Distribution Agreement

In presenting this thesis as a partial fulfillment of the requirements for an advanced degree from Emory University, I hereby grant to Emory University and its agents the non-exclusive license to archive, make accessible, and display my thesis or dissertation in whole or in part in all forms of media, now or hereafter known, including display on the world wide web. I understand that I may select some access restrictions as part of the online submission of the thesis or dissertation. I retain all ownership rights to the copyright of the thesis or dissertation. I also retain the right to use in future works (such as articles or books) all or part of this thesis or dissertation.

Signature:

_____ _____

Leon Foy McSwain **Date**

Investigating the Role for Y-Box Binding Protein 1 in Medulloblastoma Radiation Resistance and Post-transcriptional Regulation of Migration and Metastasis

By
Leon Foy McSwain
Doctor of Philosophy
Graduate Division of Biological and Biomedical Sciences
Cancer Biology

Anna Marie Kenney, PhD.
Advisor

Tobey MacDonald, MD
Committee Member

Jennifer Spangle, PhD
Committee Member

David Yu, MD
Committee Member

Wei Zhou, PhD
Committee Member

Accepted:

Kimberly J. Arriola, PhD
Dean of the James T. Laney School of Graduate Studies

Date

Investigating the Role for Y-Box Binding Protein 1 in Medulloblastoma Radiation Resistance and Post-transcriptional Regulation of Migration and Metastasis

By

Leon Foy McSwain

B.S. General Biological Sciences, University of Georgia, 2015

Anna Marie Kenney, PhD

Advisor

An abstract of a dissertation submitted to the faculty of the James T. Laney School of Graduate Studies of Emory University in partial fulfillment of the requirements for the degree of Doctor of Philosophy in the Graduate Division of Biological and Biomedical Sciences

Cancer Biology

2023

Abstract

Brain tumors represent a vast landscape of ailments ranging from the genomic and transcriptomically simple to the very complex and therapeutically adaptable. While relatively genetically straightforward, Medulloblastoma (MB) still represents a formidable tumor in pediatric patients for which treatments consist of total resection, harsh chemotherapy, and radiation resulting in numerous sequelae lasting into adulthood. From the mid to late 2010s the advent of transcriptomic technology, such as microarray and RNA sequencing afforded a closer look into the cell biology and, thus, potentially exploitable protein dependencies within these tumors. However, even considering this, modern therapies continue to consist of these antiquated techniques with a lack of modernization. This dissertation is an attempt to understand not only the sensitization of Medulloblastoma to the standard of care therapies mentioned above, but also to explore post-transcriptional regulation of proteins where differential RNA sequencing analysis may not detect oncoprotein dependencies due to a lack of transcriptional differences amongst patients.

The introductory chapters of this dissertation are an exploration of proteins medulloblastomas depend upon for mediating resistance to radiation and chemotherapy, some of which are druggable and have clinical trials pending. Y-Box Binding Protein 1 (*YBX1*) binding and signaling through some of these proteins, including Poly-ADP-Ribose Polymerase (PARP) and *TP53,* is thought to be responsible for mediating the radiation resistance phenotypes seen across many cancer types. Key DNA damage repair signaling proteins, such as RAD50 and MRE-11, are also published as binding partners for YB1. The 4th chapter of this dissertation explores the findings of those studies, and in some cases challenges them, in an investigation of sensitizing MB to radiation through YB1 silencing.

The final chapters of this dissertation challenge the frequently utilized transcriptomic technologies mentioned previously by exploring the RNA binding protein (RBP) functions of YB1 and introduce novel MB targets for reducing migration, metastasis, and proliferation. RNAs targeted by RBPs may show a lack

of differential RNA levels between samples while the corresponding proteins coded for by these RNAs show drastically different levels. Here we have elucidated a novel signaling axis whereby YB1 regulates PlexinD1 protein levels by post-transcriptional mRNA binding and translational regulation. We also explore a binding partner, Sema3E, through which PLXND1 signals to mediate migration and proliferation.

Altogether, these studies are a step forward in sensitizing MB to standard of care, and a contribution to understanding tumor biology and mRNA translational regulation as a whole, potentially applicable outside of medulloblastoma.

Investigating the Role for Y-Box Binding Protein 1 in Medulloblastoma Radiation Resistance and Post-transcriptional Regulation of Migration and Metastasis

By

Leon Foy McSwain

B.S. General Biological Sciences, University of Georgia, 2015

Advisor: Anna Marie Kenney, PhD

A dissertation submitted to the faculty of the James T. Laney School of Graduate Studies of Emory University in partial fulfillment of the requirements for the degree of Doctor of Philosophy in the Graduate Division of Biological and Biomedical Sciences

Cancer Biology

2023

Acknowledgements and Dedications

I dedicate this dissertation to the many who've supported me over the years. Those who I would like to thank utmost are my two psychiatrists, Drs. Katherine Bertachi and Alyson Goodwyn, and my therapist, Julius Peterson. Together, they helped me to persevere during the most challenging time of my life, helping to diagnose my cPTSD and work through my disease treatment. I would like to thank Dr. Anna Kenney, my advisor, for supporting me during my lab transition after being dismissed from another lab. This was a period of growth for me. Secondarily, I would like to dedicate this dissertation to my two grandfathers who passed during my time at Emory, Clifford McSwain, who was an intellectual inspiration and LGBT supporter (in fact, he was gay), and Leon Caldwell, a mechanic from whom I derive my manual dexterity and willingness to help others who passed from COVID-19. And of course this work would be nothing without the support of my undergrads: Victor Chen, Tiffany Huang, and Grace Zhou who are some of the hardest working people I know. They helped me to develop my mentorship and become the teacher I am today. I would like to thank Kiran Parwani for contributing components of my DNA Repair MB review. I would also like to thank Claire Pillsbury for being my friend, intellectual and emotional confidant, and for her contributions to my first paper on YB1. I would like to thank my committee, David Yu, Jennifer Spangle, Wei Zhou, and Tobey MacDonald. Finally, to all the people who I have befriended and who have provided me emotional and social support over the years: my OG Emory group (Jasmine Lee, Jenny Shim, Sherri Smart), my cycling friends (Benjamin Kasavan, Mariah, Carolyn Ma, Sam Bockner, Rebeccah Parker, Tom, and Felix, from The Fixie and SOPO), Haritha Kunhirama (our postdoc), my closest friend and room-mate for the duration of my PhD, Erik Ringen, who helped me through it all and taught me R, and of course my two cats Ira and Lakshmi who I adopted the day I moved to Atlanta from Athens.

Table of Contents

Abbreviations: WNT = Wingless, SHH = Sonic Hedgehog, DDR = DNA Damage Response, MB = Medulloblastoma, DSB = Double Strand Break, SSB = Single Strand Break, NHEJ = Non-Homologous End Joining, HR = Homologous Repair, BER = Base Excision Repair, NER = Nucleotide Excision Repair, ATM = ataxia telangiectasia mutated, ATR = ataxia telangiectasia and Rad3-related protein, Chk1 = Checkpoint Kinase 1, Chk2 = Checkpoint Kinase 2, PTCH = Patched, Smo = Smoothened, PARP = Poly ADP Ribose Polymerase 1, BBB = Blood Brain Barrier, CGNP = Cerebellar Granular Neural Precursor, PVN = Perivascular Niche, APE1 = Apurenic/apyrimidinic endonuclease 1, MGMT = O6-MethylGuanine-DNA Methyltransferase. KD = Knockdown, KO = Knockout, OE = Overexpression, MRI = Magnetic Resonance Imaging, STR = Subtotal Resection, GTR = Gross Total Resection, LCA = Large Cell Anaplastic, DNV = Desmoplastic/Nodular, MBEN = medulloblastoma with extensive nodularity; LP = Lumbar Puncture

Chapter 1

An introduction to Medulloblastoma

Authors contribution and acknowledgement of reproduction:

Portions of this chapter are published as part of the manuscript “Medulloblastoma and the DNA damage response” in Frontiers, 2022. SWS conceived these portions (see chapter 2).

1.1 Current Clinical Approaches to Medulloblastoma

Medulloblastoma (**MB**) is the most common malignant brain tumor affecting children. Standard treatment of non-infant medulloblastoma requires maximal safe surgical resection followed by radiation and chemotherapy (**Figure 1**).[1] Within the last ten years, microarray and methylome profiling from multiple groups has led to the identification of four major molecularly distinct MB subgroups – Wingless (**WNT**), Sonic Hedgehog (**SHH**), **Group 3**, and **Group 4 (Figure 2).**[2–4] While WNT and SHH MB are driven by alterations in WNT and SHH pathways respectively, oncogenic drivers of Group 3 and Group 4 tumors are less clear.[5,6] The amplification of *MYC*, *MYCN*, and mutations in *TP53*, are common molecular alterations driving DNA damage induced apoptotic resistance and frequently enriched upon relapse.[5,7] While c*MYC* amplification is predominant in Group 3 MB and is associated with poor patient prognosis, this occurs in other subgroups as well.[8] Furthermore, following SHH stratification into 4 molecularly distinct categories (SHHα; SHHβ; SHHδ; SHHγ) it was found that p53 mutations are enriched in SHHα and patients have a worse prognosis.[9] Thus, prognosis varies based on subgrouping and in fact WNT patients have the best outcome compared to those of other subgroups with *MYC* amplification or *TP53* mutation.[10]

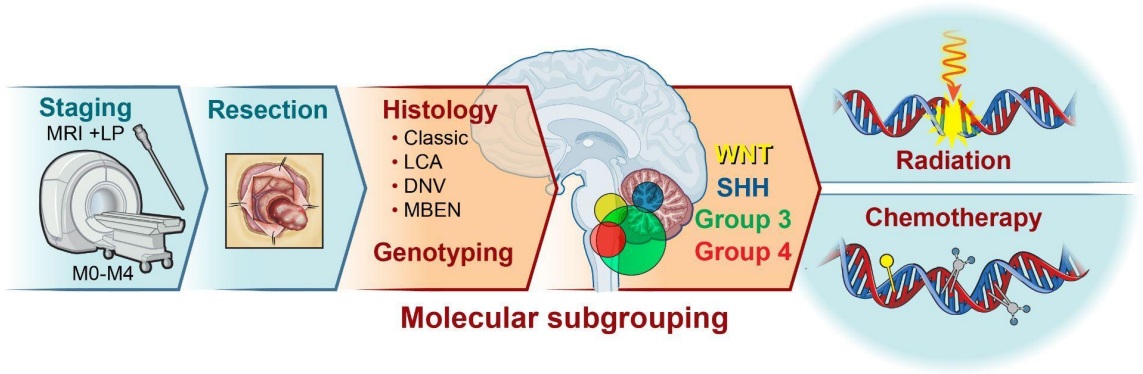

Figure 1: Medulloblastoma is a tumor of the Cerebellum

Medulloblastoma constitutes the most common childhood malignant brain tumor, accounting for approximately 20% of all central nervous system tumors. Patient stratification consists of categorization based on age and presence of metastasis, histology, and genotyping. Following initial staging*, maximal surgical resection is typically attempted for all patients. Subsequent histology and molecular profiling introduce subgroup classification and potential alterations to the treatment protocol. While most patients receive some combination of radiation and chemotherapy, the patients age, location of tumor,[11] extent of spread, histology, and subgroup inform the intensity and duration of treatment. Acronyms: MRI: Magnetic Resonance Imaging, LCA: Large Cell Anaplastic, DNV: Desmoplastic/Nodular, MBEN: medulloblastoma with extensive nodularity; LP: Lumbar Puncture *may be delayed till after surgery).

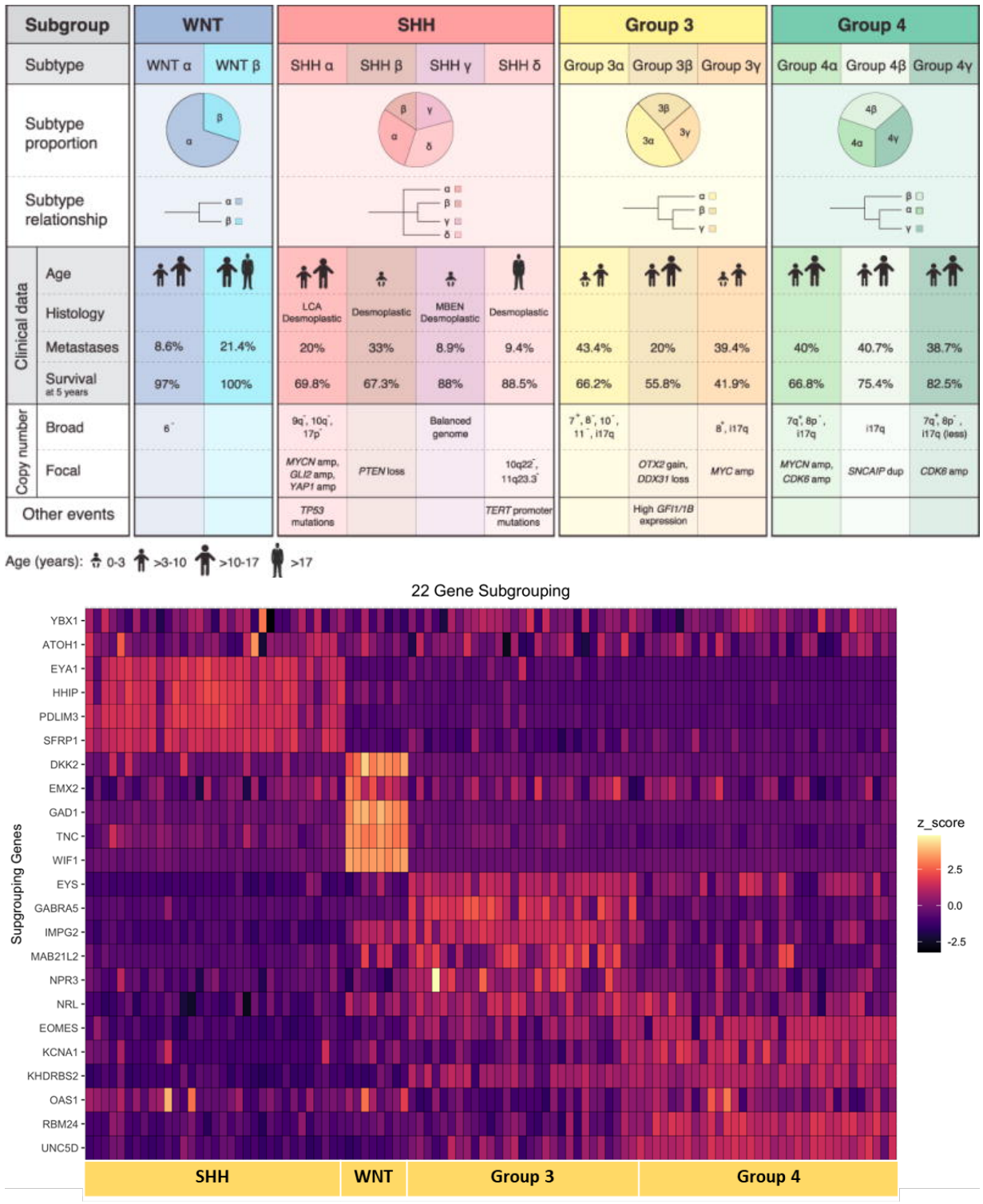

Figure 2: Molecular subgrouping of Medulloblastoma

(TOP) Medulloblastoma can be genetically sub-grouped into 4 molecularly distinct profiles on

the bases of genetic alterations and transcriptome. SHH is defined by alterations to the SHH pathway, *TP53*, *TERT,* and *MYCN.*** (Bottom) Distinct sets of transcripts from these same earlier studies were initially developed to define MB subgroups but have since been replaced. *YBX1* and *ATOH1* are addendums to these data where YB1 RNA is not enriched or specific to any one subgroup but is instead highly expressed across all groups (see chapter 4). Image generated in R using GSE85217.

** Szalontay and Khakoo, "Medulloblastoma: An Old Diagnosis with New Promises", Current Oncology Reports, 2020

Despite recent genomic MB characterization and subsequent tumor stratification, clinical treatment paradigms are still largely driven by histology, degree of surgical resection, and presence or absence of metastasis rather than molecular profile.[12] Patients usually undergo resection of their tumor followed by craniospinal radiation (**CSI**) and a 6 month to one year multi-agent chemotherapeutic regimen. Traditionally, radiation has been recognized as the mainstay of treatment for non-infant MB patients (>3 yo). Prior to the 1950s, MB was considered a universally fatal diagnosis. In 1953, Patterson and Farr published a case series of 27 patients treated with CSI and observed a 3-year survival of 65%.[13] This landmark paper led to the widespread acceptance of CSI as the therapy for MB. However, the long-term neurocognitive sequelae of radiation therapy, along with the advent of cytotoxic agents, propelled the addition of chemotherapy in the 1970s.[14] Since then improvement in survival has been incremental, comprising better surgical and radiation techniques, better supportive care, and combination/intensification of agents.

Over the last decade, modifications to the above therapeutic regimen have been primarily driven by molecular subgrouping. Given the good outcomes of patients with WNT tumors, there is an effort to reduce the radiation dose for these patients.[12] Additionally, administration of carboplatin concomitant with radiation was recently found to be beneficial specifically for Group 3 patients.[15] Multiple clinical trials are underway to evaluate the efficacy of targeted therapies, particularly in SHH MB, although none have made it to clinical practice yet. Additionally, many proteins have been investigated for potential synergism with MB standard of care which are explored extensively in chapters 2 and 4.

1.2 Medulloblastoma: Developmental Biology Gone Awry

Of course, early therapies preceded our understanding of brain tumor cell biology, which is crucial to the development of novel therapies and began with studies on the development of the cerebellum. Developmental biology is something of a complex tango involving numerous morphogens and ligand gradients responsible for patterning, foliation, limb development and beyond. Here we will focus on cerebellar development and the Sonic Hedgehog signaling axis, also named based on *Drosophila* mutational phenotypes consisting of excessive hair growth (**Figure 3**).

The significance of appropriate signaling termination during development cannot be overstated and is exemplified in the development of many tumors, one of the most classical being *TP53* germline mutations, the cause of Li Fraumini syndrome which can drive MB development. Of course, cerebellar development is no different, and with that comes the potential for SHH signaling dysregulation. In the setting of cerebellar development, the SHH ligand, secreted from purkinje

neurons, regulates the proliferation of cerebellar granular neural precursors (CGNPs). As expected, constitutive SHH signaling would result in the cerebellar hyperplasia and, potentially, the development of a tumor. Classically, however, the overexpression of select oncogenes rarely leads to tumor development, hence the significance of tumor suppressor loss, of which many are implicated in driving medulloblastoma development. The patched receptor, for example, can suffer from translocation or deletion, halting the suppression of oncogenic SMO → Gli signaling, and the basis of the PTCH floxed spontaneous MB mouse model. Prominent oncogenes responsible for driving MB development include Telomerase Reverse Transcriptase (*TERT*), for which single nucleotide polymorphisms (SNVs) results in overexpression and numerous phenotypic effects, and the overexpression of SMO, the hallmark oncogene utilized for the *NeuroD2-SmoA1* spontaneous mouse model.[16,17]

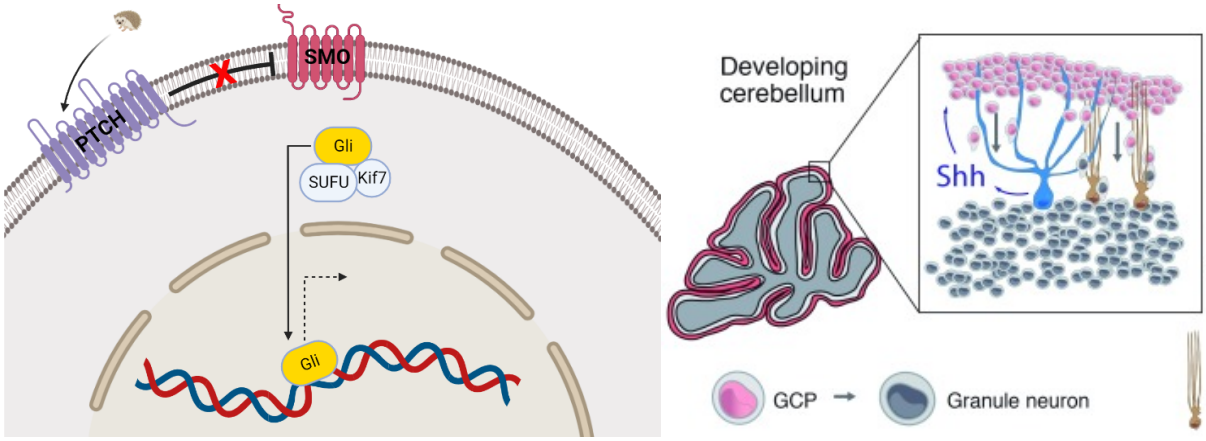

Figure 3: SHH signaling and the developing cerebellum

(**Left**) SHH signaling is defined by constitutive suppression of Smoothened (SMO) receptor by Patched (PTCH) and the transcription factor Gli is suppressed by SUFU, preventing its nuclear translocation. When PTCH is bound by SHH ligand, suppression of SMO is stymied and the Gli transcription factor can translocate to the nucleus to mediate proliferation, among many other

phenotypes. (**Right**) During cerebellar development, SHH ligand gradients regulate the proliferation and eventual differentiation of cerebellar granular neural precursor cells (CGNPs) into granular neurons resulting in cerebellar foliation and layering.[18]

It is clear, then, how these early tumorigenic events can be harnessed to create models for studying medulloblastoma development and, in fact, are correlative with human medulloblastomas as exemplified by UMAP of spontaneous SHH and Group3 models and MB patients showing uniquely conserved sub-cell tumor populations representing proliferative, progenitor, and immune cell populations, among others, making them such phenomenal tumor models (Chapter 4). [19]

1.3 Metastasis and Medulloblastoma

MB patients that present with metastasis, which are primarily leptomeningeal (**Figure 4**), have a considerably shorter overall survival compared to their non-metastatic counterparts. Additionally, radiation or therapy induced metastasis results in a substantially worse prognosis, with an overall survival average of ~3 months, compared to patients who present initially with metastasis.[20] Early attempts to identify molecular determinants of metastatic positive patient outcome were met with difficulty as tumor models at the time were lacking, such as when MacDonald et al discovered PDGFRA as a driver of migration derived from patient microarray data, or the lack of either a publication history or small molecule inhibitors for genes nominated from differential expression analysis between Met- and Met+ patients.[21,22] And while these gene signatures may prove useful for clinical prognostics, only actionable targets would allow for translation into the clinic. A handful of studies have since been published proposing molecular targets implicated in driving migration and metastasis.

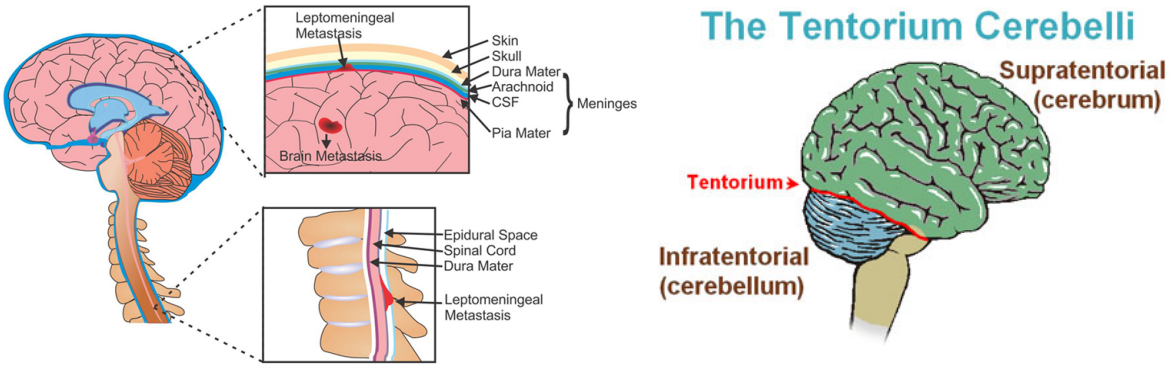

Variable	SHH	Group 3	Group 4
No. of Cases	3/26 (11.5%)	10/28 (35.7%)	14/46 (30.4%)
Metastases Location			
Supratentorial	0	5	10
Suprasellar	0	0	7
Infratentorial	2	7	7
Spinal	1	9	8

Figure 4: MB metastasis are primarily leptomeningeal in nature

(Left) An illustration of leptomeningeal anatomy as the primary site of MB metastasis. Cells achieving anoikis and stemming from the primary tumor will presumably travel through the CSF until they implant in one of four regions: supratentorial, infratentorial, suprasellar, or spinal (**Right**).[23,24] (**Bottom**) Statistics on incidence of metastasis in MB patients from SHH, Group 3, and Group 4 patients. [25]

ERBB2 was one of the earliest nominated metastatic drivers in MB. Overexpression of ERBB2 in Daoy cells followed by microarray identified S100A4 calcium binding protein as a signaling effector amongst other proteins previously implicated by MacDonald et al. such as RAS/MAPK

and cytokine signaling. ERBB2 was found to promote transcription of S1004A while inhibiting ERBB2 with OSI-744 resulted in a decrease in S100A4 protein levels, reducing invasion potential.[26] Another metastatic candidate, VEGF, surprisingly plays no role in promoting migration or metastasis in multiple studies. Initially, VEGF was found to correlate negatively with leptomeningeal positive patient outcomes; however, this study was not specific to MB patients.[27] This narrative was contradicted by a lack of Daoy cell responsiveness to bevacizumab when supplied with VEGFA high conditioned media.[28] However, this study did find uPA, a urokinase receptor ligand, to be highly enriched in the benign meningothelial meningioma cell conditioned media used to stimulate Daoy cells. uPA and its receptor uPAR are both enriched in MB cells following radiation and signal through Focal Adhesion Kinase (FAK) to enhance migration, a phenotype abrogated upon uPA depletion.[29] These data are suggestive of a mechanistic reason for increased metastatic incidence following standard of care therapy. In more recent studies, MATH1 (ATOH1), a CNS developmental transcription factor, and LDHA, secreted from MYC-driven cells, were shown to promote extensive leptomeningeal spread *in vivo* using SHH and Group3/4 models, respectively.[30,31] Altogether, while these studies do nominate several potential drivers of MB metastasis, none have translated into the clinic. This could be attributed to the methods of research which may not account for initial resection and standard of care or the difficulty of integrating an anti-metastatic drug into the clinical trial pipeline. In fact, a majority of the research has been more mechanistically focused with few treatment-based *in vivo* studies, not unlike the narrative presented in chapter 6.

1.4 Conclusions

In the context of medulloblastoma, there remain many questions to be answered with, currently, only sub-par tools. Given the importance of support cells like astrocytes in the proliferation and maintenance of brain tumors, modeling therapeutic response in a monoclonal *in vitro* cell population is a poor reflection of true response to oncogenic inhibition and the *in vivo* tools available, such as PDX models, may not allow us to effectively model immune responses or study proteins for which drugs are not available. Additionally, the blood brain barrier (BBB), an epithelial lining of brain vascular that prevents the entry of many peripherally administered drugs and antibodies, continues to pose a major hurtle for brain tumor therapeutic development. While some small molecule inhibitors such as vismodegib or prexasertib show excellent BBB penetrance and activity, pharmacologic resistance remains a concern and may require combination therapies such as STAT inhibition alongside vismodegib.

Chapter 2

A Review: Targeting Proteins Involved in the DNA Damage Response to Radiation and Chemotherapy in Medulloblastoma

Author's Contribution and Acknowledgment of Reproduction

This chapter is reproduced with edits from a literature review manuscript published in Frontiers in Oncology, 2022.

LFM and AMK contributed to the conception of the review. AMK, JS, and DH sponsored the review. LFM designed the layout and writing of the review. SWS and KP contributed individual sections to the review, including Clinical perspectives and AKT signaling, respectively.

2.1 Abstract

Despite genomic MB characterization and subsequent tumor stratification, clinical treatment paradigms are still largely driven by histology, degree of surgical resection, and presence or absence of metastasis rather than molecular profile. Patients usually undergo resection of their tumor followed by craniospinal radiation (**CSI**) and a 6 month to one-year multi-agent chemotherapeutic regimen. While there is clearly a need for development of targeted agents specific to the molecular alterations of each patient, targeting proteins responsible for DNA damage repair could have a broader impact regardless of molecular subgrouping. DNA damage response (**DDR**) protein inhibitors have recently emerged as targeted agents with potent activity as monotherapy or in combination in different cancers. Here we discuss the molecular underpinnings of genomic instability in MB and potential avenues for exploitation through DNA damage response inhibition.

2.2 DNA Damage Signaling

Since the standardization of medulloblastoma treatment from the mid-1980s to the mid-2000s, surgical resection, radiation and chemotherapy continue to serve as the primary treatment modalities for MB patients.[32,33] While radiation delivery optimization and dose reduction preserves vital tissue proximal to the primary tumor site, posterior fossa irradiation and on-target off-tumor effects of chemotherapy remain important considerations for therapeutic development.[34,35] Targeting proteins involved in resolving DNA damage from either ionizing radiation (**IR**) induced single and double strand breaks (**SSBs** and **DSBs**) or adducts formed by chemotherapies could permit lower therapeutic dosing and more effective targeting of tumor cells.[36]

2.3 Targeting Proteins involved in the DNA damage response to Radiation and Chemotherapy

The DNA damage responses to IR-induced SSBs and DSBs, and adducts formed by chemotherapies, are extensively reviewed elsewhere.[37,38] Here we will discuss the central tenets of the DDR, including detection, downstream signaling, and repair, as they pertain to MB therapy resistance and potentially targetable DDR proteins. Firstly, exposure to ionizing radiation results in the accumulation of SSBs and DSBs, which the cell will repair through one of the two methods: homologous recombination (**HR**) or the more error prone non-homologous end joining (**NHEJ**) (**Figure 2**).[39] Comparatively, DNA adduct forming agents, such as those commonly used to treat MB including cisplatin, lomustine, cyclophosphamide, and temozolomide, require alternate repair proteins to perform base excision repair (**BER**) or nucleotide excision repair (**NER**) (**Figure 2**). Proteins important for detection, signaling, and repair, including ATM/ATR, CHK1/2, and PARP function in both types of damage repair while APE1 and CK2 facilitate DNA adduct repair,

specifically. Other proteins discussed include AKT, a mediator of radiation resistance in the MB stem cell niche, p53 the "guardian of the genome," which when mutated, results in substantially worse standard of care response primarily due to defective cell death signaling downstream of damage recognition, and proteins that regulate p53.

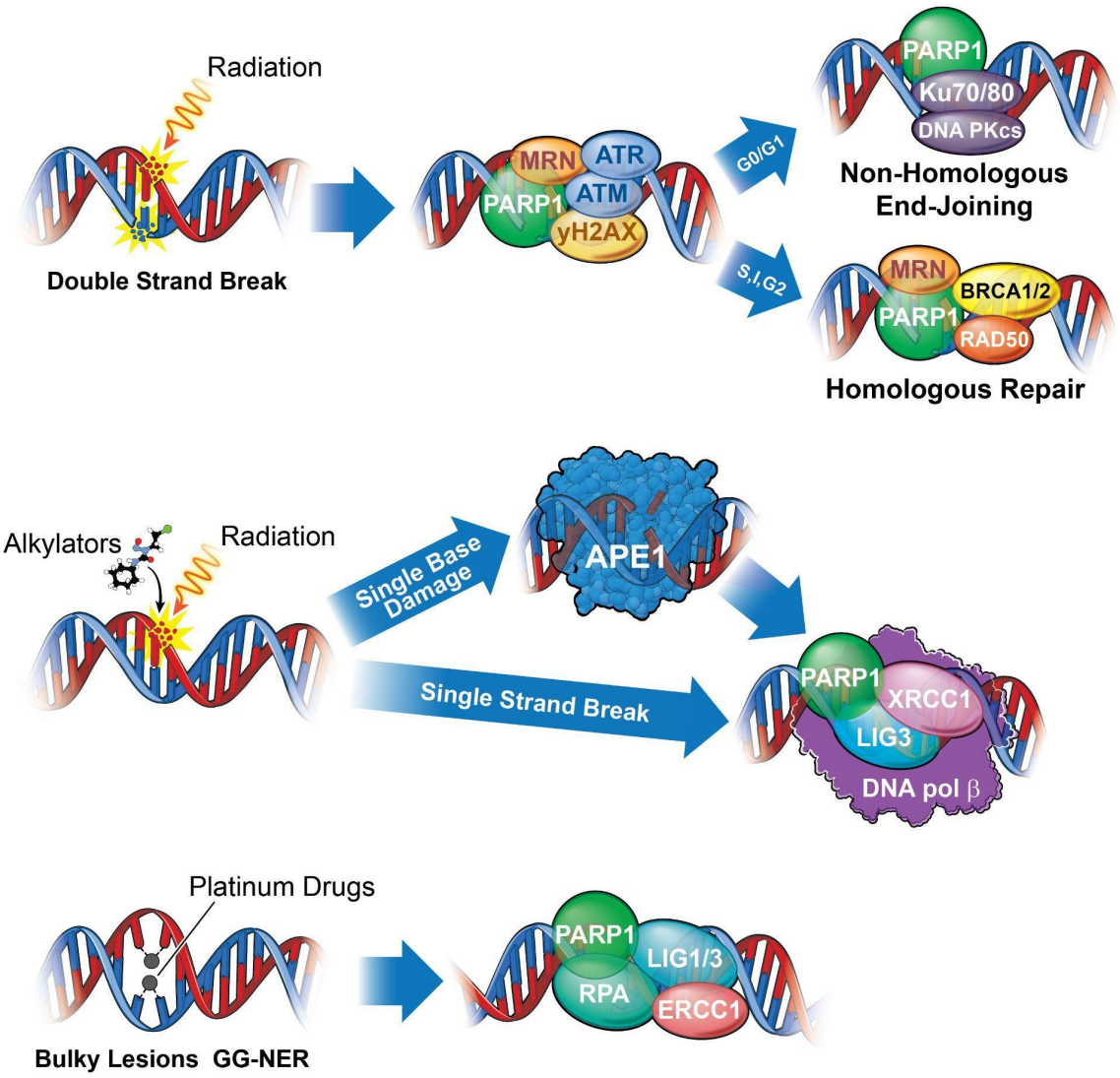

Figure 1: A summary of the DNA damage response in Medulloblastoma

Numerous DNA damage response signaling axes mediate DNA repair following medulloblastoma standard of care. Chemotherapies utilized, including temozolomide, cisplatin, lomustine, and cyclophosphamide (with cisplatin and cyclophosphamide constituting standard of care), bind directly to DNA to create bulky lesions repaired through a combination of either Base Excision Repair (**BER**), Nucleotide Excision Repair (**NER**), MGMT (Not shown), and **HR** or **NHEJ,** while IR mediated DSBs are repaired through NHEJ and HR.

(**Top**) The deleterious effects of Ionizing radiation results primarily from DNA double strand breaks (DSBs) repaired either through Homologous Repair (**HR**) or Non-Homologous End Joining (**NHEJ**). While PARP, M/R/N (a complex of 3 proteins: MRE-11, RAD50, NBS), and ATM function universally to recognize strand breaks, cells in G0/G1 lack sister chromatids and will repair through a more error prone NHEJ, while those in S, Interphase, or G2 will repair through HR, utilizing the sister chromatid to replace the missing bases. Proteins directly involved in repair of double strand breaks include Ku70/80 and DNA-PKcs for NHEJ and M/R/N, BRCA1/2, and RAD50 for HR. Upstream effectors, ATM and ATR, will signal through Chk1 and 2 to arrest the cell and either repair or commit apoptosis (**Figure 4**). (**Middle**) Single strand breaks resulting from radiation or excision of damaged base pairs by APE1 (such as those resulting from alkylation) are identified by PARP1 and repaired by XRCC1, DNA Ligase III (LIG3), and DNA polymerase beta. (**Bottom**) Bulky lesions resulting from platinum based drugs such as cisplatin or carboplatin can be repaired either through transcription coupled NER (TC-NER) or global genomic NER (GG-NER). While it remains unclear what role PARP may play in TC-NER, it serves as a recognition and recruitment protein for GG-NER, functioning

alongside DNA Ligase I or III (LIG1/3), RPA, and ERCC1 proteins. Bifunctional alkylating agents and chloro-ethylating agents, such as cyclophosphamide or lomustine, respectively, can methylate guanine. Methylated guanine can be repaired through MGMT (not shown), through direct removal of guanine methyl group, potentially resulting intrastrand cross-linking (**ICL**) requiring a combination of NER and HR or NHEJ to repair) or interstrand cross-linking, repaired through NER. Platinum drugs mediate interstrand cross-linking, repaired predominantly through NER. Finally, Temozolomide can be repaired either through BER (requiring APE1) or MGMT [40].

2.3.1 ATR-Chk1

Dozens of proteins function together to recognize and initiate repair of damaged DNA; however, ATR and ATM can initiate cell cycle arrest, damage repair, and apoptosis by signaling through Checkpoint Kinase 1 and 2 (**Figures 1 and 4**).[41] More specifically, the ATR-Chk1 signaling axis has emerged as a key player in postnatal cerebellar development and MB therapeutic resistance, and Chk1 is upregulated across MB subgroups.[42] Saran and colleagues investigated SHH signaling in a patched 1 receptor heterozygous IR inducible SHH MB model (hereafter referred to as the ***PTCH*$^{+/-}$ model**), where radiation induces a "second hit" to the smoothened receptor inhibitor, *PTCH*, resulting in constitutive SHH signaling and tumorigenic transformation. The group uncovered a link between *PTCH* heterozygosity and tumor formation following IR exposure in postnatal day 4 (**P4**) but not P10 mice as a result of differences in p53 activation.[43,44] Subsequently, SHH pathway dysregulation was linked to ATR-Chk1 pathway inactivation in the *PTCH*$^{+/-}$

model.[45] Through overactivation of the SHH signaling cascade via *PTCH* inactivation and overexpression of Gli1 protein, the phosphorylation and activation of Chk1 is attenuated, resulting in abrogation of the S-phase cell cycle checkpoint and chromosomal aberrations. In an ATR-deleted mouse model ($ATR^{hGFAP\text{-}Cre}$) of cerebellar granular neural precursor cells (**CGNP**s), the putative cell of origin for SHH MB, cells develop extensive chromosomal abnormalities leading to cerebellar hypoplasia.[46] From the same study, ATR deletion results in abrogation of cell cycle checkpoint activation, evidenced by PCNA and pHH3 positive staining, and accumulation of γH2AX, a marker of DNA damage, ultimately resulting in p53 accumulation, caspase-3 cleavage, and apoptosis. Additionally, ATR deletion from a smoothened overexpressing SHH model through cre-recombination ($SmoM2;Atr^{G\text{-}cre}$), inhibits tumor formation; all of which suggest a requirement for ATR in maintaining genomic stability during cerebellar development and tumor formation, nominating the ATR-Chk1 axis as a potential therapeutic target.

What we ultimately seek to therapeutically exploit by targeting the ATR-Chk1 pathway are cells with unstable genomes; in fact, many cells amenable to ATR-Chk1 signaling inhibition are *MYCN* or c*MYC* amplified or overexpressing. SHH and WNT subgroups overexpress *MYCN* while Group3 and WNT subgroups overexpress *cMYC*.[8] *MYCN* and *cMYC* increase the number of firing replication origins, causing collision between replication and transcriptional complexes, resulting in fork stalling and collapse and the accumulation of DDR marks at the sites of active DNA replication.[47–49] However, the simultaneous regulation of cell cycle check-points and DDR allows cells to maintain a complex balancing act between genomic instability and tumor maintenance, which depends upon the ATR-Chk1 signaling axis.[49] An example of this can be found in *MYCN* expressing SHH MB. Sonic Hedgehog signaling drives *MYCN* expression in both CGNPs and MBs of the $PTCH^{+/-}$ model, and *MYCN* overexpression can drive cell proliferation independent of

SHH signaling.[50] Coincidently, the genomic instability resulting from *PTCH1* deletion can lead to the amplification of regions of chromosome 12, including the *MYCN* gene.[51] Through transcriptional upregulation of the MRE11/RAD50/NBS1 (**M/R/N**) complex downstream of ATR-Chk1 in CGNPs, *MYCN* drives not only a genomically unstable, highly replicative state, but also an increase in proteins required for recognition and repair to counter the instability.[47]

The lack of enzymatic activity and hydrophobic pockets paired with an intrinsically-disordered N-terminal make *MYCN* a challenging drug target.[52] Given these challenges, alongside the potentially broader impact of DNA repair protein inhibition, much of the research has focused on sensitization of cells to genomic stress through inhibition of either Chk1 or Wee1, a target of Chk1.[53] The correlative relationship between protein expression and cell sensitivity to protein inhibition is not applicable in the case of Chk1. While all MB subgroups demonstrate elevated Chk1 expression and worse prognosis with high Chk1 expression, as mentioned previously, the relative expression of *cMYC* is a greater predictor of responsiveness to Chk1 inhibition.[42] In earlier studies utilizing AZD-7762, a Chk1 inhibitor, numerous cell lines demonstrated response as measured through reductions in cell viability, accumulation of γH2AX, and increase in apoptotic markers. Daoy, D283, D425, UW-228, and HD-MB03 all show varying degrees of Chk1 inhibitor response; however, high *cMYC*-expressing cells such as D283 and HD-MB03, both Group 3 cell lines, are more sensitive to damage as seen through a higher ratio of reduced viability to γH2AX foci formation.[42,54] Lower levels of damage accumulation are required to push the cell fate towards apoptosis. *In vivo* and synergism studies subsequently emerged using AZD-7762, MK-8776, Rabusertib, or Prexasertib (all Chk1 inhibitors) in combination with cisplatin or gemcitabine. Inhibition of Chk1 in Group 3 cells, including D425, D283, and SU-MB002, but not SHH PDX models, results in cell cycle checkpoint abrogation and a greater accumulation of DNA damage

and subsequent cell death following simultaneous exposure to cisplatin or gemcitabine.[55]

Genomic surveillance is crucial for cerebellar development, tumorigenesis, and tumor maintenance. While ablation of the ATR-Chk1 axis results in cerebellar hypoplasia in non-tumor models, downregulation during SHH tumor development leads to extensive chromosomal abnormalities and abrogation of tumor development. This complex balancing act is a requirement for maintaining a highly proliferative, tumorigenic state. The *cMYC* amplification and overexpression of Group 3 models creates a reliance on the ATR-Chk1 axis for viability where inhibition could result in cell death, a phenotype potentially exploitable in WNT tumors given their MYC status. And even though SHH PDX models do not appear responsive to CHK1 inhibition in recent studies, inhibition of MYCN → M/R/N signaling is unexplored. *MYC* amplification alongside Chk1 upregulation may serve as reliable biomarkers for Chk1 pathway inhibition, particularly in Group 3 patients who have the worst prognosis. Currently, Prexasertib in combination with Cyclophosphamide or gemcitabine is in a phase 1 clinical trial for refractory Group 3 and Group 4 patients.[1ct]

2.3.2 PARP

Poly-ADP-ribose Polymerase, or PARP, plays numerous roles in the DNA damage response, but is most notable for damage recognition and repair protein recruitment through ribosylation of damaged DNA and auto-ribosylation. While PARP1 is not typically required for cell survival, because it facilitates repair of IR induced strand breaks through both NHEJ and HR, and repair of bulky adducts through NER (**Figure 2**), inhibition could sensitize MB cells to existing therapies and even synergize with the aforementioned Chk1 inhibitors.[56–58] In fact, while *BRCA1* and

BRCA2 mutation status are positive predictors of PARP1 inhibitor response due to synthetic lethality in the setting of other tumor types, this is not a requirement and other gene signatures can serve as predictors of therapeutic response where the use of single molecular markers prove to be insufficient.[59] Additionally, the *BRCA1/2* mutation status across MB patients remains unclear, though RNAseq data have shown upregulation of gene signatures associated with *BRCA1/2* mutation in Group3 and 4 and a subset of SHH patients.[17]

A role for PARP1 in MB tumor formation emerged through studies of p53 null mice. While *TP53* ablation alone is not sufficient for brain tumor formation, in $TP53^{-/-}$; $PARP1^{-/-}$ mice, neuronal cells are predisposed to malignant transformation.[60,61] Saran and colleagues, using a p53 wild type $PTCH^{+/-};PARP1^{-/-}$ model of SHH MB, demonstrated that *PARP1* ablation leads to increased frequency of preneoplastic lesions, accumulation of γH2AX foci, and CGNP genomic instability.[62] Chromosomal rearrangements resulting from *PARP1* abrogation led to a second hit in the *PTCH1* allele, increasing the incidence of tumor formation. The absence of PARP also increases phosphorylation of Ser18-p53, suggesting that the majority of genetically unstable cells undergo apoptosis while few cells escape to accelerate tumor formation. Pre-treatment of *in vitro* MB models, D283, D556, and UW228-2, with olaparib prior to irradiation results in greater accumulation of γH2AX foci that are sustained longer than control.[63] In fact, olaparib is blood brain barrier (**BBB**) penetrant and could serve as an effective brain tumor therapy[64] Considering the genomic instability of CGNPs following *PARP1* and *ATR* ablation, there is also a potential for synergism between PARP and ATR inhibition. While not yet studied in the setting of MB, in glioma-bearing mice the combination of VE822, an ATR inhibitor, and olaparib leads to a 60% increase in survival compared to control-treated.[65]

In addition to PARP's role in radiation induced strand break repair, it also mediates base excision repair. As mentioned above, PARP1 is critical for resolution of adducts by functioning as a component of the BER complex, consisting of DNA ligase III (*LIG3*), DNA Polymerase β *(POLB),* and XRCC1.[56,66] Adducts formed by lomustine, cisplatin, and cyclophosphamide, which serve as cytotoxic chemotherapies to treat MB, require functional BER or NER for resolution.[67,68] Unfortunately, the combination of PARP inhibitors with cyclophosphamide does not improve response rate over cyclophosphamide alone, at least in the setting of breast cancer, and combinations with lomustine are understudied[69]. However, the administration of PARP inhibitors alongside platinum-based drugs like cisplatin has the potential to enhance targeting of tumor cells while reducing secondary cytotoxicities.[70] In fact, compared to veliparib-mediated catalytic inhibition of PARP1, which abrogates PARylation, olaparib demonstrates superior DNA-PARP trapping, resulting in not only a lack of repair, but also replication fork stalling and double strand breaks. Olaparib synergizes with cisplatin and temozolomide, an emerging MB therapeutic for recurrent patients.[71–74] In Group 3 and 4 xenograft models generated using D384, D425, and D283 cell lines, D384 and D425 show a robust response to combination therapy with temozolomide and another PARP inhibitor rucaparib, whose DNA trapping kinetics are comparable to those of olaparib.[75,76]

Historically, PARP inhibition induced apoptosis through synthetic lethality when combined with *BRCA1/2* mutations in breast cancer patients resulting from unrepaired strand breaks. However, *BRCA1/2* mutation is not a requirement for the use of PARP inhibitors. PARP1 is crucial to DDR activation through its PAR catalytic activity, which is exemplified in developmental MB models where ablation leads to genomic instability and cell death following radiation. While there is a reliance of MYC amplified cells on the ATR-Chk1 signaling axis, PARP inhibition appears to be

relevant across all subgroups not only in the context of radiation but also when combined with platinum-based drugs and temozolomide. Inhibiting PARP could have a broader impact compared to ATR-CHK1 in cells without *MYC* amplification or overexpression in combination with standard of care therapies and could afford dose decreasing to ameliorate toxicities from chemotherapy, namely cisplatin. Currently, olaparib is in a phase 2 clinical trial for patients with advanced or refractory solid tumors, including MB.[2ct]

2.3.3 APE1

Apurinic/apyrimidinic endonuclease 1 (**APE1**) not only regulates DNA binding of transcription factors through cysteine residue redox regulation, it is also responsible for DNA incision proximal to adducts formed by platinum-based drugs and alkylating agents such as cisplatin and temozolomide (**Figure 2**).[77,78] The production of oxygen free radicals from ionizing radiation also produces abasic sites in the DNA reparable through APE1, the abrogation of which leads to unrepaired DNA and cell death.[79–81] Additionally, due to the potential for PARP inhibitor resistance, targeting APE1 could sensitize PARP inhibitor resistant cells to chemotherapy and radiation.[82]

Similar to a requirement for PARP and ATR in maintaining genome integrity during cerebellar development, due to the high CNS oxidative stress in postnatal mice, APE1 can protect cells against postnatal oxidative DNA damage.[83] 100% of Mice lacking APE1 die within 30 days of birth concomitant with accumulation of extensive γH2AX accumulation. And while p53 ablation in these mice rescues their viability, the absence of p53 alone does not result in tumor burden by post-natal day 20 whereas 100% of $(Ape1^{L/L};p53^{L/L})^{Nes\text{-}cre}$ mice develop tumors by day 15. From the same study, APE1 deficient astrocytes maintain radiation induced DNA damage compared to

controls and are sensitized to cisplatin. Similarly, after uncovering a role for APE1 in mediating resistance of glioma to adjuvant radiation and alkylating agent based chemotherapy, Silber and colleagues extended these findings to MB and primitive neuroectodermal tumors.[84–86] In patients deemed high risk as indicated by tumor invasion into the surrounding brain, APE1 endonuclease activity is elevated.[87] In UW228-2 cells treated with siRNA against APE1 in combination with temozolomide, survival is decreased compared to control. These data point to a requirement for APE1 to mediate cisplatin adduct resolution in MB. Given the barriers to small molecule inhibitor development for some targets and potential lack of BBB penetrance, the utilization of siRNA conjugated nanoparticles has emerged as a viable alternative, potentially alleviating inhibitor resistance and issues with BBB penetrance.[88] UW228 cells exposed to nanoparticle conjugated siRNA against APE1 *in vitro* sustain radiation induced DNA damage.[83,89] Only recently did a selective APE1 inhibitor emerge in high throughput drug screening of non-small cell lung cancer (**NSCLC**)[90]. The application of NO.0449-0145 induces DNA damage *in vitro* and in an *in vivo* xenograft model and overcomes cisplatin and erlotinib resistance; however, the BBB penetrance and applicability in MB would require further investigations.

2.3.4 CK2 and MGMT

Casein Kinase II (**CK2**), a pleiotropic protein with diverse functions from Epithelial to Mesenchymal Transition (**EMT**) regulation to DNA damage repair, has become a potential therapeutic target in MB.[91] While CK2 regulates redox activity of APE1 through post-translational modification, its role in DNA repair comes from signaling through O6-MethylGuanine-DNA Methyltransferase (**MGMT**), a DDR protein capable of mediating temozolomide resistance.[92–94] Unlike protein complexes that mediate BER and NER, MGMT can function alone to repair *O*6-

AG and *O*4-alkylthymine adducts formed by alkylating agents.[95] Even though MGMT promoter methylation in CpG rich sequences and subsequent overexpression is well known for mediating temozolomide resistance in glioblastoma, the clinical relevance of targeting MGMT in MB has only recently emerged.[96]

In 2018 Li and colleagues uncovered a CK2 → β-Catenin → MGMT signaling axis in SHH MB.[94] Knockout of either isoform, *CSNK2A1* or *CSNK2B*, results in decreased tumorigenic potential. In a high throughput screen using CX-4945, an orally bioavailable and BBB penetrant selective inhibitor of CK2, temozolomide was found to synergize with CK2 inhibition.[97,98] Indeed, CK2 KO leads to a decrease in MGMT and β-Catenin and an increase in apoptosis following temozolomide exposure, which was rescued by re-expression of β-Catenin. These data point to CK2 as a modulator of MGMT activity and temozolomide resistance in MB. There are other DDR proteins involved in recognition, repair, and signaling found to be CK2 substrates, including p53, BRCA1, XPB, XRCC1, XRCC4, Histone H1, and Rad51.[99] CK2 is also implicated in driving proliferative and migratory phenotypes and inhibition of apoptosis in multiple cancers, including MB.[99] Initial studies showed binding of CK2 to the smoothened receptor and promotion of SHH signaling.[100] Proteomic analysis of CGNPs showed increased phosphorylation of CK2 motifs in postnatal day 7 mice, implicating CK2 as a driver of cerebellar developmental programming[101]. Subsequent CK2 knockdown or treatment with the CK2 inhibitor 4,5,6,7-Tetrabromobenzotriazole (**TBB**) destabilizes Gli2 and decreases Gli1 expression, downstream mediators of SHH signaling. More importantly, D175N mutation in CK2 confers resistance to TBB but not CX-4945 likely due to ATP-binding cavity enlargement, further demonstrating CX-4945 robustness. These findings point to a broader impact of CK2 targeting and the potential for radiation and chemotherapy sensitization and inhibition of oncogenic phenotypes. CX4945 is currently in a multi-phase clinical trial for

recurrent, SHH subgroup MB.[3ct]

2.3.5 AKT and PI3K (Section Contributed by Kiran Parwani)

AKT, or protein kinase B (**PKB**), is a member of the AGC serine/threonine kinase family that plays major roles in cellular growth, survival, and DNA repair.[102,103] Receptor tyrosine kinases (**RTKs**) such as PDGFR, VEGFR, and IGF-1R are some of the primary drivers of AKT phosphorylation in tumors, including MB, typically due to the amplification of the receptors or ligands, or the presence of an autocrine feedback loops.[104,105,106,107,108] Overexpression or following ligand binding to these receptors leads to dimerization, autophosphorylation, and activation of phosphoinositide 3-kinase (**PI3K**) which is recruited to the receptor and activated.[109] PI3K then catalyzes the conversion of PIP2 to PIP3, recruiting AKT via its pleckstrin homology domain to be phosphorylated by PDK1, on Thr308, and mTORC2, on Ser473 (**Figure 3**).[110,111] Dual phosphorylation at these marks is a requirement for full activation of AKT, leading to downstream activation of mTORC1 and modulation of cell growth and proliferation.[112]

In the context of DNA damage, ATM, ATR, and DNA-PKs can all phosphorylate and activate AKT even in the absence of upstream RTK activation; and while the mechanism through which ATM and ATR activate AKT is unclear, DNA-PKs can directly phosphorylate AKT at serine 473.[113] Additionally, PARP indirectly releases AKT from SIRT1 inhibition and accumulates adenosine monophosphate (**AMP**) driving AMP-activated protein kinase (**AMPK**) mediated activation of AKT. AKT can also modulate DDR through feedback mechanisms involving DNA damage signaling sensors and effectors.[113] Activated AKT increases *cMYC* transcription and inhibits the cyclin-dependent kinase inhibitor $p21^{Cip1}$, a target of p53, both of which promote cell cycle progression.[114,115] Additionally, AKT suppresses ATR/Chk1 signaling and subsequent HR,

yet AKT can be activated in an ATM/ATR-dependent manner and repair DSBs through DNA-PKcs mediated NHEJ. As many DNA damaging agents target dividing cells,[116] it is important to highlight that potential resistance to these agents can occur often due to AKT driven NHEJ.[117] p-AKT accumulates in irradiated lung carcinoma and prostate cancer cells and activates DNA-PKs to induce NHEJ.[118] Conversely, AKT inhibits HR by mediating BRCA1 and RAD51 cytoplasmic retention.[119] Active AKT phosphorylates Bad, Bax, and Bcl-2, inhibiting apoptosis and promoting cell survival.[120] Together, these signaling roles drive a pro-repair, pro-survival phenotype that could be exploited therapeutically.

Many of these AKT signaling phenotypes are conserved in the setting of medulloblastoma, including both pro-survival and growth and the DNA damage response. In the CGNP developmental model of SHH MB, SHH signaling drives expression of insulin growth factor (**IGF**), resulting in an autocrine feedback loop between IGF and IGF1R to promote CGNP

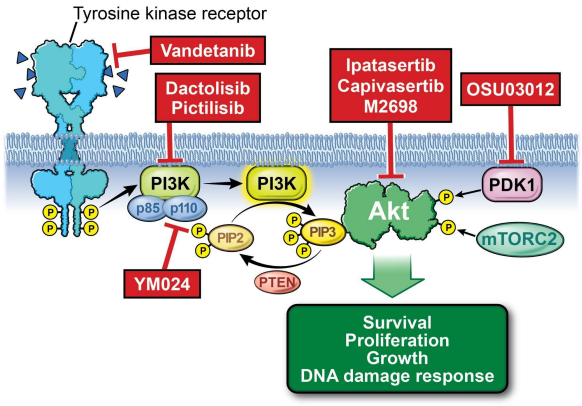

Figure 2: The role of AKT in DNA damage A) Canonical AKT signaling begins with the activation of a receptor tyrosine kinase (e.g., VEGFR, EGFR, or IGFR). Receptor activation, by binding of a ligand, dimerization, and autophosphorylation, causes binding and activation of p85 and p110, the respective regulatory and catalytic subunits of PI3K. Activated PI3K will go on to catalyze the conversion of PIP2 to PIP3, a process which can be reversed by the tumor suppressor PTEN. If PIP3 is formed, it will recruit AKT to

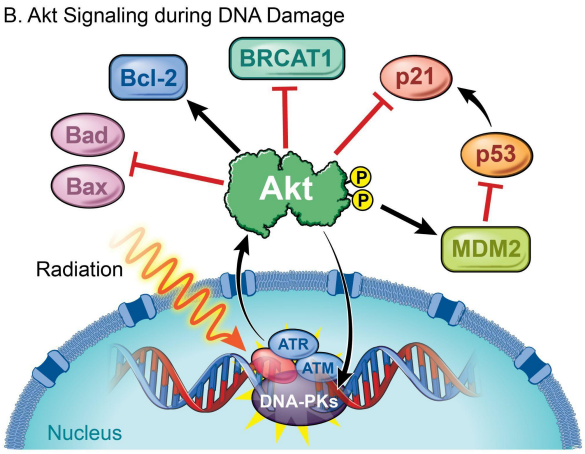

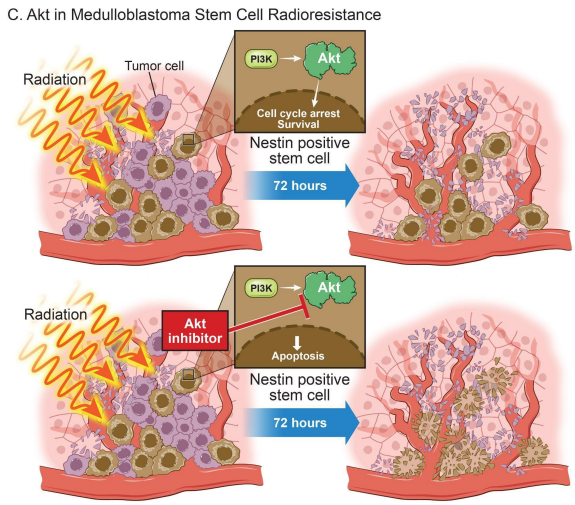

the membrane at which point AKT will be phosphorylated by PDK1 and mTORC2. This dual phosphorylation fully activates AKT, allowing it to affect several downstream processes such as cell survival, proliferation, growth, and the DNA damage response. B) Following exposure to radiation , repair proteins (e.g. ATM, ATR, DNA-PKs) are recruited to the damaged site to facilitate repair. The activation and recruitment of these proteins correlates with an increase in phosphorylated AKT. p-AKT then inhibits apoptosis through Bad and Bax inhibition and Bcl-2 activation. p-AKT will also inhibit the downstream target of p53, p21, to inhibit cell cycle arrest. A feedback loop exists in that AKT can also phosphorylate and activate these proteins to aid in DNA repair. AKT facilitates NHEJ by phosphorylating DNA-PKs and inhibits HR by promoting cytoplasmic localization of BRCA1 and Rad51. C) Irradiation decreases the population of tumor cells at the perivascular niche with the exception of stem cells which are largely radioresistant. Nestin-positive stem cells in the perivascular niche treated with radiation activate the PI3K/AKT pathway to undergo cell cycle arrest and re-enter the cycle 72 hours later, driving MB survival and recurrence. AKT inhibition prior to irradiation abrogates perivascular stem cell radiation resistance, leading to apoptosis of these cells.

proliferation, supporting a role for AKT as a developmental protein.[121] Additionally, irradiated P1 and P10 mice harbor increased p-AKT in non-irradiated and irradiated cerebella at P1 compared to P10.[122] There is also interplay between p53 levels and p-AKT activity in that P10 cerebella are more resistant to MB formation and sensitive to radiation-induced cell death due to an increase in p53 expression and lower p-AKT activity. Furthermore, AKT constitutes a source of resistance to smoothened inhibitors and is strongly associated with poor outcomes.[123] Indeed, smoothened

receptor inhibition alongside PI3K through Vismodegib and Dactolisib, respectively, synergizes to decrease cell viability in both SHH and Group 3 cell models.[124] From the same study, combination of cisplatin and Dactolisib, but not Vismodegib, results in significant decrease in viability compared to single agent supporting a role for the PI3K/AKT signaling axis in post-DNA damage survival. Inhibition of the upstream AKT kinase, PDK1, with OSU03012 results in a decrease in p-AKT S473 and a sensitization to both doxorubicin and cyclophosphamide but not temozolomide in Group 3 models.[125] Subsequently, it was found that many MB cells and patient samples overexpress the oncogenic PI3K catalytic subunit p110α isoform responsible for phosphatidylinositol phosphorylation. YM024-mediated inhibition of the p110α subunit abrogates doxorubicin-induced AKT phosphorylation at S473, sensitizing cells to doxorubicin.[126] Inhibition of AKT phosphorylation by targeting upstream RTKs can also sensitize MB to DNA damage. Treatment of SHH-*TP53*-mutated MB and MYC-amplified MB cells with Vandetanib, a multi-kinase inhibitor targeting RET, VEGFR2, and EGFR, reduces cell migration and cell viability.[127] When combined with Pictilisib, a PI3K-inhibitor, AKT phosphorylation and protein levels are decreased compared to monotherapy. Following combination, cells are sensitized to etoposide, a chemotherapy which binds and forms a ternary complex between topoisomerase II and DNA. Thus, targeting AKT directly or indirectly would not only decrease tumor growth but will also sensitize cells to DNA damage.

There is also a role for AKT in mediating post-radiation survival of cancer stem cells residing in the perivascular niche (**PVN**), the putative cells of recurrence for many brain tumors.[128] Following radiation, AKT is phosphorylated and activated in nestin-positive mouse MB stem cells.[129] The PI3K/AKT/mTOR axis also regulates hypoxia-inducible factor 1-alpha (**HIF-1α**) mediated expression of VEGF, leading to the vascularization of the tumor, supporting a role for AKT in the

development and maintenance of the PVN stem cell niche.[130] These findings are further supported by Hambardzumyan et al. who demonstrated that radiation-treated PVN resident nestin-positive stem cells activate the PI3K/AKT pathway, undergo cell cycle arrest, and re-enter cell cycle 72 hours later.[131] Furthermore, inhibiting AKT prior to irradiation sensitizes cells in this niche to treatment, demonstrating that these cells' inherent radiation resistance can be partially overcome through AKT inhibition.

AKT signaling is vital in cell cycling and proliferation which drive tumorigenesis. These processes render cells resistant to DNA damaging agents by the additional upregulation of DNA damage repair proteins which can result in a feedback loop that activates AKT. Previous studies have clearly demonstrated that inhibiting AKT sensitizes MB to DNA damage *in vitro*, making AKT a compelling target *in vivo* that has the potential to be combined with irradiation and chemotherapy. The challenge in AKT targeting lies in ensuring that inhibitors are potent enough to overcome the activation of upstream proteins, such as the receptor tyrosine kinases that activate AKT. Currently, there are several AKT inhibitors in clinical trials as both monotherapy and combination therapy for other solid tumors. Ipatasertib and Capivasertib treatments result in an increase in progression free survival in patients harboring solid tumors such as breast and ovarian cancers.[132] However, despite these treatment options, minor toxicities such as hyperglycemia and skin rash still occurred with nausea and fatigue presented when AKT inhibition was combined with chemotherapy.[133] M2698 is a BBB penetrant, ATP-competitive inhibitor of AKT1/3 and p70S6K, a downstream target of AKT, that exhibits significant growth arrest in many solid tumor cell lines. M2698 treated mice orthotopically-implanted with GBM cells exhibit increased survival and reduced brain tumor burden.[134] Samotolisib, a PI3K isoform inhibitor, is currently in phase 2 clinical trials for patients with relapsed or refractory advanced solid tumors, including medulloblastoma.[4ct]

2.4 p53

p53 expression and mutation status emerged in the early 1990s as a biomarker for poor therapeutic response and shorter overall survival in MB due to the role of p53 in DNA repair and cell fate following genomic insult (**Table 1**).[135–137]

In the absence of external cell stressors, p53 is degraded to prevent cell cycle inhibition or inappropriate apoptotic induction; thus, any dysregulation of the p53 pathway resulting from mutations in *TP53* or alterations to proteins responsible for p53 degradation, namely WIP1 and MDM2, is made apparent by atypical alterations to p53 levels.[138–140] While *TP53* mutations are infrequent in MB, occurring in approximately 10%-15% of patients, p53 status and the potential for p53 therapeutics even outside of *TP53* mutant patients remain important considerations.[7,141–143] When activated downstream of ATM-Chk2 and ATR-Chk1 following DNA damage, p53 signals through BAX, NOVA, and PUMA to initiate cell death and p21 to inhibit cell cycling, bringing about a potential therapeutic window and an explanation as to why *TP53* mutant patients have a substantially worse prognosis (**Figure 4**).[144]

2.4.1 p53 status as a predictor of Chk1 and PARP inhibition

Given the emergence of DDR specific therapeutics and the role of p53 in mediating cell death and cell cycle checkpoint activation, *TP53* mutation status should be considered as a potential predictor for patient response to inhibition of the previously discussed DDR proteins. While *TP53* wild type CGNPs and mutant Daoy cells demonstrate Chk1 signaling axis requirements, Daoy cells may no longer represent MB patients and targeting Chk1 in novel SHH PDX models shows no survival

Table 1: p53 mutation status and effect on medulloblastoma patient survival				
Subgroup	Wt p53 Percent	Mut p53 Percent	Wt p53 5-Year OS	Mut p53 5-Year OS
SHH	211 Patients* 83.0%	43 Patients* 16.9%	76% ± 4%*	41% ± 17%*
WNT	83 Patients* 82.2%	18 Patients* 17.8%	94% ± 5%*	86% ± 13%*
Group 3	72 Patients* 100%	0 Patients* 0%	Avg 54.6%**	
Group 4	121 Patients* 99%	1 Patient* 1%	Avg 75.0%**	

*161 Zhukova N, Ramaswamy V, Remke M, et al. Subgroup-specific prognostic implications of TP53 mutation in medulloblastoma. *J Clin Oncol*. 2013;31(23):2927-2935.
**162 Ray S, Chaturvedi NK, Bhakat KK, Rizzino A, Mahapatra S. Subgroup-Specific Diagnostic, Prognostic, and Predictive Markers Influencing Pediatric Medulloblastoma Treatment. *Diagnostics (Basel)*. 2021;12(1). doi:10.3390/diagnostics12010061

Table 1: p53 mutation status and effect on medulloblastoma patient survival

p53 mutant SHH patients respond poorly compared to p53 WT SHH while p53 mutant WNT patients do not show a drastically worse response compared to p53 WT WNT patients. Group3 and 4 patients rarely present with p53 mutations.[161] p53 mutations and MYC amplification are present at higher frequencies at relapse and impact patient outcome for all subgroups (not shown).[7]

advantage, regardless of p53 status.[42,47,54,55,145] However, Group 3 PDX models, both *TP53* wildtype, D283, TKMB870, and SU-MB002, and *TP53* mutant cells, D425, in addition to a MYC amplified p53 dominant negative syngeneic mouse model, respond to Chk1 inhibition.[55] These data suggest that p53 status is not a predictor of Chk1 response in the setting of Group 3 MB, which is supported by findings in other cancers.[146] However, a requirement for p53 functionality in PARP inhibitor mediated cell death in MB is less clear. p53 mediated apoptosis in *PTCH*$^{+/-}$

model following PARP ablation suggests that p53 is required for apoptotic induction in the absence of PARP.[62] Additionally, the Group 3 models tested for combination of olaparib and radiation, D283 and D556, are *TP53* wild type; and while UW228 is *TP53* mutant and responsive to olaparib and radiation, it may no longer be representative of SHH MB.[63,145] However, when testing combinations of PARP inhibitor and temozolomide in D425 and D384, both Group 3 models, p53 status does not predict PARP inhibitor response, and in fact D425, a *TP53* mutant model, tumor growth inhibition is greater compared to D384 and D283 from the same study.[75] Thus, p53 may be required for therapeutic response following PARPi combined with radiation whereas for PARPi plus temozolomide, p53 may not be required.

2.4.2 p53 and Medulloblastoma Development

p53 plays a significant role in mediating cellular response to radiation and chemotherapy, including induction of apoptosis through BCL-2 and BCL-XL inhibition and transcriptional activation of BAX, NOXA, and PUMA and regulation of G1 and G2 cell cycle checkpoints through numerous targets including p21 and 14-3-3-σ.[147,148] The dysregulation of p53 signaling pathway components introduces mechanisms of therapeutic resistance to standard of care therapy, and, potentially, any of the aforementioned DDR therapeutics. The importance of p53 for apoptosis of pre-neoplastic cerebellum is made apparent through developmental SHH MB modeling where inactivation of p53 alongside other tumor suppressors predisposes to MB development. The absence of p53 and the G1 restriction point protein Rb in CGNPs of the external granular layer leads to induction of MB via unabated cell cycling.[61] The genomic instability resulting from ablation of these tumor suppressors drives MB development through the amplification of *MYCN* and *PTCH2*, an isoform of the frequently mutated *PTCH1* of SHH MB possessing smoothened

inhibitory features.[149,150] Furthermore, in the absence of *PTCH1*, Rb inhibition mediated through ablation of *CDKN2C* (Ink4c or p18), an inhibitor of proteins responsible for Rb inhibition (CDK4, CDK6, and CyclinD1), leads to the formation of MB even in the presence of wild type *TP53*.[151]

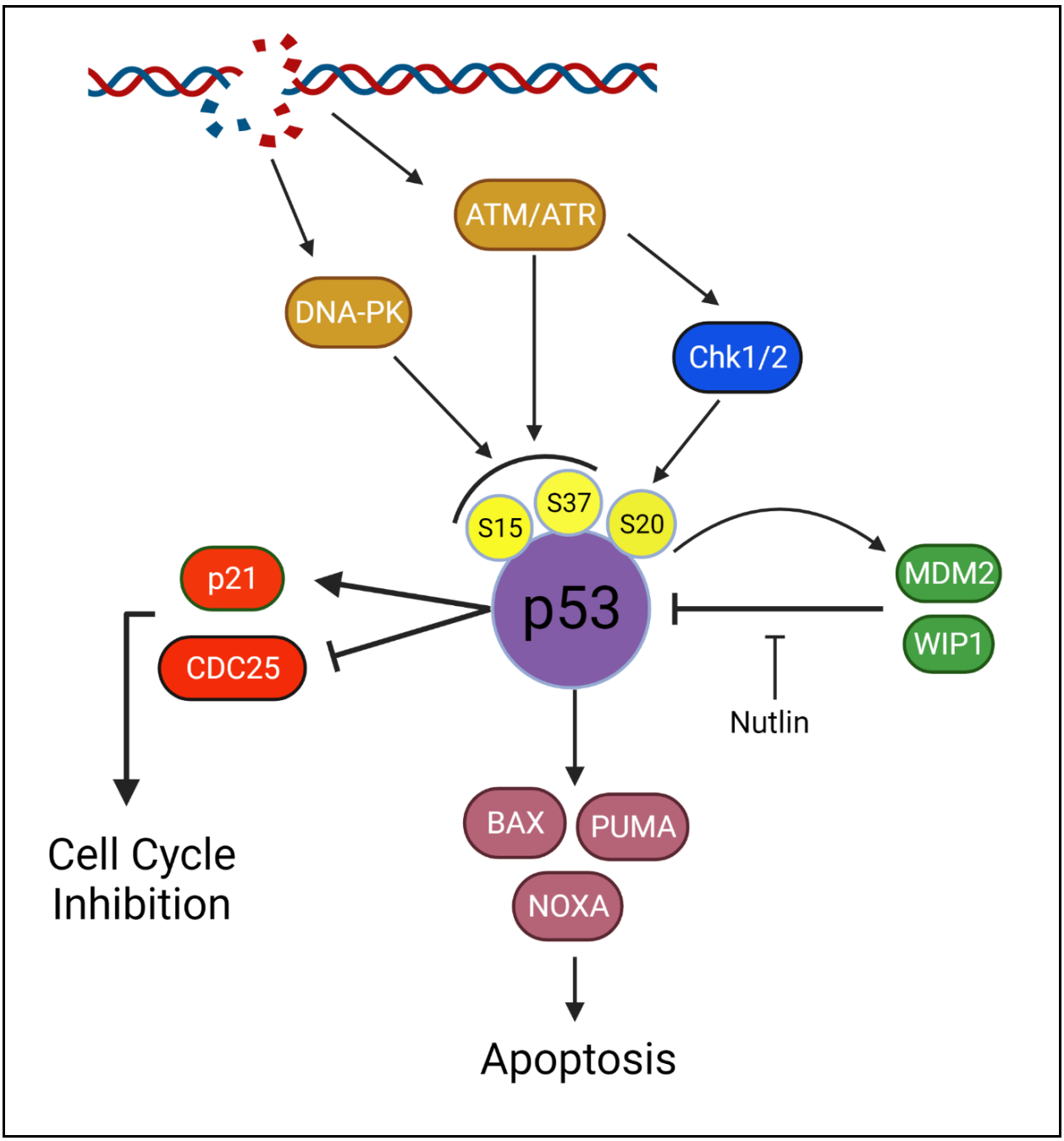

Figure 3: Activation of p53 following DNA damage

P53 is a downstream effector following double strand DNA breaks and plays a crucial role in tumorigenesis. Following Damage detection by ATM/ATR or activation of DNA-PKcs, p53 is phosphorylated at Ser15 or Ser37. ATM and ATR will also activate Chk1 and 2 resulting in phosphorylation of p53 at Ser20. Together these phospho-sites inhibit p53 degradation by preventing MDM2 binding and facilitate p53 tetramerization, a crucial step in p53 activation. P53 will activate p21 and inhibit CDC25 A,B, and C to activate the cell cycle checkpoint and inhibit cycling. P53 will also transcriptionally upregulate pro-death proteins, BAX, PUMA, and NOXA. Upon overcoming inhibition by BCL-2 family apoptotic inhibitors (not shown), BAX, PUMA, and NOXA will activate apoptosis. Inhibition of the MDM2-p53 interaction with nutlin allows for p53 accumulation and apoptosis, ideally in cells heavily reliant on p53 suppression for survival.

These data provide a mechanism by which loss of p53 or restriction point inactivation in combination with SHH mitogenic signaling would lead to unabated cell cycling and tumor development. Overall, in the absence of restriction point and cell cycle checkpoint safeguards, the effects of DNA damage are exacerbated as the cell cannot appropriately respond to damage.

More direct evidence for the importance of intact DDR for MB suppression follows from p53 and DDR protein ablation studies. Mice deficient for KU80 or DNA Ligase IV, proteins required for NHEJ mediated DSB repair, in a *TP53* null background, accelerates MB formation leading to shorter overall survival.[152,153] Tumorigenesis is also achieved through combined loss of p53 and other DDR pathways, including HR and BER. The absence of XRCC2, which forms a complex

with Rad51 paralogs to prepare DNA filaments for HR repair, results in embryonic lethality that is rescued by *TP53* ablation, driving MB formation.[154,155] Furthermore, requirements for BER and SSB repair, pathways crucial for cisplatin adduct resolution, is made evident again by the simultaneous ablation of *TP53* and DNA Polymerase β or XRCC1.[156] *POLB*$^{-/-}$;*TP53*$^{-/-}$ and *XRCC1*$^{-/-}$;*TP53*$^{-/-}$ mice overexpress MYCN and CDK6 and develop aggressive classical MBs resembling the SHHα subtype. The absence of genomic guardians in CGNPs amplifies their tumorigenic potential and further delineates a requirement for intact DNA damage signaling in the developing cerebellum. p53 loss is required for MB development when DNA repair mechanisms are no longer present. Where DNA damaging reagents are utilized for pediatric MB patients with defective p53, DDR signaling pathways cannot activate p53 mediated apoptosis or senescence, creating potential opportunities for therapeutic resistance.

2.4.3 Targeting the p53 response

While the p53 inactivating mutations are the most apparent method for p53 pathway dysregulation, alterations to p53 regulators or signaling effectors are also described in MB and can be therapeutically harnessed for p53 signaling modulation when combined with DNA damaging reagents. MDM2, or Double Minute 2, is an E3 ubiquitin ligase responsible for the degradation of p53 in the absence of cell stress; thus, MDM2 dysregulation may lead to inappropriate p53 degradation, resulting in cell cycle checkpoint abrogation or apoptotic resistance. And while MDM2 is only amplified in a small percentage of adult MB, manipulation of p53 levels through MDM2 inhibition could be viable in patients without MDM2 overexpression and enhance the effects of DNA damage therapies.[157,143] MDM2 ablation from the *PTCH*$^{+/-}$ model results in p53 accumulation, decreased CGNP expansion, and aberrant cerebellar foliation.[158] It follows from this

reasoning that disrupting the interaction between MDM2 and p53 could enhance p53 mediated apoptosis and cell cycle inhibition, made possible by MDM2 inhibitors such as nutlin.[159] MDM2 inhibition by nutlin in *TP53* wild type MB cells, HDMB03, ON2-76, D341, and D283, results in the accumulation of p53, p21, and sub G1 population size; however, *TP53* mutant cells, Daoy and UW228, are unaffected.[160] Additionally, when combined with a DNA intercalating agent, doxorubicin, nutlin further enhances the apoptotic and cell cycle inhibitory activity of p53.[161]

The interaction between MDM2 and p53 can also be modulated by other proteins, including BAI1, I2PP2A, and WIP1. BAI1, or Brain-specific angiogenesis inhibitor 1, inhibits angiogenesis and upregulates p53 activity through MDM2 inhibition.[162,163] Therein, *ADGRB1* (BAI1) ablation in the $PTCH^{+/-}$ model results in substantial decreases in p53 and p21, and an approximately 50% increase in MB tumor formation. Furthermore, epigenetic reactivation of BAI1 through KCC-07, a MBD2 (Methyl-CpG-binding domain protein 2) inhibitor, potentiates the activity of p53 and cell cycle inhibition, bestowing a survival advantage in mice harboring D556 xenograft tumors.[163] BAI1 epigenetic reactivation can also be achieved by inhibiting EZH2, an epigenetic transcriptional repressor responsible for H3K27 methylation.[164] Application of the EZH2 inhibitor, tazemetostat, yields a mild survival advantage in *TP53* wild type MB xenograft models. Another MDM2 antagonist, I2PP2A or Phosphatase 2A Inhibitor 2 also known as SET, inhibits PP2A which dephosphorylates MDM2, rendering it incapable of degrading p53. The application of COG112 in primary SmoA1 SHH MB mouse cells inhibits I2PP2A, allowing PP2A to dephosphorylate MDM2, resulting in accumulation of p53, p21, and a decrease in cell viability of *TP53* wild type ONS-76 cells.[165] Synergism between radiation or chemotherapy and I2PP2A or EZH2 inhibition remains to be determined.

A final protein of interest, WIP1/PPMD1 or wild-type p53-induced phosphatase 2, is a serine/threonine phosphatase belonging to the PP2C family, which can positively regulate p53 degradation.[166,167] WIP1 is capable of dephosphorylating p53 at Ser15 (facilitating MDM2 binding), direct upregulation of MDM2 activity, and contributing to DDR termination through pATM and γH2AX dephosphorylation. Thus, targeting WIP could amplify the ATM-Chk2 signaling axis, augmenting DNA damage recognition and p53 activation, and potentially sensitizing to DNA damaging reagents. WIP1 is overexpressed in a considerable population of MB cell lines and patient tumors as a result of chromosome 17q copy number gains, present in ~46% of patients sampled.[168] And while the overexpression of WIP1 mildly abrogates accumulation of p53Ser15 phosphorylation following UV exposure and increases the expression of p21 in MB, and knockdown sensitizes to ionizing radiation in Diffuse Intrinsic Pontine Glioma (*DIPG*), the level of sensitization achievable in MB is not clear.[169] Secondarily, similar to the pleiotropic nature of CK2, WIP1 is known to influence not only DDR, but also proliferation and invasiveness. Utilizing the RCAS nestin-tva mouse model, when co-infected with transgenes overexpressing SHH ligand and WIP1, 34% of mice develop spontaneous tumors compared to 8% of mice with SHH overexpression.[170] Importantly, WIP1 overexpression alone was not sufficient to induce spontaneous tumor formation. WIP1 overexpression also drives expression of SHH signaling targets, Gli1 and Ptch1, and enhances proliferation in CGNPs independent of p53 inhibition.[171] Finally, in both smoothened-overexpressing and *PTCH*$^{+/-}$ MB models, *PPM1D* knockout dramatically suppressed *de novo* tumor formation. Thus, targeting WIP1 could not only reduce proliferative and tumorigenic phenotypes, but also sensitize to MB DNA damaging therapies.

Historically, MB patients harboring *TP53* mutations have had a substantially worse prognosis than

their WT counterparts likely due to ineffective apoptotic signaling following standard of care therapies. And while the vast majority of cancer therapies focus on inhibiting genes mediating resistance, the activation of tumor suppressors is beginning to emerge as a potential alternative. Inhibition of MDM2 oncogenes as a way to reactivate p53 is being tested in clinical trials for hematologic and solid tumors.[5ct] Results for preclinical research for p53 activation through MDM2 and WIP1 inhibition is mixed, however, and the efficacy of these inhibitors in patients is to be determined. Secondarily, for patients with *TP53* mutations, MDM2 and WIP1 inhibition will likely have no effect because mutant p53 is dominant negative over any endogenous WT p53. Over the last two decades researchers have turned to gene therapy as a way to reintroduce p53 through recombinant viruses, a more relevant approach for *TP53* mutant tumors.[6,7ct] This localized method to protein expression may not carry the same systemic issues as administering an MDM2 or WIP1 inhibitor, however, gene therapy is challenging and carries potentially dangerous side effects for constructs capable of mutating into self-replicating viruses. Presumably, given the role of a p53 virus would be to transiently express p53, this rids the potential for inappropriate genomic integration and cellular transformation. Thus, given the rapidly developing landscape of gene therapy, WT p53 expression could develop into a viable therapeutic option.

2.5 Conclusions

Given the lack of success with molecular therapy in medulloblastoma and the only recently emerging impact of molecular subgrouping on patient treatment, DNA damaging therapeutics will remain the backbone therapy in MB patients for the foreseeable future. DNA damage proteins are highly conserved in their response to genotoxic therapies across patients; however, the responsiveness may be contingent upon numerous factors, including underlying genomic

instability driven by MYC amplification, or the presence of secondary mutations or tumor suppressor inhibition such as *TP53* loss or mutation. These factors may drive apoptotic resistance and potentially advantageous mutagenesis. Alternatively, variations to proteins playing either a direct or indirect role in the DDR, such as increased Chk1 expression, elevated APE1 activity, or phosphorylation of AKT, can prime tumors for responsiveness to DNA damage. Together, these alterations may lead to the clonal evolution of therapeutically resistant cells from a once minority cell population such as those of the perivascular niche, ultimately resulting in patient relapse. The targeting of DDR proteins is broadly applicable even outside of a synthetically lethal context, such as with PARP dependence in *BRCA1/2* mutation positive cancers, and numerous inhibitors against PARP1, ATR, Chk1, and MDM2 are being tested in combination with standard of care radiation and chemotherapy in the setting of medulloblastoma and beyond.[172–174]

Chapter 3

Y-Box Binding Protein 1: a Pleiotropic Oncogene

3.1 Abstract

Y-box binding protein 1 (YB1) is a diverse oncogene implicated in a variety of cellular processes stemming largely from the cold shock domain responsible for nucleic acid binding. The regulation of YB1 is complex and consists not only of protein synthesis and stability, but also post-translational modifications affecting differences in the cleavage, nuclear translocation, and nucleic acid or protein interactions. The roles for YB1 in fetal development can be hijacked by cancer cells to drive proliferation, migration and metastasis, and therapeutic resistance to not only radiation and chemotherapy standards of care, but also small molecule inhibitors for many proteins. These characteristics make YB1 an interesting and promising therapeutic target.

3.2 Structure and Regulation of YB1

Since the discovery and characterization of YB1 in 1988 from Didier et al. as a protein capable of binding and inhibiting the transcription of MHC II through a Y-box (CCAATT) in the promoter, hundreds of papers have been published not only on the role of YB1 in fetal development, but also as a major oncogene across numerous cancers (**Figure 1 and 2**).[175] The early publication history on YB1 as a DNA damage response protein, a transcription factor for cyclins, and as a suppressor of apoptosis in the early 2000s paved the way for a body of literature on the numerous developmental and oncogenic roles of YB1. And while the effects of YB1 phenotypically are of great significance, the regulation of YB1 protein takes many forms and influences the diverse phenotypes YB1 mediates.

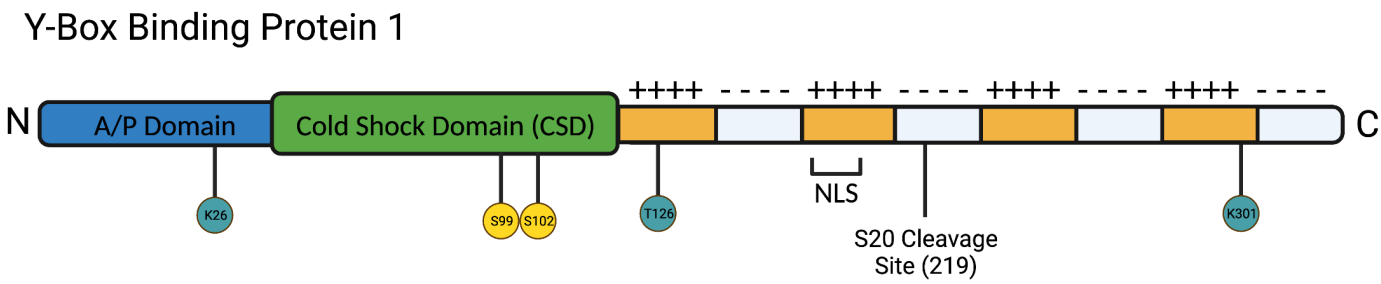

Figure 1: Structure of Y-Box binding protein 1

YB1 Cold Shock Domain (CSD) is crucial for DNA and RNA binding. Sumoylation of lysine 26 is implicated in YB1 DNA damage response, serine 99 phosphorylation regulates RNA binding, serine 102 phosphorylation regulates nuclear functionality, O-linked-N-acetylglucosaminylation at threonine 126 regulates transcriptional activity, and lysine 301 is important for extracellular secretion.

YB1 can be subjected to many post-translational modifications; however, one of the more highly studied and debated of these includes serine residue phosphorylation. Serine 102 was found to be

phosphorylated by AKT1 in breast cancer cells through direct binding to facilitate anchorage-independent growth by the Dunn group.[176] Given AKT proteins are phosphorylated and activated in response to receptor tyrosine kinases (RTK) such as IGFR, EGFR, PDGFR, and VEGFR, which are widely active and dysregulated in cancer, the group hypothesized that a HER2 → AKT1 → pYB1S102 axis would provide anoikis resistance to facilitate a lymphatic or hematogenous route for metastasis. Indeed, phospho-null mutations at S102 (S102A) abrogated anchorage independent growth. Shortly thereafter, the Sorensen group found AKT to phosphorylate YB1, resulting in a release of YB1 inhibition on the 5' cap of mRNAs to allow for translation,[177] a phenotype conserved following phosphorylation of serine 99.[178] Given AKT functions as a downstream signaling effector of many receptors, it stands to reason that other groups observe a decrease in YB1 phosphorylation following inhibition or depletion of other RTKs or their signaling effectors such ERK1/2 and p90RSK. In cell free reactions containing ERK1/2 and YB1, ERK1/2 can phosphorylate YB1 at S102 resulting in greater gel shift when incubated with DNA containing hypoxia response elements (HRE) such as those found in the VEGF promoter, suggesting YB1 phosphorylation enhances promoter binding.[179] The Dunn group then established that Ribosomal S6 Kinase (p90 RSK) downstream of the Ras/Raf/MEK/ERK1/2 axis can also phosphorylate YB1 at S102.[180] Pharmacologic inhibition or protein depletion of RSK resulted in a reduction of S102 phosphorylation without changes in YB1 protein levels leading to a reduction in EGFR transcription and decreases in ERK1/2 phosphorylation. This would indicate not only transcriptional effects but also a positive feedback loop between YB1 and ERK1/2 to prolong pathway activation. From the two previous studies, phosphorylation appears to facilitate YB1 binding to HREs or the EGFR promoter to promote transcription; however, the effect of S102 phosphorylation on nuclear translocation was unclear. Unfortunately, it remains this way as

different groups publish differential requirements of S102 phosphorylation for nuclear entry. For example, in 2016 Miao et al. showed an increase in the percent phosphorylation of YB1 S102 following plating of cells on fibronectin coated plates; however,

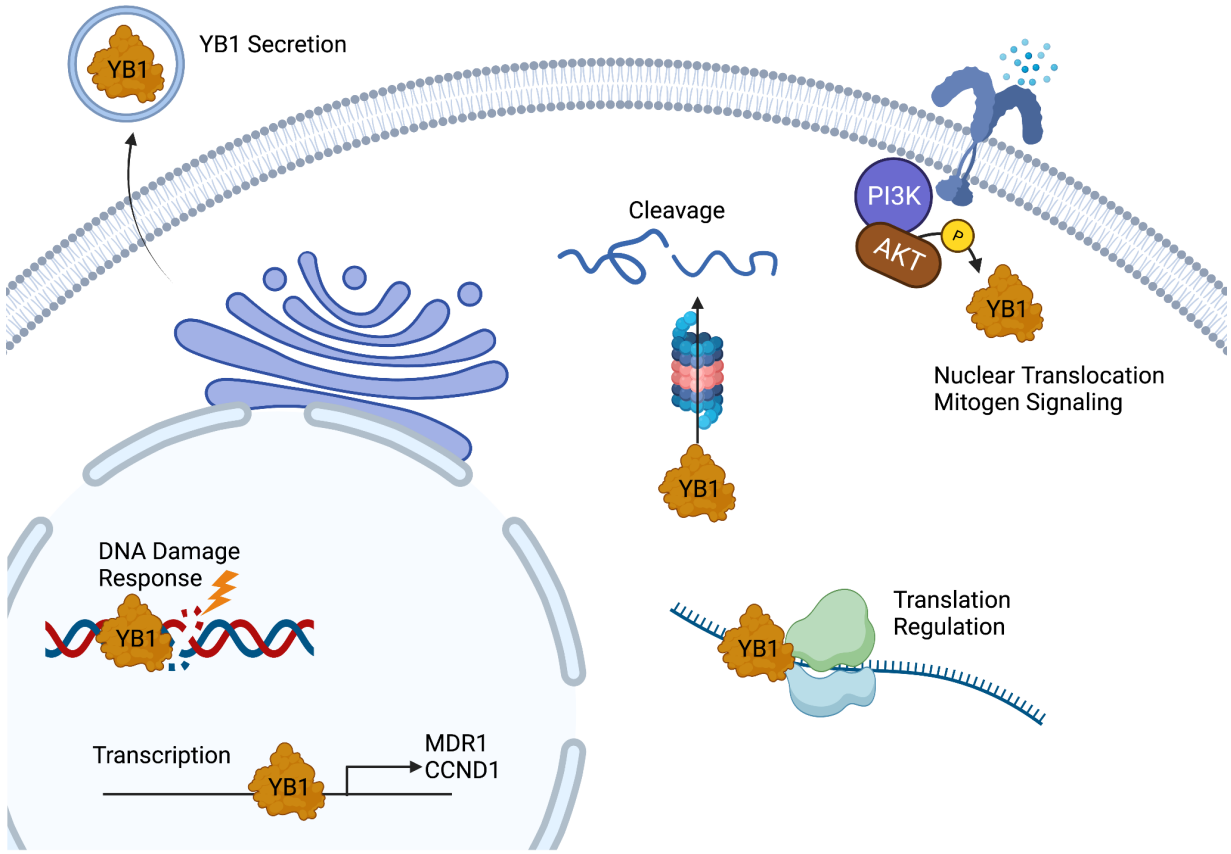

Figure 2: The many functions of YB1. YB1 can regulate translation or transcription through its Cold-Shock domain. Cleavage of YB1 can alter nuclear localization. YB1 can be phosphorylated by AKT or ERK to promote nuclear translocation and is associated with mitosis. YB1 binds to damaged DNA and promotes repair. YB1 can be secreted as an extracellular mitogen to promote proliferation and migration.

this was not followed by a dramatic increase in the nuclear compartment of total YB1. This data would be suggestive of a more nuclear mechanism for YB1 phosphorylation as opposed to phosphorylation being a prerequisite for nuclear translocation.[181] In agreement with these findings, 2 years later another group proposed a mechanism by which RSK translocates to the nucleus to phosphorylate nuclear YB1, indicating nuclear shuttling prior to phosphorylation.[182] On the other hand, some groups have proposed the requirement of S102 phosphorylation for nuclear entry, primarily relying on S102A or S102D phospho-null or phospho-mimetic site directed mutants of YB1, respectively. While these studies do show strict cytoplasmic localization of phospho-null mutants and cytoplasmic and nuclear distribution of phospho-mimetics in immunofluorescence data, western blotting data from the same studies may contradict this whereby cell stimulation without the addition of ectopic YB1 does not result in alterations to YB1 cytoplasmic/nuclear distribution.[183] Overall, while YB1 can be phosphorylated to promote DNA or RNA binding, the effect of YB1 phosphorylation on nuclear shuttling remains unclear, though it would seem phosphorylation of endogenous YB1 is likely not a requirement for nuclear shuttling.

While phosphorylation is the predominant post-translational modification studied for YB1, there are several other modifications published to regulate YB1 protein stability or functionality, including Acetylation, PARylation, Sumoylation, and O-linked- N-acetylglucosaminylation (O-GlcNAcylation). Acetylation of YB1, for example, affects YB1's ability to bind and regulate the translation of mRNAs such as HIF1α. Following HDAC1/3 inhibition under hypoxic conditions, YB1 loses the ability to bind and promote translation of HIF1α due to a lack of de-acetylation.[184] Alternatively, the addition of O-GlcNAcylation at threonine 126 improves promoter binding and transcriptional activation of target genes as measured through luciferase reporter, similar to the

effects of S102 phosphorylation.[185] Interestingly, O-GlcNAcylation can promote cerebellar development and SHH MB tumor initiation through the SHH pathway, indicating a potential YB1 PTM crucial for its functionality in cerebellar and tumor development, especially given our groups previous publications.[186] Additionally, some groups have placed emphasis on the PARylation of YB1 by PARP1 as a bi-product of YB1 involvement in the DNA damage response. In a cell free reaction, the YB1 c-terminal domain interacts with PARP1, resulting not only in improved binding between DNA and PARP1, but also the PARylation of YB1 by PARP1.[187,188] Unfortunately, the effect of PARylation on YB1 functionality was not clear given the nature of cell free reactions. Finally, some groups have shown interactions between YB1 and RNA to affect the stability of YB1 protein. For example, depletion of MIR22HG through siRNA results in a decrease in YB1 protein that is rescued by MG132 inhibition of proteasomal degradation but not by cycloheximide inhibition of translation.[189] YB1 stabilization by micro-RNAs is corroborated by numerous published studies and now represents a major mechanism for YB1 protein stabilization in the cell. And while the aforementioned post-translational modifications or micro-RNA binding affect the stability or functionality of YB1, regulation of transcription and translation still play a major role in the dynamic regulation of YB1 in development and in cancer.

Regulation of YB1 protein takes the form of both transcription factor mediated mRNA production or tight regulation of YB1 translation through 5'cap or 3'UTR protein binding to either promote or inhibit translation. In fact, much of the YB1 RNA in the cell is stored in ribonucleoprotein granules (or simply RNPs), allowing for rapid changes in translation. The Ovchinnikov group, who've published extensively on the biochemical properties of YB1, initially demonstrated an inhibitory feedback loop whereby YB1 binds its own mRNA to inhibit translation.[190,191] In fact,

YB1 commonly serves as a positive control for RIPseq including in our own research (Chapter 6). Poly-A-binding protein (PABP) can then bind and displace YB1 from the 3'UTR of its own mRNA to recruit eukaryotic initiation factor 4 complex (eIF4G) to promote translation of YB1. Stimulation of the mTOR pathway, responsible for mediating cell proliferation and other oncogenic phenotypes, can also promote YB1 translation.[192] For this, researchers ligated a YB1 5'UTR onto a luciferase report to show that luciferase translation is significantly reduced independent of eIF4E following mTOR1/2 inhibition with PP242, suggestive of an mTOR → YB1 translational regulation.[193] Finally, heterogeneous nuclear ribonucleoprotein Q (hnRNP Q) was also shown to bind the 3'UTR to inhibit YB1 translation by displacing PABP.[194] Thus, while a number of proteins, including YB1, can bind and regulate YB1 translation, transcriptional regulation is less characterized.

The few published mechanisms of YB1 transcriptional regulation involve two proteins highly relevant to neurodevelopment and neural tumors: cMyc (*MYC*) and Math2 (*NeuroD6*). cMyc is a major, frequently amplified, oncogene responsible for driving Group3 and 4 Medulloblastoma development and metastasis, resulting in therapeutic resistance and poor overall survival (Chapter 2). Not only is Myc robustly expressed during neuro-development within the medullary hindbrain (**Figure 3**), it is responsible for driving proliferation, sensitizing to apoptosis, and in the case of MB, promoting genomic instability.[195] In experiments with cMyc and non-cMyc expressing cells, Uramoto et al. found that YB1 expression is dramatically enhanced in cMyc and p73 expressing cells when co-transfected with a YB1 promoter expression plasmid containing an intact CACGTG E-box.[196] Interestingly, NeuroD6, a basic Helix-Loop-Helix transcription factor also binds an CAGGTG E-box. Implicated in cortex development and highly expressed in the brain throughout

development (**Figure 3**), NeuroD6 is required for YB1 transcription. In gel mobility shift assays using nuclear extracts, the CAGGTG E-box was required for YB1 promoter binding by Math2 and when supplementing nuclear extracts from 5 day old brains with an excess of a DNA fragment from the YB1 promoter containing an E-box, Math2 is quenched away from the endogenous YB1 promoter resulting in lower YB1 protein.[197] These elegant experiments implicate a Math2 → YB1 axis in neurodevelopment potentially conserved with Myc and a final transcription factor, NeuroD2. NeuroD2 is a CNS developmental transcription factor and has 98% base pair similarity to NeuroD6 in the basic Helix-Loop-Helix motif responsible for DNA binding and transcription initiation.[198,199] NeuroD2 binds a CACCTG E-box, similar to NeuroD6 and cMyc, and is expressed in the medullary hindbrain (**Figure 3).** While no publication has reported a role for NeuroD2 in driving YB1 expression, the similarity of E-box sequences amongst NeuroD2, NeuroD6, and Myc and the demonstrated role for NeuroD6 and Myc in driving YB1 transcription, nominate NeuroD2 as a transcriptional regulator of YB1. Thus, a NeuroD2 → YB1 axis may participate in cerebellar development or medulloblastoma tumor formation given NeuroD2 is required for granule cell survival up to p20 of the postnatal period paired with a known role for YB1 in CGNP proliferation (discussed below).[200,201]

Understanding the myriad of post translational modifications, RNA binding stabilization, and transcriptional regulation of YB1 mRNA or protein in the cell are an important prerequisite to YB1's developmental and oncogenic phenotypes, or the therapeutic manipulation of YB1 functionality or protein levels, to be discussed next.

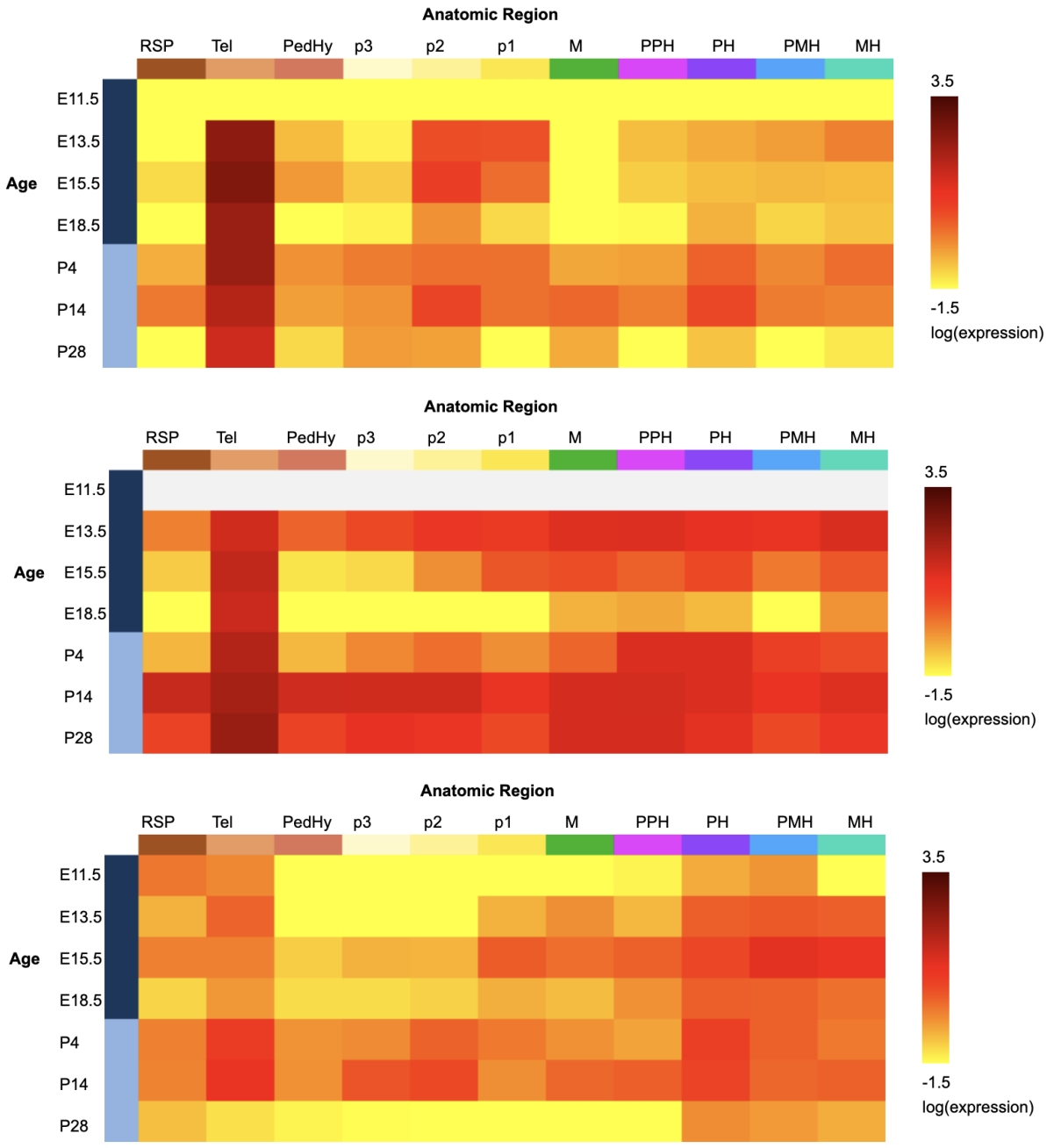

Figure 3: Neuronal Embryonic and Perinatal Expression of NeuroD6 (Top), NeuroD2 (Middle), and cMyc (Bottom)

Heatmaps of embryonal and perinatal transcription factor expression of NeuroD2, crucial for cerebellar development, NeuroD6, implicated in cortex development and the transcription of YB1, and cMyc, implicated in the transcription of YB1.

Abbreviations: CSPall, central subpallium (striatum/pallidum); D, diencephalon; DPall, dorsal pallium (isocortex and entorhinal cortex); F, forebrain; H, hindbrain; M, midbrain; MH, **medullary hindbrain (medulla)**; MPall, medial pallium (hippocampus, taenia tecta, subiculum); NP, neural plate; p1, prosomere 1 (pretectum); p2, prosomere 2 (thalamus); p3, prosomere 3 (prethalamus); PedHy, peduncular hypothalamus; PH, pontine hindbrain (pons proper); PMH, pontomedullary hindbrain; PPH, prepontine hindbrain; RSP, rostral secondary prosencephalon; SP, secondary prosencephalon; SpC, spinal cord; Tel, telencephalic vesicle.

https://developingmouse.brain-map.org

3.3 YB1 in Embryonic and Tumor Development

Developmental signaling frequently presents inappropriately during cancer development, maintenance, or metastasis. Thus, the dynamic phenotypes associated with YB1 could stem from its involvement in embryonic and postnatal neural development. In fact, YB1 is required for embryonic development as exemplified by the lack of viable homozygous null pups when *YB1*-/+ mice are intercrossed.[202] Around E13.5, embryos start becoming non-viable with a large percent surviving until birth at which point they perish shortly thereafter. These fetuses are characterized by embryonic growth retardation, exencephaly, and multi-organ hypoplasia, indicative of a requirement of YB1 for proliferation or migration. And while the group found no global changes

to mRNA or protein in mouse embryonic fibroblasts isolated from these embryos, there were changes to DNA damage susceptibility. At earlier stages of embryonic development, YB1 null E10 embryos exhibit deficiencies in neural tube closure and erythropoiesis of the fetal liver.[203] Proliferation, premature senescence, and F-actin formation are reduced in YB1 null derived mouse embryonic fibroblasts (MEFs). The increased senescence in YB1 null cells was later shown to be a result of YB1 binding and repressing p16 transcription in MEFs following serial passages.[204] While these studies show effects of YB1 deletion on gross embryonic phenotypes, the mechanistic regulation of YB1 is unclear. Once the previously discussed Kobayashi group established that Math2 transcriptionally regulates YB1 in p5 pup brain nuclear lysate, they went on to explore co-expression of YB1 and Math2 in perinatal pup brains. Hippocampal YB1 cytoplasmic staining was correlative to nuclear Math2 staining in terms of immunofluorescence intensity and immuno-blotting. The greatest intensities for Math2 and YB1 were observed at p5 with expression continuing upwards of 4 weeks, but with substantially reduced intensity.[197] These studies reveal not only some global requirements for YB1 in embryonic development, but a more CNS focused signaling role for YB1 in regulating proliferation and neural tube formation. In fact, our group has shown YB1 to be required for CGNP proliferation, extending a requirement for YB1 to cerebellar development that could be regulated by NeuroD2.

The development of tumors is not unlike embryonic development, especially in the case of pediatric tumors. As discussed in chapter 2, genomic instability resulting from Myc amplification and overexpression, for example, is a primary driver of cell transformation and tumor development. A case for YB1 in maintaining genomic stability was made in the previously discussed studies where YB1 deletion results in sensitization to mitomycin c, cisplatin, and

oxidative stress. Following YB1 overexpression in murine mammary epithelial cells (ECs), breast carcinomas are induced via mitotic failure, centrosome amplification, and increased proliferation in 12-15 months.[205] YB1 high cells were then found to drive chromosomal non-disjunction, aneuploidy, and double minutes leading to the amplification of HER2.[206] These cells exhibit bi-nucleation and checkpoint slippage, similar to a phenotype we've observed in our cells (Chapter 4). Furthermore, YB1 was shown to drive stemness and proliferation in the subventricular zone and in neural stem cells prior to differentiation with CNTF or IGF1 after which YB1 protein dropped along with Sox2, BMI1, Musashi-1, and Nestin.[207] From the same study, differentiation following YB1 depletion is conserved in glioblastoma neurospheres, resulting in a reduction to the same stem markers and neurosphere growth. These data point to an overarching theme of YB1 genomic stability maintenance during fetal and tumor development and to YB1 as a driver of stemness, cell fate, and proliferation.

3.4 YB1 Drives Proliferation and EMT

The developmental regulatory properties of YB1 extend into multiple cancer subtypes with phenotypes including enhanced proliferation, stemness, and epithelial to mesenchymal transition. Many of the proliferative phenotypes driven by YB1 stem from CCAAT Y-box promoter binding and transcriptional initiation (**Figure 4**). Through a combination of both EMSA and reporter assays, the Royer group found YB1 to bind to the promoters and facilitate transcription of CyclinA2 and CyclinB1in HeLa cells.[208] YB1 was also shown to regulate CyclinD1 and CyclinE1 through Y-box promoter binding.[209,210]

The transcriptional regulation of cyclins provides an avenue for YB1 to promote cell cycling and proliferation and has been shown in a number of cancers including cervical, lung adenocarcinoma,

hepatocellular carcinoma, and pancreatic ductal adenocarcinoma.[208–211] This YB1 → Cyclin axis is potentially conserved in SHH MB as our group has shown CyclinD1 to decrease following YB1 depletion in SHH MB primary mouse cells. YB1 can also regulate proliferation through HER2, EGFR, IGF, and POLA transcription. YB1 can promote transcription of the catalytic subunit of DNA replication initiation complex (POLA) through 3'

ABCB1
TCTACATAAGTTGAAATGTCC**CCAAT**GATTCAGCTGATGCGCGTTTCTCTACTTGCCCTT
TCTAGAGAGGTGCAACGGAAGCCAGAACATTCCTCCTGGAAATTCAACCTGTTTCGCAGT
TTCTCGAGGAATCAGCATTCAGTCAATCCGGGCCGGGAGCAGTCATCTGTGGTGAGGCTG
ATTGGCTGGGCAGGAACAGCGCCGGGGCGTGGGCTGAGCACAGCCGCTTCGCTCTCTTTG
CCACAGGAAGCCTGAGCTCA - TSS

CCNB1
GAACGCCTTCGCGCGATCGCCCTGGAAACGCATTCTCTGCGACCGGCAGCCG**CCAAT**GGG
AAGGGAGTGAGTGCCACGAACAGG**CCAAT**AAGGAGGGAGCAGTGCGGGGTTTAAATCTG
AGGCTAGGCTGGCTCTTCTCG - TSS

CCNA2
CCCCTGCTCAGTTTCCTTTGGTTTACCCTTCACTCGCCTGCGACCCTGTCGCCTTGAATG
ACGTCAAGGCCGCGAGCGCTTTCATTGGT**CCATT**TCAATAGTCGCGGGATACTTGAACTG
CAAGAACAGCCGCCGCTCCG - TSS

CCND1
CGCGCCCCCTCCCCCTGCGCCCGCCCCCGCCCCCCTCCCGCTC**CCATT**CTCTGCCGGGC
TTTGATCTTTGCTTAACAACAGTAACGTCACACGGACTACAGGGGAGTTTTGTTGAAGTT
GCAAAGTCCTGGAGCCTCCA - TSS

Figure 4: Y-box's in promoters of MDR1 (*ABCB1*), CyclinB1 (*CCNB1*) and CyclinA2 (*CCNA2*). CyclinA2 promoter Y-box deviates by an adenine while still preserving YB1 binding and transcriptional activation.[208] This Y-box sequence is conserved in the CyclinD1 (*CCND1)* promoter, also shown to be responsive to YB1 levels.[210]

TSS: transcription start site

inverted Y-box repeat sequence indicating an alternate mechanism for YB1 to regulate cell cycling apart from cyclin transcription.[212] As a departure from regulation of proteins directly involved in cell cycle progression or DNA replication, the Dunn group found YB1 transcriptionally upregulates HER2 and EGFR expression that is abrogated upon YB1 depletion resulting in reduced proliferation.[213] This axis is conserved in the setting of glioma where YB1 interacts with Kindlin-2 and β-Catenin to bind the EGFR promoter and enhance RTK/AKT signaling and proliferation.[214] Our group also showed YB1 to bind the IGF2 promoter to induce an autocrine feedback loop between YB1 and Insulin growth-factor receptor to promote proliferation in SHH MB. Finally, YB1 depletion results in an increase in PTEN mRNA and a decrease in PIK3CA mRNA in HEK

and breast cancer cells, respectively, indicating potential transcriptional regulation by YB1.[215,216] Altogether, YB1 is a major transcriptional regulator of genes involved in cell cycle progression or mitogenic pathways such as RTKs or related proteins, including IGF, PTEN, and PI3KCA.

YB1 involvement in mitogenic signaling also includes direct protein-protein interactions and non-canonical cell secretion. Following activation of AKT by HER2 or IGF1R in breast cancer, AKT binds YB1 to mediate S102 phosphorylation resulting in anchorage independent growth (anoikis).[176] In melanoma cells, depletion of ERK1/2 or AKT3 results in a decrease in pYB1 with AKT3 depletion specifically resulting in decreased total YB1 protein.[217] Alternatively, pharmacological inhibition of PI3K, PDGFR, or ERK1/2 with LY294002, Sorafenib, or PD98059, respectively, resulted in abrogation of YB1 S102 phosphorylation. Stimulation of prostate cancer cells with EGF to activate EGFR results in increased pYB1 S102 through direct interaction with ERK1/2. On the other hand, silencing YB1 leads to increased proteasomal degradation and decreased phosphorylation of ERK1/2 resulting in decreased proliferation.[218] These studies indicate phosphorylation and activation of YB1 following RTK/AKT activation and extensive interactions between YB1 and MAPK signaling to regulate proliferation in cancer cells. And while the majority of YB1 proliferative signaling occurs through transcription or MAPK signaling participation, YB1 can also be secreted as an extracellular mitogen. For example, monocyte stimulation with lipopolysaccharide results in YB1 secretion with a requirement for Lys301 and 304 (**Figure 1**).[219] Inhibition of the canonical secretory pathway with brefeldin A does not abrogate YB1 secretion in micro-vesicles while calcium signaling stimulation with ionomycin or the addition of extracellular ATP, at least in the setting of melanoma, enhances the secretion of YB1 through a non-canonical secretory pathway.[220] Additionally, supplementing cell media with

recombinant YB1 drives proliferation, cell cycling, and migration, indicating a receptor or binding partner for YB1 that is not yet established in the literature.

Proliferation constitutes a major facet of oncological signaling; however, cell migration and tumor metastasis are equally important. YB1 influences migration and metastasis through translational regulation of angiogenic or mesenchymal transcripts or by promoting expression of matrix metalloproteinases. In a breast cancer model, YB1 can shift cells from a proliferative to migratory state by binding an Internal Ribosome Entry Site (IRES) in the 5'UTR of Snail and Twist, independent of 5' cap initiation, to drive EMT and enhance metastasis.[221] YB1 translational regulation of snail is conserved in cervical cancer and our group has also shown YB1 to regulate developmental migratory protein translation (Chapter 6).[222] The Sorensen group went on to discover that YB1 is a major metastatic driver in sarcoma through the translational regulation of HIF1α.[223] Rescuing YB1 depleted cells with ectopic HIF1α restores metastasis revealing a linear migratory signaling axis. Contrary to the previously discussed publications, however, cyclinD1 levels increased in this study following YB1 depletion in agreement with a "go or grow" phenotype. On the other hand, a transcriptional role for YB1 in cell migration stems largely from promoting matrix metalloproteinase (MMP) expression, membrane bound and soluble proteins that promote angiogenesis and metastasis.[224] In pancreatic ductal adenocarcinoma (PDAC), YB1 upregulates MMP2 while suppressing p27 mediated senescence to enhance liver metastasis.[225] Alternatively, YB1 promotes expression of MMP1 through promoter binding in breast cancer that is abrogated upon YB1 depletion and rescued with ectopic MMP1.[226] Finally, YB1 can also regulate migration or invasion in a number of other cancers including hepatocellular carcinoma, gastric cancer, and lung adenocarcinoma; however, no clear mechanism of regulation is

presented.[227–230] Altogether, there appears to be a strong correlation between YB1 high cells and metastatic potential driven primarily through the YB1 cold shock domain.

3.5 YB1 in the DNA Damage Response and Genomic Stability

A role for YB1 in genotoxic cell response to cisplatin, mitomycin C, and UV radiation was established shortly after YB1 discovery in 1996 by the Kohno group followed by studies on sensitization which paved the way for YB1 involvement in multiple aspects of stress response including DNA binding, DDR protein interactions, p53 inhibition, drug efflux protein expression, and chromosome segregation.[231,232] YB1 direct involvement in the DDR response again derives from cold shock domain DNA binding. In a cell free reaction, YB1 can bind and promote strand separation of cisplatin modified or mis-repaired base containing DNA, particularly if there is a Y-box.[233] Secondary to this, YB1 can bind multiple DNA repair proteins to affect repair pathway decision or chromosomal stability. For example, YB1 can inhibit NEIL1, a DNA glycosylase responsible for base excision repair (BER) following ROS damage of DNA not dissimilar from the role of APE1 (Chapter 2), another BER protein YB1 interacts with, which creates a nick in the phosphodiester backbone of DNA following DNA glycosylase removal of damaged bases.[234,235] Alternatively, a role for YB1 in mismatch repair is evidenced by inhibition of MutSα localization through interactions with PCNA, resulting in increased microsatellite instability of YB1 high cells.[236] YB1 also participates in the global-NER (Chapter 2) response to intra-strand cross linking caused by UV and chemo through localization and activation of XPC-HR23B in a cell free reaction.[237] These data nominate YB1 as an inhibitor of BER and a promoter of global-NER; however, YB1 also participates in damage recognition through PARP1 and there is limited published data to support a role for YB1 in homologous recombination.

PARP1 is a prime candidate for tumor sensitization to standard of care (Chapter 2) and a relationship between PARP1 and YB1 is extensively explored in cell free reactions from the Lavrik group. Not only can PARP1 ribosylate YB1 (see 2.2), but the C-terminal domain of YB1 can promotes interaction with PARP1 to stimulate PARP1 ribosylation of damaged DNA and YB1.[238] In addition, high concentrations of YB1 can overcome PARP1 inhibition by Olaparib , allowing PARP1 to ribosylate DNA and overcome PARP1 inhibition.[239] While MB cells can be sensitized to DNA damage through PARP inhibition with Olaparib, discussed in chapter 2, YB1 high cells could benefit from simultaneous inhibition of PARP and YB1 given the potential for YB1 to overcome PARP inhibition. Altogether, these data would suggest YB1 promotes recognition of single and double strand breaks (SSBs and DSBs, respectively) induced by ionizing radiation or chemotherapy as a prerequisite to non-homologous end joining or homologous recombination. This leads to the limited evidence for YB1 participation in repair of SSBs or DSBs resulting from genotoxic insult. For example, following doxorubicin treatment and DSB induction, a proteolytic fragment of YB1 (amino acids 1-219), binds MRE11 and RAD50, two components of the M/R/N complex (Chapter 2) responsible for damage recognition and induction of homologous recombination pending MRE11 mediated strand resection.[240] Unfortunately, more mechanistic studies are required to conclude any meaningful effect of this interaction given doxorubicin sensitization could be due to multiple factors. YB1 was also shown to co-precipitate with H2AX following S139 phosphorylation, a marker of chromatin de-condensation following DNA damage that is required for repair protein recruitment, through direct interaction with hnRNP R.[241] Given a lack of enzymatic function for YB1, these findings nominate YB1 as a scaffolding protein to facilitate protein-protein or protein-DNA interactions.

Apart from the direct involvement of YB1 in DDR discussed, there are many "indirect" mechanisms for YB1 mediated resistance to genotoxic therapies, including drug efflux and apoptotic regulation. Expression of multidrug resistance protein 1 *(ABCB1 or MDR1),* drives efflux of cisplatin, a major backbone chemotherapy for many cancers including MB, was found to be correlative with YB1 shortly following YB1 discovery.[242] The *ABCB1* gene promoter, in fact, contains a Y-box (**Figure 4**), allowing YB1 to bind alongside other transcription factors to enhance drug efflux. In HEK cells, depletion of APE1 abrogates YB1 - MDR1 promoter binding in an EMS assay resulting in cisplatin and etoposide sensitization, putatively as a result of MDR1 down-regulation.[243] In fact, in lung cancer tissue, APE1 and MDR1 are positively correlated, indicating preservation of signaling in patients. These findings were corroborated by another group showing APE1/YB1 MDR1 promoter localization and enhanced RNA Pol II loading.[244] The role of APE1 in the DNA damage response makes it another candidate for inhibition (Chapter 2), and given YB1 and APE1 together can promote MDR1 expression, targeting YB1 and APE1 simultaneously could improve responsiveness to chemotherapy. Activation of MDR1 transcription by YB1 is triggered in numerous ways including taxane or cisplatin exposure or activation of mitogenic upstream signaling. In gastric cancer, *RACQL4* (ATP-dependent DNA helicase Q) expression correlates with cisplatin sensitivity. In rescue experiments, YB1 can bind and promote MDR1 expression from a luciferase reporter and *RACQL4* dramatically enhances the expression of MDR1. However, in the absence of YB1 *RACQL4* cannot promote transcription of MDR1.[245] This would indicate not only a requirement of YB1 for MDR1 expression in gastric cancer, but that *RACQL4* can dramatically enhance expression, driving chemo resistance. YB1 depletion also leads to a reduction in ABCC3 protein levels, another drug efflux protein, to sensitize gastric cancer cells to doxorubicin.[246]

Apoptotic regulation by YB1 represents another indirect mechanism for DNA damage resistance outside of drug efflux that is important for maintaining a genomically unstable cell environment. p53, the "guardian of the genome", discussed extensively in chapter 2, is crucial for cell response to genotoxic insult and chromosomal instability (**Figure 5**) and can be regulated by YB1. In an EMS assay, Lasham et al. found YB1 to bind the *TP53* promoter at -138 to -127 bp relative to the transcription start site (AGC TCT GGC TTG) and YB1 overexpression in 3T3, HeLa, and

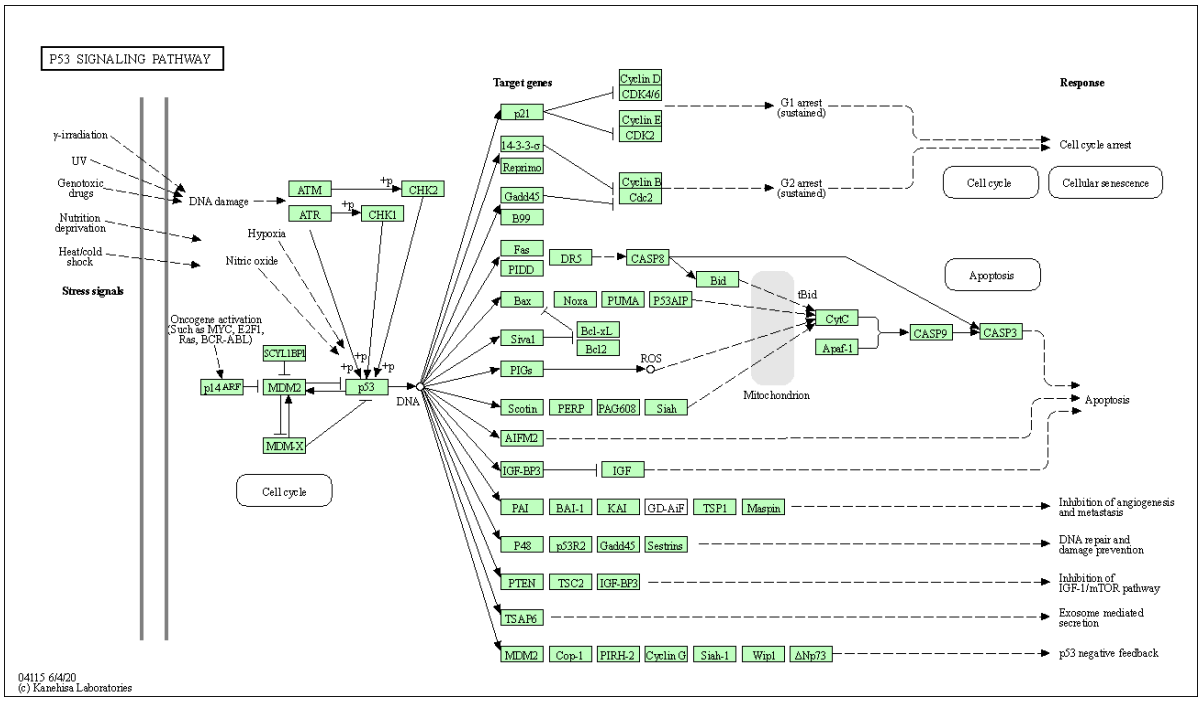

Figure 4: p53 apoptotic signaling
https://www.genome.jp/pathway/hsa04115

RKO cells alongside a p53 reporter results in reduced p53 expression.[247] Additionally, YB1 depletion results in elevated p53 and BAX expression and induction of apoptosis in a p53 dependent manner. And while YB1 can inhibit p53 transcription to a large degree, it can also directly bind to p53. The interaction between YB1 and p53 is sufficient to prevent p53

transcriptional induction of pro-apoptotic factors such as *NOXA* and *BAX* but not *CDKN1A*, which is attributed to the lower binding affinity of p53 to the *NOXA* and *BAX* promoters compared to *CDKN1A* promoter.[248] The Braithwaite group who published the two previous studies also showed a requirement of wild type p53 for nuclear localization of YB1; however, this phenotype is not consistent and even in our p53 mutant and null models YB1 is present in the nuclear and chromatin compartment.[249] The apoptotic inhibitory relationship between YB1 and p53 is conserved in the settings of liver cancer and glioma.[250,251] YB1 can also directly regulate apoptotic factors irrespective of p53. In leukemia, YB1 binds and promotes translation of BCL2, an anti-apoptotic protein, to enhance cell survival.[251] Alternatively, YB1 depletion in HUVECs and HPAECs results in a decrease to BCL-XL, another anti-apoptotic protein.[252] These data point to YB1 as a major regulator of cell viability and there are important considerations due to the impact of p53 suppression on MB standard of care response.

While p53 mutations result in a dramatically worse response to radiation and chemotherapy, YB1 high cells may suppress wild type p53 to limit apoptotic induction. A global response to radiation and chemo may consist of AKT activation (chapter 2), phosphorylation and activation of YB1, p53 suppression, and the convergence of these pathways on the DNA damage response to facilitate repair of DNA, efflux of chemotherapies, and suppression of cell death or senescence. The YB1 anti-apoptotic signaling axes are crucial not only in the response to therapy, but also in maintaining cell viability from genomic instability. A role for YB1 in maintaining genomic stability stems from an involvement in cell division and chromosome segregation during mitosis. In published works, phosphorylated YB1 localizes to centromeres during mitosis and, when depleted, results in microtubule detachment during telophase and misshapen nuclei.[253] Additionally, in YB1 high

cells, phospho-YB1 can be found at the spindles and cells tend to show abnormal nuclear morphology, bi-nucleation, and extensive chromosomal abnormalities.[206] These are phenotypes we have noticed in our own studies of YB1 (Chapter 4) where phospho-YB1 localizes to centromeres during mitosis as indicated by pYB1 and DAPI staining and following radiation YB1 intact cells become multinucleated. In fact, similar to the effect of patched deletion on MYCN amplification in murine MB models (chapter 2), YB1 overexpression results in gene amplification, likely stemming from a role in chromosomal disjunction and interactions with cMYC. As discussed in chapter 2, cMYC amplification and overexpression can drive a highly proliferative state while suppressing apoptotic signaling that is vulnerable to DDR signaling inhibition by targeting Chk1 with prexasertib. A role for MYC in YB1 mediated genomic instability potentially results from a transcriptional and translational relationship between MYC and YB1 where YB1 can stabilize and facilitate translation of cMYC mRNA.[254,255] MYC was also found to upregulate YB1 transcription, indicating a feed forward loop between YB1 and MYC that could have several effects on the cell including genomic amplification, suppression of apoptosis, and enhanced DNA repair and drug efflux.[256] Therefore, to return to the aforementioned role for YB1 in the global response to radiation, YB1 high cells may accelerate damage repair and suppress cell death while also accumulating genomic alterations potentially leading to greater mutational signature and shorter overall survival.

3.6 YB1 in the Clinic: Resistance and Targeting

The diversity and sheer number of oncogenic phenotypes YB1 elicits make it a highly desirable drug target; however, not unlike MYC, there is no clear enzymatic function and both the C and N-terminals are disordered. This has made creating therapies for YB1 challenging. In 2017, Nakano

et al. developed an amido-bridged nucleic acid (AmNA)-modified antisense oligonucleotide (ASO) targeting YB-1.[252] Amino-bridge modification enhances cell entry allowing for IV administration of ASOs which the group used to deplete YB1 *in vivo* to inhibit tumor growth. In 2021, another group developed a small molecule inhibitor for YB1, SU056, for use in ovarian cancer models; however, there are no other publications corroborating these results.[257] Finally, in 2023 a third group published on a drug based on its ability to disrupt YB1-RNA interactions through cold-shock domain binding; however, it is not clear whether this would impeded protein protein or protein-DNA interactions for YB1.

3.7 Conclusions

The multifaceted oncogenic phenotypes driven by YB1 ranging from basic mitogen to direct therapeutic resistance make it a highly desirable therapeutic target. Many of the proteins YB1 interacts with or regulates translation or transcription of including PARP1, APE1, MYC, and p53, are crucial to the therapeutic response of Medulloblastoma to standard of care, including radiation and chemotherapy (Chapter 2). Additionally, the diversity of signaling outside of direct signaling interactions between YB1 and these proteins means there is a potential for synergism. Unfortunately, the blood brain barrier penetrability of small molecule inhibitors or ASOs for YB1 is unclear and additional studies are needed to corroborate YB1 inhibitors or ASOs.

Chapter 4

YB1 Modulates the DNA damage Response in Medulloblastoma

Author's Contribution and Acknowledgment of Reproduction

This chapter is reproduced with edits from a manuscript published in Scientific Reports, 2023. LFM and AMK contributed to the conception, design, and methodology of the study. AMK and DH sponsored the study. LFM, VC, and TH performed western blotting, immunofluorescence, comet, and proliferation assays. CP performed flow cytometry. JR performed IHC. All authors read the manuscript and approved the final version.

4.1 Abstract:

Y-box binding protein 1 (*YBX1* or YB1) is a therapeutically relevant oncogene capable of RNA and DNA binding and mediating protein-protein interactions that drive proliferation, stemness, and resistance to platinum-based therapies. Given our previously published findings, the potential for YB1-driven cisplatin resistance in medulloblastoma (MB), and limited studies exploring YB1-DNA repair protein interactions, we chose to investigate the role of YB1 in mediating radiation resistance in MB. MB, the most common pediatric malignant brain tumor, is treated with surgical resection, cranio-spinal radiation, and platinum-based chemotherapy, and could potentially benefit from YB1 inhibition. The role of YB1 in the response of MB to ionizing radiation (IR) is not studied, but relevant for determining potential anti-tumor synergy of YB1 inhibition with standard radiation therapy. We have previously shown that YB1 drives proliferation of cerebellar granular neural precursor cells (CGNPs) and murine Sonic Hedgehog (SHH) group MB cells. While others have demonstrated a link between YB1 and homologous recombination protein binding, functional and therapeutic implications remain unclear, particularly following IR-induced damage. Here we show that depleting YB1 in both SHH and Group 3 MB results not only in reduced proliferation, but also synergizes with radiation due to differential response dynamics. YB1 silencing through shRNA followed by IR drives a more NHEJ-dependent repair mechanism, leading to faster γH2AX resolution, premature cell cycle re-entry, checkpoint bypass, reduced proliferation, and increased senescence. Our research shows that depleting YB1 in combination with radiation sensitizes SHH and Group 3 MB cells to radiation.

4.2 Introduction

For decades, the standard of care for medulloblastoma (MB) treatment has consisted primarily of surgical resection and a combination of radiation and cisplatin-based chemotherapy.[258] And while patient survival has greatly benefited from this regimen, there are significant sequelae that result, including endocrine abnormalities, hearing loss, and neurocognitive decline. Additionally, some MB molecular subgroups, including *TP53*-mutant Sonic hedgehog-activated (SHH) and Group 3, have a substantially worse survival outcome with a higher incidence of relapse, while Wingless (WNT) and Group 4 respond well.[259,260] In addition to the investigation of small molecule inhibitors to target genetic and transcriptomic alterations specific to the four subgroups (Wingless - WNT, Sonic Hedgehog (SHH), Group 3 and Group 4), clinical trials have also focused on targeting proteins that mediate resistance to DNA damaging therapies.[261] We previously showed that Yes-Associated Protein (YAP) drives Y-box binding protein 1 (YB1) expression resulting in proliferation of cerebellar granular neural precursors (CGNPs) and NeuroD2-SmoA1 derived primary SHH mouse medulloblastoma cells (referred to as MBCs) through Insulin-like growth factor 2 (IGF-2) promoter binding and an Insulin-like growth factor receptor (IGFR) autocrine feedback loop.[201] Given the overexpression of YB1 across the four molecular-defined MB subgroups, WNT, SHH, Group 3 and Group 4, we sought to determine whether YB1 plays a role in the MB radiation response. The mechanistic properties regulating YB1 cellular localization and functionality are well established but are lacking and inconsistent between cancer models with respect to YB1's role in the response to ionizing radiation (IR). Compared to anatomically matched control brain, YB1 expression is elevated in several types of brain tumors, both adult and pediatric, including glioblastoma multiforme, ependymoma, anaplastic astrocytoma and diffuse intrinsic pontine glioma.[6] YB1 can also drive a variety of stemness, metastasis, proliferation, angiogenesis,

and drug resistance phenotypes in other cancers including neuroblastoma, breast, lung, colorectal, and others.[262,263] YB1 nuclear transport appears to be a prerequisite to drive these phenotypes, a mechanism induced by environmental stressors and preceded by serine 102 phosphorylation and c-terminal cleavage.[182,264]

In addition to these phenotypes, several groups have emphasized a role for YB1 in the DNA damage response, focusing on direct interactions with DNA or repair proteins. YB1 was shown to mediate strand separation of cisplatin-bound DNA in addition to driving expression of the MDR1 receptor, resulting in cisplatin efflux.[233,265–267] In addition, following etoposide or doxorubicin treatment of NIH3T3 cells, the proteolytic YB1 fragment was found to interact with Mre-11 and Rad50, proteins responsible for homologous recombination.[240] Considering the more deleterious effects of IR involve double strand breaks (DSBs) repaired through homologous recombination (HR) or non-homologous end joining (NHEJ), any role for YB1 in this process could lead to synergism. While YB1 was found to potentiate PARP1-mediated ribosylation of DNA following IR induced DSBs leading to PARP inhibitor resistance, *in vivo* studies have not corroborated these findings and targeting YB1 could ameliorate the need for PARP inhibition.[239] Additionally, even though YB1 was found to colocalize with p53 and WRN following UV treatment, authors did not see any colocalization between YB1 and γH2AX, a marker of chromatin de-condensation proximal to sites of DNA damage.[268] Thus, a direct and functional role for YB1 in the response to IR remains to be seen.

In the present study, we extend our previous findings on YB1 as a driver of proliferation into Group 3 MB and demonstrate the functional consequences of YB1 depletion following IR in both SHH and Group 3 MB. We show that YB1 knockdown (KD) cells utilize differential repair

pathways, fail to recognize and activate cell cycle checkpoints, resulting in decreased proliferation and increased senescence in YB1 depleted cells.

4.3 Results

4.3.1 YB1 is expressed across all MB subgroups and overexpression is associated with decreased survival in an SHH primary mouse model

Previously, we have shown that YB1 RNA is elevated across MB subgroups.[9,201] We sought to corroborate YB1 RNA levels with corresponding protein expression data by immunoblotting cell lysates from NeurD2-SmoA1 primary SHH mouse MB cells (MBCs), a PTCH receptor deficient spontaneous SHH tumor mouse derived MB cell line (Pzp53Med[269]), human SHH MB cell lines (Daoy, UW228, and ONS-76) and Group 3 and 4 MB cell lines (D341, D556, BT52, D283, and CHLA01). Interestingly, YB1 protein is robustly expressed across all cell lines (**Figure 1a**). Immunohistochemistry (IHC) of 3 patient samples from both SHH MB *TP53*-wild type and mutant tumors, whose patients respond poorly to standard of care, shows that YB1 is highly expressed in all samples (**Figure 1b and Supp. Fig. 1a and b**).[270] Given challenges with stable protein knockdown in primary MB mouse models, we chose to transiently overexpress YB1 in NeurD2-SmoA1 derived primary cells followed by orthotopic implantation into the cerebella of p5 mice to determine whether YB1 is a driver of tumor growth in SHH medulloblastoma. Mice implanted with YB1-overexpressing MBCs had a median survival of 26.5 days compared to mice injected with GFP control-transduced MBCs, which had a median survival of 60.5 days ($p<0.0001$) (**Figure 1c**). Finally, single cell sequencing of SHH primary MB mouse models published by Riemondy et al. allowed us to further assess a potential role for YB1 in cell subpopulations within the tumor (**Figure 1d**).[19] In the SHH-Math-Cre-SmoM2 primary SHH model, YB1 is elevated in most cell

populations, particularly in those representing immune, active cell cycling (MS-A1 and MS-A2), and progenitor (MS-B1). In the MYC driven p53 dominant negative Group 3 spontaneous mouse model (GP3-Myc-dnP53), YB1 is highly elevated in sub-populations corresponding to active cell cycling (MP-A1, -2) and progenitor (MP-B1,-B2, -B3) compared to differentiated neoplastic subpopulations (MP-C1, -C2) (**Supp. Fig 1c**).[271] In addition to data showing worse survival in mice harboring YB1 overexpressing tumors and robust YB1 protein express across all subgroups, the single cell sequencing expression profiles suggest that YB1 inhibition in stem or progenitor-like populations previously implicated in driving relapse could sensitize to radiation resulting in improved radiation response given the results of this study.

Figure 1: YB1 is expressed across all MB subgroups and overexpression is associated with shortened survival in an SHH primary mouse model

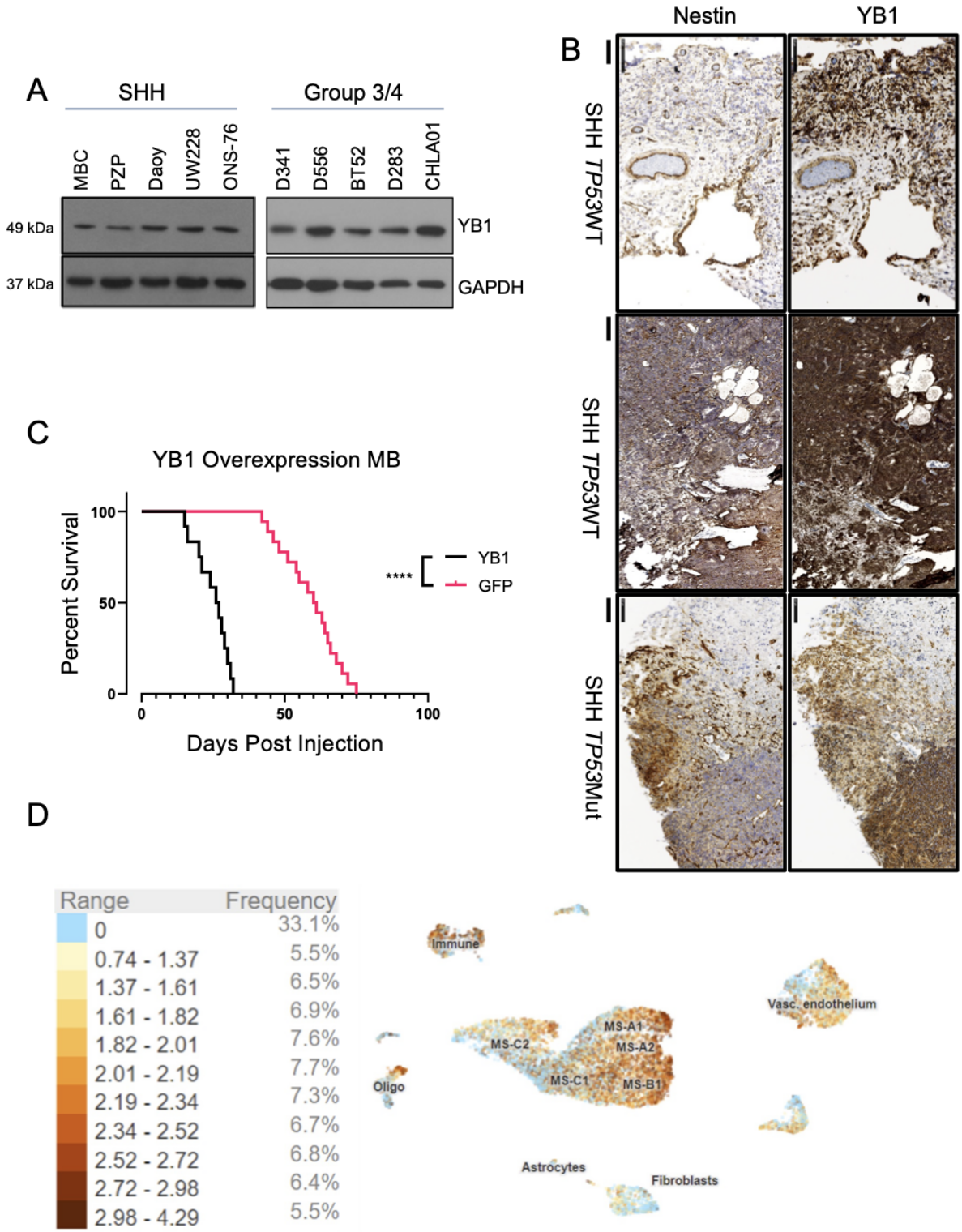

Figure 1: YB1 is expressed across all MB subgroups and overexpression is associated with shortened survival in an SHH primary mouse model (A) Immunoblotting cell lysate from SHH cells (MBC (primary NestinD2-SmoA1), Pzp53Med (Ptch-LacZ-p53^{null}), Daoy, UW228, and ONS-76), and group 3/4 cells (D341, D556, BT52, D283, and CHLA01) with GAPDH as control. (**B**) Immunohistochemistry of SHH subgroup samples from both *TP53* wild type and mutated patients showing positive staining of both Nestin (Stem marker) and YB1 (Left scale bar = 100μm, quantification **Supp Fig. 1a and b**). (**C**) Survival analysis of BL6 mice orthotopically implanted with NestinD2-SmoA1 primary cells following adenoviral overexpression of YB1 (GFP median survival 26.5 days YB1 median survival 60.5 days $p<0.0001$). (**D**) UMAP of previously published single cell sequencing analysis of SHH-Math-Cre-SmoM2 showing enrichment of YB1 in numerous cell populations collected from UCSC Cell Browser: active cell cycling (MS-A1 and MS-A2) and progenitor (MS-B1). Expression profile is subdivided into 10 expression ranges apart from no expression and percent of all cells within each range listed on right.

4.3.2 YB1 depletion results in differential cell cycling and nuclear morphology after IR damage

To characterize the result of YB1 depletion on cell cycle distribution up to 48 hours (**h**), human SHH MB ONS-76 short-hairpin control (**shGFP**) and YB1 knockdown (**KD**) (**shYB1**) cells were exposed to 10 Gray (**Gy**) IR at 24 and 48h post-plating with all conditions grown for 72h followed by EdU incorporation and staining with Live/Dead Aqua (**Figure 2a and Supp. Fig 2**). As shown, the cell cycle distribution between non-treated YB1 KD and control cells is very similar. YB1 KD cells have a modest decrease in S-phase and increase in G2/M compared to control, consistent with a role for YB1 in the transition to and completion of mitosis.[272] Following radiation, a greater proportion of control cells have entered the terminal sub-G1 phase 48h compared to KD cells ($p=0.0275$, **Figure 2b and c**). At 48h cells show significant differences not only in cell cycle ratios, but also in nuclear morphology. Control cells have an increase at 48h post-radiation in proportions of cells in doublets as detected via flow cytometry ($p=0.0026$, **Figure 2d, doublets not included in analysis**). To confirm that this doublet morphology was not a technical artifact of flow cytometric analysis, we stained cells for LaminA/C in both ONS-76 and UW228, a *TP53* mutated cell line (**Figure 2e and Supp. Fig. 3**). The elevated nuclear fractionation indicated by the LaminA/C staining in control irradiated compared to YB1 depleted cells 48h following radiation in both ONS-76 and UW228 suggests these cells are experiencing mitotic catastrophe and incomplete cytokinesis.[273] The increase in sub-G1 populations paired with observed changes in nuclear morphology of control-irradiated cells phenotypically resemble the chromosomal instability of YB1 high cells observed breast cancer.[205,206] Given the potential for induction of chromosomal instability, we chose to further explore the potential for YB1 involvement in DNA repair following radiation.

Figure 2: YB1 depletion results in differential cell cycling and reduction of aberrant nuclear morphology following radiation

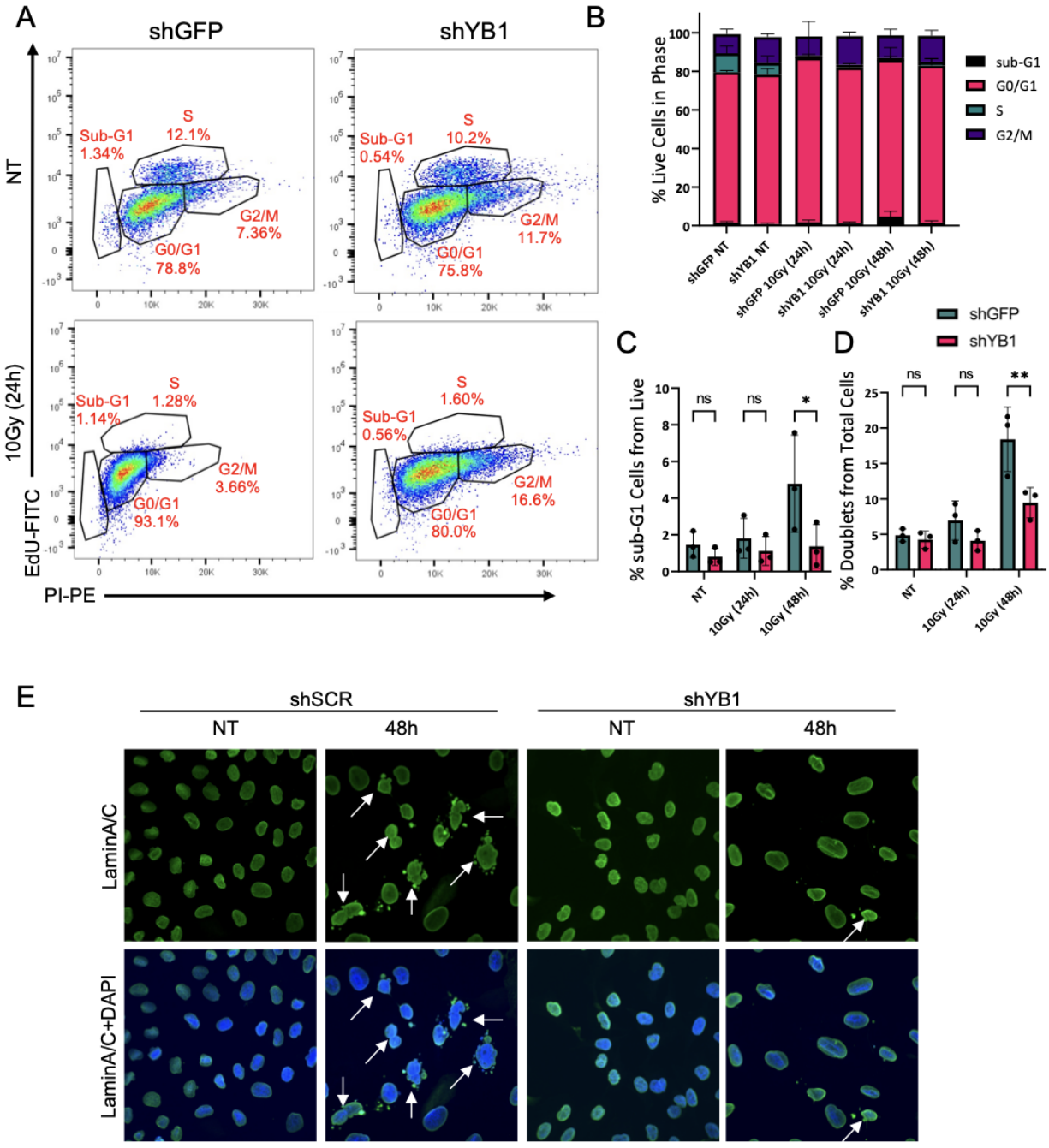

Figure 2: YB1 Knockdown results in differential cell cycling and reduction of aberrant nuclear morphology following radiation (**A**) ONS-76 shGFP and shYB1 cells were untreated (NT) or treated with 10Gy and analyzed for cell cycle phase proportions (sub-G1, G0/G1, S, and G2/M) at 24 (shown) and 48h using EdU and PI. Quantification of cell cycle phase distribution (SD and Means **Supp Fig. 2** n=3) (**B**). At 48h post-irradiation, shYB1 shows significantly lower proportions of cells in sub-G1 (shGFP vs shYB1 95% CI = 0.36-6.47 p=0.0275 n=3) (**C**) and cells appearing in doublets (shGFP vs shYB1 95% CI = 3.303-14.56 p=0.0026 n=3) (**D**) (doublets excluded from cell cycle analysis). **(E)** shSCR and shYB1 non-treated and treated with 10Gy were stained with LaminA/C and DAPI 48h after 10Gy irradiation. shSCR cells demonstrate more aberrations in nuclear morphology (UW228 and additional images **Supp Fig. 3**).

4.3.3 Irradiation of YB1 depleted cells results in differential γH2AX resolution and CHK2 phosphorylation in SHH and Group3 MB cells

Differences in cell cycle ratios and nuclear morphology between control and KD cells suggest that YB1 may influence DNA repair pathway choice, with YB1 driving a more time-consuming repair in addition to a potential role in G2/M regulation. To determine whether YB1 plays a direct role in the DNA damage response to IR and to investigate DNA damage accumulation and resolution up to 24h following radiation, we performed cellular fractionation and radiation time courses in the NeuroD2-SmoA1 primary MBCs. We exposed MBCs to 2Gy radiation and assessed cytoplasmic, nuclear, and chromatin fractions to determine YB1 intracellular distribution by immunoblotting (**Supp. Fig4a**). We found that YB1 is robustly distributed between all subcellular fractions; however, there was no difference in nuclear or chromatin YB1 levels between irradiated and non-irradiated cells up to 30min. Given toxicity of lentivirus in combination with radiation in primary cells, we irradiated YB1 overexpressing MBCs. Following 6h of recovery from initial exposure, γH2AX persists in YB1-overexpressing cells compared to GFP-infected control MBCs and YB1 overexpressing cells show lower levels of cleaved caspase 3 (CC3), a marker of cell death, compared to control (**Figure 3a and Supp. Fig. 4b**). When we performed immunofluorescence (**IF**) with these cells, we observe γH2AX foci persistence in YB1 depleted cells compared to irradiated control, thus corroborating the western blot data (**Figure 3b and c**). We chose to confirm these effects in sh control or shYB1 ONS-76 and D341 cell lines, representing human models of SHH and Group3 MB, respectively. 24h after IR damage, both cell lines show the opposite of YB1-overexpressing MBCs in that γH2AX intensity persists in control cells compared to YB1 KD cells at 24hrs (**Figure 3d and e and Supp. Fig. 5**). Human SHH MB Daoy (*TP53* mutant) cells also shower lower γH2AX 6 and 24h in YB1 KD cells compared to control

(**Supp. Fig. 4c**). Moreover, in D341 cells, phospho-Chk2 intensity is higher at 24h compared to YB1 KD cells (**Figure 3e**). The elevated γH2AX and phospho-Chk2 in cells expressing YB1 is consistent with the reduced viability and accumulation of control-irradiated cells in sub-G1 of ONS-76 48h following radiation (**Figure 2a and b)**. The γH2AX present at 24h persists regardless of cell line or control shRNA construct utilized, and in later experiments, with a scramble construct, γH2AX again is present at 24h in ONS-76 (**Figure 5**). Following radiation, a lack of γH2AX in YB1 knockdown cells at 24h and greater γH2AX intensity over control in YB1 overexpressing cells paired with differences in cell cycle re-entry at 24h is suggestive of immediate differences in repair pathway choice that may have consequences beyond the initial stages of DNA repair, such as reduced viability potentially driven by genomic instability or genomic rearrangement.

Figure 3: YB1 Depletion results in differential γH2AX resolution and CHK2 phosphorylation in SHH and Group3 medulloblastoma cells

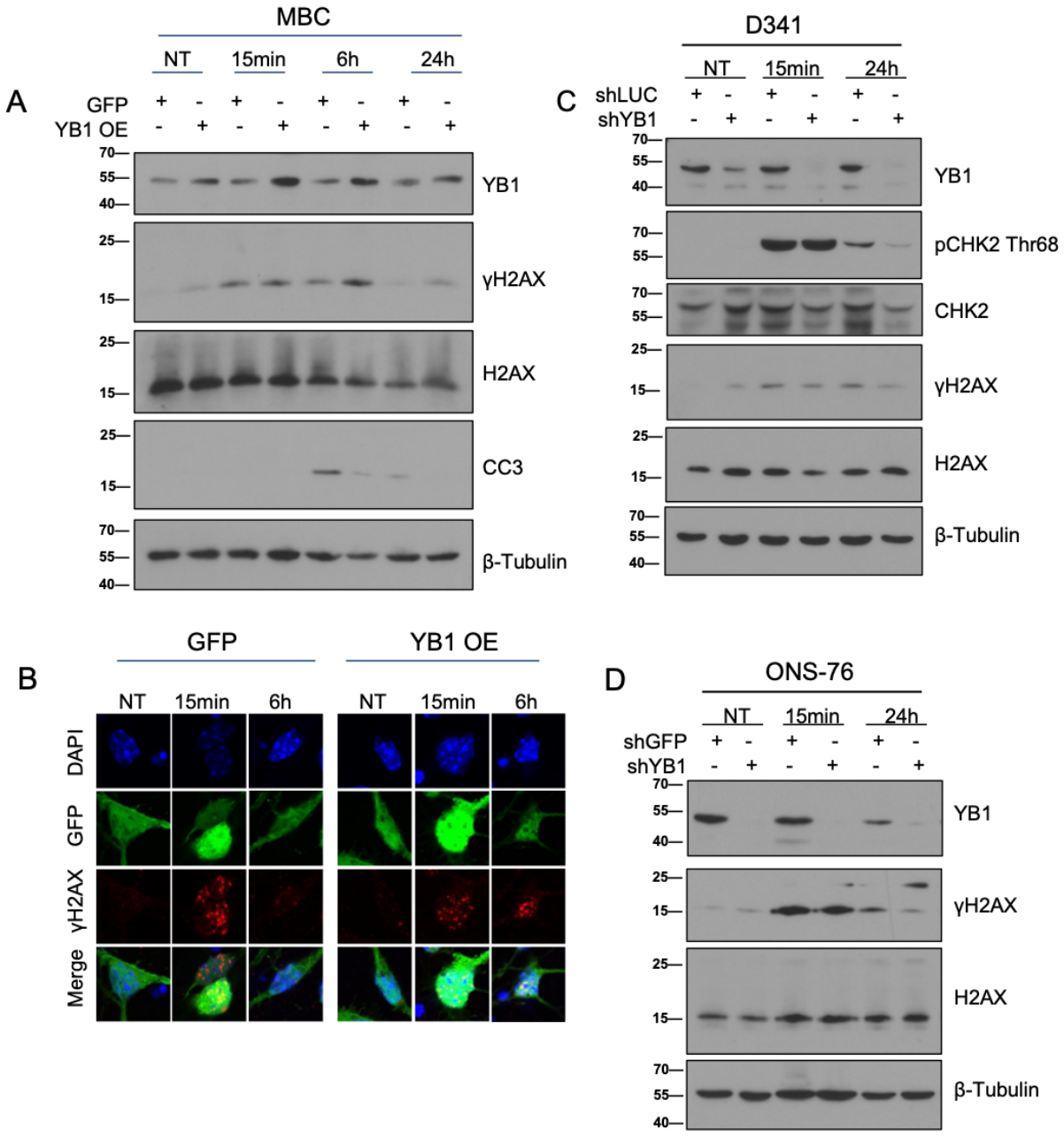

Figure 3: YB1 depletion results in differential γH2AX resolution and Chk2 phosphorylation in SHH and Group3 medulloblastoma cells (**A and B**) MBCs plated for 24h prior to infection with either control or YB1 overexpressing adenovirus. Following 48h incubation cells were irradiated with 2Gy and either lysed (immunoblotting) or fixed prior to staining (immunofluorescence). (**C**) D341 shLuc (control) and shYB1 cells irradiated with 5Gy. (**D**) ONS-76 shGFP (control) and shYB1 cells irradiated with 10Gy (Additional replicates **Supp Fig. 5**).

4.3.4 YB1 depletion results in accelerated DSB and SSB repair, γH2AX resolution, and a lack of RPA32 phosphorylation at Serines 4/8

Previous publications linked YB1 and HR through interactions between a proteolytic fragment of YB1 and Rad50 and Mre-11, components of the **MRN** complex (Mre-11/Rad50/NBS1), following chemotherapeutic exposure.[240] In our models, YB1 proteolytic processing and its effects on nuclear localization are unclear. However, given we detect full length YB1 in the nuclear and chromatin fractions, and we observe differential γH2AX beyond initial accumulation at 15 minutes, we hypothesized that cells deficient in YB1 perform less HR, a slower process than NHEJ, and will resolve DSBs, SSBs, and γH2AX foci prior to control irradiated cells.[274,275] We analyzed single cell DNA damage resolution using neutral and alkaline comet assays to understand single and double stranded break accumulation and resolution. Under both neutral (**Figure 4a1-a2**) and alkaline conditions (**Figure 4b1-b2**), shYB1 cells resolve damage faster than irradiated control irradiated cells after accumulating similar levels of damage. Furthermore, because γH2AX staining 24h after radiation (**Figure 3**) could indicate unresolved damage or apoptotic initiation, and to further test the hypothesis that YB1-deficient cells preferentially use a faster repair pathway, we incorporated an alternate scramble shRNA control and performed cell synchronization with a

greater selection of time points leading up to 24h. Following 10Gy irradiation in aphidicolin S-phase synchronized ONS-76 cells (**Figure 4 C and Supp Fig. 6**), YB1 KD cells resolve γH2AX faster than control-irradiated starting at 4h and continuing into 6h, a phenotype conserved in UW228 (**Supp Fig. 7**). Interestingly, by 6h the majority of γH2AX is resolved but re-emerges in control-irradiated cells at 24h, a phenotype conserved across cell lines regardless of short-hairpin construct used (**Figure 3 and 4**). Indeed, cells entering Sub-G1 can express γH2AX as part of apoptotic bodies.[276,277] This phenotype is made apparent in ONS-76 cells by the re-emergence of γH2AX in control-irradiated cells at 24h concomitant with an increase in Sub-G1 control-irradiated cells 24 and 48h following radiation (**Figure 2**). Finally, to begin our assessment of a potential decrease in HR mediated repair, which we expect to be highest in S-phase, we probed RPA32 at Serines 4/8 in synchronized **(Figure 4c-d and Supp Fig. 6)**. RPA32 is significantly more phosphorylated at 6h in irradiated synchronized sh control cells compared to YB1 silenced cells. Given RPA32 can be phosphorylated in response replication stress, typically seen following hydroxy-urea treatment, and is implicated in binding ssDNA prior to trading off with Rad51 for strand invasion during HR, a lack of RPA32 phosphorylation in shYB1 cells suggests a lower degree of replication stress and/or HR following radiation treatment.[278,279] The increased pRPA32, delayed γH2AX resolution, and re-emergence of γH2AX at 24h in control-irradiated cells suggest YB1 could be driving an alternate repair mechanism.

Figure 4: YB1 depletion results in accelerated physical repair, γH2AX resolution, and lack of RPA32 phosphorylation at Serines 4/8

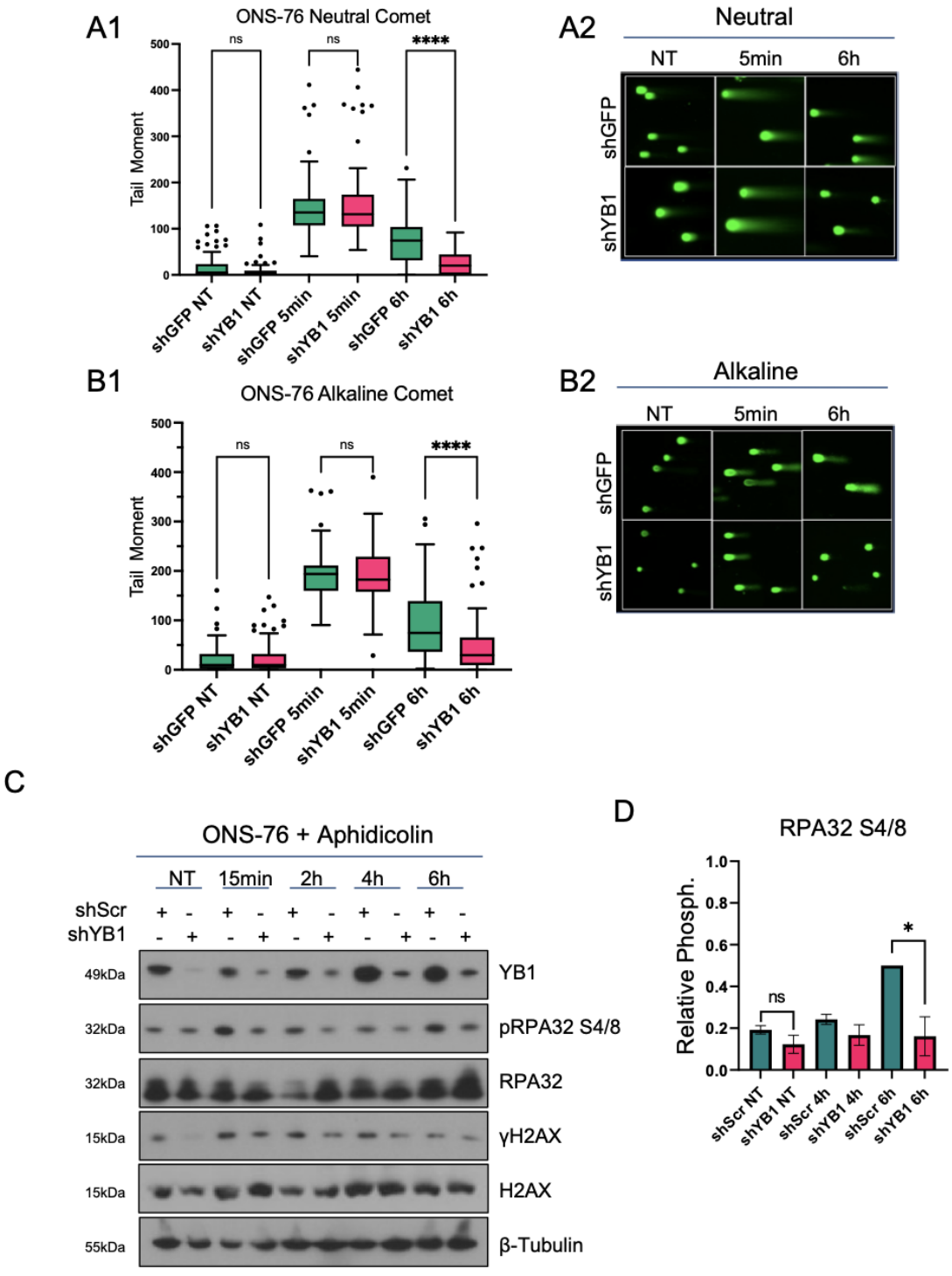

Figure 4: YB1 depletion results in accelerated physical repair, γH2AX resolution, and lack of RPA32 phosphorylation at Serines 4/8 (**A1 and A2**) Neutral comet assay tail moment of ONS-76 shGFP and shYB1 treated with 10Gy showing non-significant differences in damage accumulation (shGFP vs shYB1, shGFP 95% CI = 171-164.6 shYB1 95% CI = 135-178.3 p>0.9999 n=3 Kruskal-Wallis test) and significant differences in damage resolution at 6h (shGFP vs shYB1, shGFP 95% CI = 62.86-86.59 shYB1 95% CI = 19.06-30.49 p<0.0001 n=3 Kruskal-Wallis test). **(B1 and B2)** Alkaline comet assay tail moment of ONS-76 shGFP and shYB1 treated with 10Gy showing non-significant differences in damage accumulation (shGFP vs shYB1, shGFP 95% CI = 180.5-201.5 shYB1 95% CI = 183.3-207.0 p>0.9999 n=3 Kruskal-Wallis test) and significant differences in damage resolution at 6h (shGFP vs shYB1, shGFP 95% CI = 80.1-105.1 shYB1 95% CI = 37.84-57.05 p<0.0001 n=3 Kruskal-Wallis test). **(C)** Synchronization of ONS-76 with Aphidicolin for 24h prior to radiation time course at 10Gy (Additional replicates **Supp Fig. 6**). **(D)** Densitometry of pRPA32 S4/8 shows consistent elevation in shGFP cells compared to shYB1 6h post-IR (shGFP vs shYB1 95% CI = -0.24-0.56p=0.0223 n=3 Ratio paired t-test, internal normalization to shGFP 6h).

4.3.5 YB1 depleted cells accumulate less RAD51 and more TP53BP1 nuclear bodies during and after S-Phase repair

While differences in γH2AX, RPA32 phosphorylation, and DSB and SSB repair kinetics are emblematic of a repair pathway switch following ionization radiation damage, they are mostly suggestive. We further investigated the activation of HR or NHEJ specific proteins in ONS-76, both synchronized and non-synchronized, through IF. Given TP53BP1 is known to be involved early on in the DNA repair signaling axis to inhibit end resection and promote NHEJ, we chose to

investigate its nuclear localization following radiation.[280] Compared to 10Gy irradiated control, irradiated YB1 depleted cells show greater levels of TP53BP1 nuclear bodies in synchronized cells with greatest levels seen at 2h (**Figure 5a and b)**. RIF1, which binds to TP53BP1 to facilitate NHEJ,[281] is also enriched in YB1 depleted cells 2h following radiation (**Supp Fig. 9**). Following synchronization, however, YB1 depleted cells fail to accumulate RAD51 foci at levels comparable to control irradiated cells at 6h (**Figure 5d).** Elevated TP53BP1 and reduced Rad51 are conserved in non-synchronized irradiated YB1 depleted cells (**Figure 5c and f and Supp Fig. 8**). Finally, γH2AX foci resolve faster in synchronized-irradiated YB1 depleted ONS-76 cells (**Figure 5g**), which is consistent with western blotting (**Figure 4c**).

Figure 5: YB1 depleted cells accumulate less RAD51 foci and more TP53BP1 nuclear bodies during and after S-Phase repair.

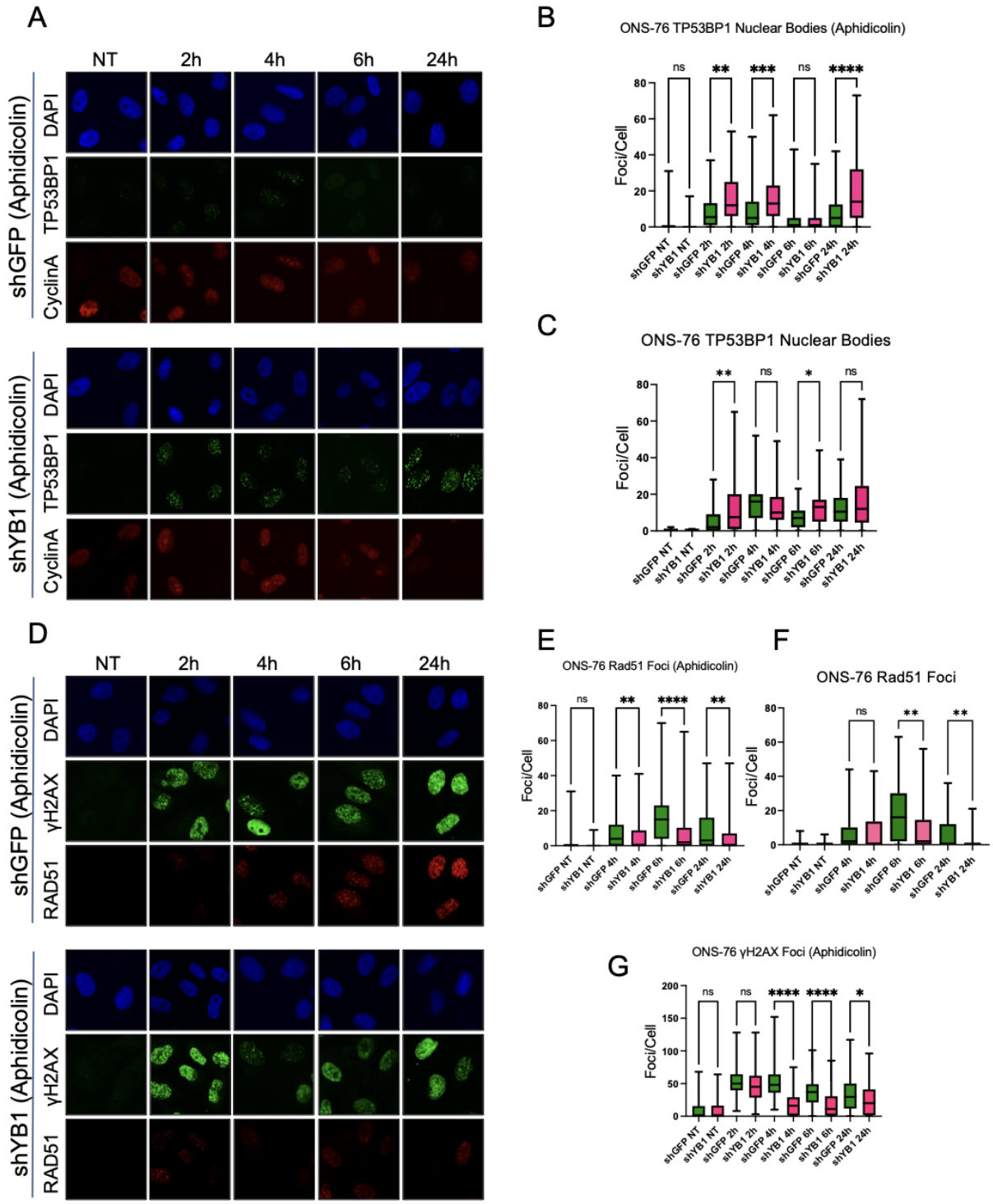

Figure 5: YB1 depleted cells accumulate less RAD51 and more TP53bp1 foci during and after S-Phase repair. (A and B) Aphidicolin S-phase synchronization of shGFP and shYB1 ONS-76 24h prior to radiation at 10Gy results in greater TP53BP1 accumulation in shYB1 cells that is sustained until 6h and reappears at 24h (2h mean rank diff. = -149.0 p=0.0045, 4h mean rank diff. = -168.9 p<0.0004, 6h mean rank diff. = 35.54 p>0.9999, 24h mean rank diff. = -208.7 p<0.0001, n=3 Kruskal-Wallis test). **(C and Supp Fig 8a)** Non-Synchronized ONS-76 exposed to 10Gy results in greater TP53BP1 accumulation in shYB1 cells that is sustained until 24h (2h p=0.0080, 4h p=0.7142, 6h p=0.0117, 24h p>0.9999, n=2 Kruskal-Wallis test). **(D and E)** Aphidicolin S-phase synchronization of shGFP and shYB1 ONS-76 24h prior to radiation at 10Gy results in reduced RAD51 accumulation in shYB1 cells up to 6h and at 24h (4h mean rank diff. = 141.0 p=0.0018, 6h mean rank diff. = 234.9 p<0.0001, 24h mean rank diff. = 135.6 p=0.0087 n=3 Kruskal-Wallis test). **(F and Supp Fig 8b)** Non-Synchronized ONS-76 exposed to 10Gy results in reduced RAD51 accumulation in shYB1 cells up to 6h and at 24h (4h p>0.9999, 6h p=0.0011, 24h p=0.0051, Kruskal-Wallis test n=2). **(D and G)** Aphidicolin S-phase synchronization of shGFP and shYB1 ONS-76 24h prior to radiation at 10Gy results in faster γH2AX resolution up to 6h that reappears in shGFP control at 24h (NT mean rank diff. = 14.48 p>0.9999, 2h mean rank diff. = 82.26 p=0.2664, 4h mean rank diff. = 406.7 p<0.0001, 6h mean rank diff. = 245.9 p<0.0001, 24h mean rank diff. = 125.3 p = 0.0205, n=3 Kruskal-Wallis test).

4.3.6 YB1 depletion results in greater canonical NHEJ and lower HR

To evaluate any changes in canonical NHEJ or HR based repair, we performed distal end joining without indels assay using the EJ7-GFP cNHEJ reporter HEK cell line and Direct Repair HR reporter assay using HEK293 DR-GFP and U2OS DR-GFP cells, respectively. Following double

sgRNA and SCEI transfection, a blunt ended double strand break is formed with a repair mechanism specific for cNHEJ (**Figure 6a)**.[282] We infected EJ7-GFP cells with lentivirus containing either sh scramble, shYB1, or shTP53BP1 as a positive control into EJ7-GFP cells to knock down YB1 or TP53BP1 (**Figure 6b and Supp Fig. 10a)** and subsequently transfected with sgRNAs to induce double strand breaks with blunt ends. Following 72 hours of recovery, YB1 depleted cells show significantly greater levels of percent positive GFP cells while TP53BP1 depleted cells show less compared to control cells (**Figure 6c)**. We infected HEK293-DR-GFP or U2OS DR-GFP cells with lentivirus containing either sh scramble, shYB1, or shCtIP as a positive control to knock down YB1 or CtIP (**Figure 6d and Supp Fig. 10a)** and subsequently transfected with SCEI plasmids to induce double strand breaks. Following 72 hours of recovery, YB1 and CtIP depleted HEK293-DR-GFP and U2OS-DR-GFP cells show significantly lower levels of percent positive GFP cells compared to control (**Figure 6e and Supp Fig 10b and c).** Together, these data support our hypothesis that YB1 depleted cells perform more canonical NHEJ and less HR.

Figure 6: YB1 depletion results in greater canonical NHEJ and lower HR

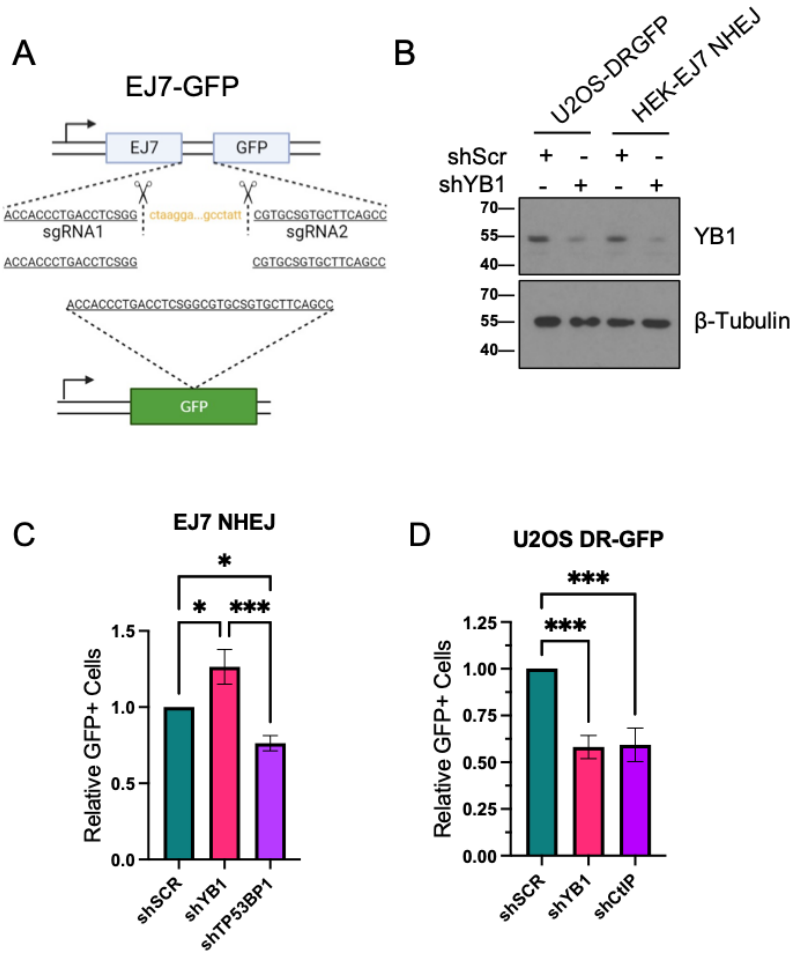

Figure 6: YB1 depletion results in greater canonical NHEJ and lower HR (A) Schematic of distal EJ without indels assay whereby two sgRNAs are co-transfected to generate blunt ends repairable through cNHEJ to restore GFP expression. (B) Western blot of YB1 KD in EJ7-HEK cells and U2OS DR-GFP cells. (C) EJ7 cNHEJ assay (shSCR vs shYB1, 95% CI = -0.46-(-0.07) p=0.0119, shSCR vs shTP53BP1 95% CI = 0.046-0.43 p=0.0197, one-way ANOVA, n=3). (D) U2OS DR-GFP assay (shSCR vs shYB1 95% CI = 0.1975-0.6395 p=0.0006, shSCR vs shCtIP 95% CI = 0.1858-0.6278 p=0.0007, one-way ANOVA, n=2).

4.3.7 YB1 knockdown results in decreased proliferation and increased senescence

We next performed *in vitro* radiation time courses on several MB-derived cell lines and counted cells beyond 48h of radiation. In SHH group cell lines (ONS-76 p53 WT and Pzp53Med p53 Null) the difference in cell counts between non-irradiated control and KD cells is not significant in ONS-76 but is significant in Pzp53Med cells, whereas following radiation there are clear reductions in proliferation of YB1 KD cells and significant increases in doubling time compared to control-irradiated cells for both cell lines (**Figure 7 a1-2 and b1-2**). Immunoblotting of lysates collected following each time course shows changes in markers which corroborate the cell count data. p21, a marker of senescence and p53 activation, is increased in ONS-76 YB1 KD cells treated with 5Gy compared to shSCR (**Supp Fig. 11a**) and, following 5Gy, there is a significant difference in β-gal positive ONS-76 cells, with YB1 depleted cells showing a higher percentage (**Figure 7a3**). YB1 depleted Pzp53Med cells treated with 5Gy have decreased LaminB1 and CyclinD2, markers of senescence and proliferation, respectively, compared to shSCR of the same dose (**Supp Fig. 11c**). In UW228, radiation at 5Gy results in a significant difference in β-gal positive cells, with YB1 depleted cells showing a higher percentage (**Figure 7c).** YB1 also appears to be a major driver of both proliferation and stable repair in Group 3 cell lines (**Figure 7 d1-2 and e1-3**). Following YB1 KD in both D425 and D341 Group 3 cells there is an increase in doubling time of non-irradiated cells which dramatically increases following radiation compared to short-hairpin control cells. For both cell lines, there was a decrease from initial plating number for the shYB1 5Gy group making doubling time incalculable. Immunoblotting of D425 cells shows a similar trend to SHH MB cells where there is a decrease in pRB, a marker of proliferation, and LaminB1 (**Figure 11b**). Altogether, radiation appears to synergize with YB1 depletion in both SHH and Group 3 MB cells to reduce proliferation and promote senescence.

Figure 7: YB1 depletion results in delayed radiation response in SHH and Group 3 Medulloblastoma

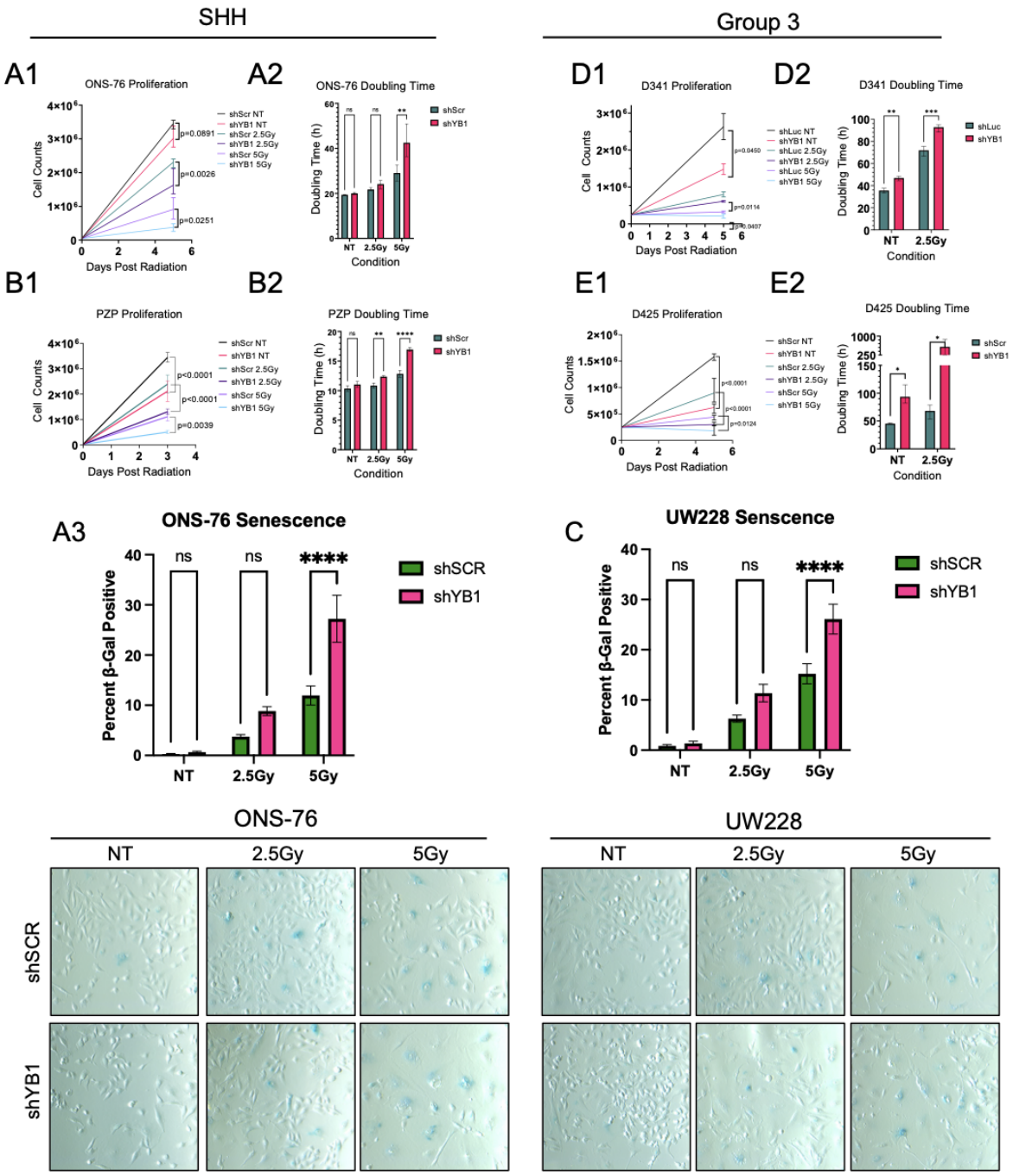

Figure 7: YB1 depletion results in delayed radiation response in SHH and Group 3 Medulloblastoma (**A1**) 5.0e4 ONS-76 cells irradiated at 2.5Gy and 5Gy, harvested after 4 days,

and counted (3.46e6 shSCR NT vs 3.02e6 shYB1 NT p=0.081; 2.31e6 shSCR 2.5Gy vs 1.63e6 shYB1 2.5Gy p=0.0026; 9.10e5 shSCR 5Gy vs 3.79e5 shYB1 5Gy p=0.0251 n=3). (**A2**) Doubling time calculated for ONS-76 (19.4h shSCR NT vs 20.0h shYB1 NT p=0.9942; 21.7h shScr 2.5Gy vs 24.1h p= 0.8034; 29.1h shScr 5Gy vs 42.5h shYB1 5Gy p=0.0015 n=3). (**A3**) β-Gal stain of ONS-76 cells following radiation time course demonstrating increased senescence of YB1 depleted cells compared to irradiated control (5Gy shSCR vs 5Gy shYB1 95% CI = -22.64-(-7.91) p<0.0001 two-way ANOVA n=3). (**B1**) 2.5e4 Pzp53Med cells irradiated at 2.5Gy and 5Gy, harvested after 3 days, and counted (3.45e6 shSCR NT vs 2.12e6 shYB1 NT p<0.0001; 2.42e6 shSCR 2.5Gy vs 1.31e6 shYB1 2.5Gy p<0.0001; 1.11e5 shScr 5Gy vs 5.1e4 shYB1 5Gy p=0.0039 n=3). (**B2**) Doubling time calculated for Pzp53Med (10.34h shSCR NT vs 11.04h shYB1 NT p=0.2149; 10.85h shSCR 2.5Gy vs 12.37h p= 0.0036; 12.84h shSCR 5Gy vs 16.95h shYB1 5Gy p<0.0001 n=3). (**C)** β-Gal stain of UW228 cells following radiation time course demonstrating increased senescence of YB1 depleted cells compared to irradiated control (5Gy shSCR vs 5Gy shYB1 95% CI = -16.75-(-5.09) p<0.0001 two-way ANOVA n=3). (**D1**) 2.5e5 D341 cells plated and irradiated followed by a 5 day incubation period (2.6e6 shLUC NT vs 1.48e6 shYB1 NT p=0.0114; 8.0e5 shLUC 2.5Gy vs 6.13e5 shYB1 2.5Gy p=0.0450; 3.3e5 shLUC 5Gy vs 2.1e5 shYB1 5Gy p=0.0407 n=3). (**D2**) Doubling time for D341 (35.50h shLUC NT vs 46.78h shYB1 NT p=0.0074; 71.83h shLUC 2.5Gy vs 92.76h p=0.0001 n=3). (**E1**) 2.5e5 D425 cells plated and irradiated followed by a 5 day incubation period (1.58E6 shSCR NT vs 6.25E5 shYB1 NT p<0.0001; 8.97e5 shSCR 2.5Gy vs 3.02e5 shYB1 2.5Gy p<0.0001; 4.43e5 shSCR 5Gy vs 1.85e5 shYB1 5Gy p=0.0124 n=3). (**E2**) Doubling time for D425 (45.2h shSCR NT vs 93.7h shYB1 NT p=0.0281; 68.1h shSCR 2.5Gy vs 575.4h p=0.0140 n=3). All comparisons performed using 2-way ANOVA, see **Supp Fig. 11** for growth and doubling times statistics.

4.4 Discussion

Here we extend our previous findings of YB1 as a driver of cell proliferation in SHH MB to include Group 3 MB and we demonstrate that in both MB subgroups, YB1 appears to promote a more stable, HR-based mechanism of repair that is required for appropriate IR-induced damage signaling. In the past, a role for YB1 in the radiation response was inconsistent and lacked a functional outcome. Many studies have placed emphasis on the importance of YB1 proteolytic cleavage for nuclear entry and functionality.[283] However, in our SHH cells, cleavage does not appear to be required for nuclear entry or functionality as exemplified by full length nuclear and chromatin fraction YB1. Additionally, there is a decrease in YB1 S102 phosphorylation following radiation of MBCs (not shown), a phospho-site implicated in regulation of nuclear entry and driving DNA-binding and oncogenic phenotypes.[284–286] Thus, our data are in keeping with previous reports of YB1 being constitutively active in SHH MB through S102 phosphorylation and nuclear entry even in the absence of exogenous insult or proteolytic cleavage, while the decreased post-radiation phosphorylation is likely a result of checkpoint activation and cell cycle exit.

We show that silencing YB1 alongside radiation likely forces MB cells to use a repair method that is more rapid and less amenable to mitotic catastrophe and apoptosis up to 48h following IR, as exemplified by accelerated γH2AX reduction, enhanced repair of DNA double strand breaks, and a lack of multinucleation and re-accumulation of γH2AX in knockdown cells at 24h. However, while silencing YB1 allowed for faster recovery up to 48h, there is an expense to viability beyond 48h. It is also known that NHEJ can be faster than HR and that Rad51 and RPA32 S4/8 are positive markers of HR.[275,287] On the contrary, TP53BP1 and RIF1 can inhibit early repair events such as

end resection through CtIP inhibition.[281] Altogether, depleting YB1 may drive the cells to utilize a faster and a more NHEJ reliant repair pathway resulting in genomic instability and the reduced proliferation seen 3-5 days following irradiation as exemplified through less RAD51 foci, lower RPA32 phosphorylation, more TP53BP1 nuclear bodies, and more RIF1 foci in YB1 depleted cells. On the other hand, some factors may impact the accumulation and recognition of damage. In fact, damage accumulation may be contingent upon chromatin compaction, thereby affecting damage resolution. While YB1 is implicated in maintaining an open chromatin state which could make DNA more vulnerable to damage,[288] this does not appear to be the case as all non-synchronized cells accumulated comparable levels of γH2AX and single and double strand breaks 15 min following IR damage.[289–291]

Finally, patients with SHH-activated and *TP53* mutant MBs have a worse outcome likely due to the necessity of p53 for radiation and chemotherapy-induced apoptosis.[292] Even though Pzp53Med are p53 null and Daoy, UW228, and D425 cells are p53 mutated, all demonstrate differential repair kinetics between control and knockdown cells similar to ONS-76, MBC, and D341 cells, all of which are *TP53* WT. Indeed, depleting YB1 in Pzp53Med and D425 cells still results in lower rates of proliferation compared to control 3 and 5 days following IR damage, respectively. Secondarily, 24hrs following IR, Daoy YB1 KD cells do not re-accumulate γH2AX compared to control, a phenotype seen in ONS-76 and D341. While binding and inhibition of p53 by YB1 was previously reported, our data suggests p53 is not required for YB1 KD MB cell radiation response; however, whether YB1 binds and inhibits p53 in WT cells to promote survival is unclear.[248,293] Additionally, MYC amplification, a biomarker for poor outcome in Group 3 MB patients, is present in D425 and D341 cells, both of which respond favorably to YB1 KD in combination with radiation treatment. Given that cMYC was recently shown to synergize with Chk1 inhibition likely

due to replication-driven genomic instability, the proliferation decrease in non-irradiated cells following YB1 KD could result from a similar requirement for DNA repair signaling to maintain genomic stability, which is further exacerbated by radiation.[55] Taken together, our data point to YB1 as a potential therapeutically relevant target in both SHH and Group 3 MB not only because YB1 drives proliferation, but also because YB1 participates in the DNA damage response to ionizing radiation.

4.5 Materials and methods

IHC on Human Samples

All methods were carried out in accordance with Emory University's Institutional Review Board relevant guidelines and regulations**.** De-identified patient tumor samples were provided by the Neuropathology Department of Children's Healthcare of Atlanta and studies performed on the patient tumor tissues received ethical approval by and were carried out in accordance with Emory University's Institutional Review Board (IRB Protocol #00045406). All human tissues were obtained after informed consent. Immunohistochemistry on paraffin embedded and sectioned samples was performed using a standard procedure. For this, slides were deparaffinized, dehydrated and antigen retrieval was performed using Tris-EDTA Buffer, pH 9.0 (Abcam). Tissues were blocked with 5% goat serum and stained followed by DAB.

Animal Studies

All animal experimental protocols were conducted in accordance with the Emory University Institutional Animal Care and Use Committee guidelines after approval from IACUC, protocol number PROTO201700740 (AMK)**.** NeuroD2-SmoA1[294,295] and BL6 mice were obtained from

Jackson Laboratories. For survival studies 1.5e5cells/2uL of MBCs were suspended in PBS and injected into p5 BL6 pups.

NeuroD2-SmoA1 primary cell culture:

MBCs were isolated from NeuroD2-SmoA1 mouse tumors and cultured as described previously.[294,295] Cells were seeded on Matrigel (Corning) coated plates with Neurobasal medium containing penicillin/streptomycin, 1 mmol/L sodium pyruvate, 1x B27 supplement, and 2 mmol/L L-glutamine. Primary MBCs were cultured for 4h with 10%FBS prior to media change to No FBS at which point Lentivirus or Adenovirus were added with an incubation time of 48h prior to experiment initiation or 24h prior to re-implantation into BL6 mice.

Cell Lines:

Mouse MB cell line Pzp53Med (p53 null, murine derived[269]) was a generous gift from Dr. Matthew Scott (Stanford). Human MB cell line D341 was obtained from ATCC. ONS-76 (p53 wildtype), Daoy (p53 Mut), and UW228 (p53 Mut) were a gift from Dr. Tobey MacDonald (Emory University), and D425 MB cell line is a gift of Dr. Eric Raabe (Johns Hopkins). For the purposes of this study Pzp53Med, ONS76, UW228, and DAOY are classified as SHH and D341 and D425 are classified as Group 3. ONS-76, UW228, and Pzp53Med cells were cultured in DMEM/F12 with 10% FBS. Daoy was cultured in EMEM supplemented with 10% FBS and D341 was cultured in EMEM supplemented with 20% FBS. D425 was cultured in DMEM supplemented with 10%FBS and Glutamine. Control shRNA constructs consisted of shscramble (shSCR), shGFP, and shLuciferase (shLUC). YBX1 knockdown in human cell lines was performed using TRCN0000315309 (referred to as shYB1_09) or TRCN0000315307 (referred to as shYB1_07)

and knockdown in mouse cells was performed using TRCN0000333885 (referred to as shYB1_85) or TRCN0000077210 (referred to as shYB1_10) from Millipore Sigma. For overexpression of YB1 in primary mouse cells, replication competent adenovirus was purchased from Vector Biolabs (ADV-276442) and amplified in HEK 293T cells prior to repeated freeze thaw lysis.

Source of HEK293T cells

HEK293-EJ7-GFP cells were a gift of Dr. David S. Yu (Emory University) originally obtained from Jeremy Stark (City of Hope).[32] U2OS-DR-GFP and HEK293-DR-GFP were a gift of Dr. David S. Yu (Emory University) originally obtained from Jeremy Stark (City of Hope). HEK293T packaging cells were a gift of Dr. Shubin Shahab obtained originally from ATCC (American Type Culture Collection).

Western Blotting

Tissues or cells were homogenized and lysed in RIPA lysis buffer with protease inhibitors cocktail, and phosphatase inhibitors. A total of 15–30 ug of each sample was denatured and separated on 14% SDS-PAGE gels, then transferred to immobilon-P membranes (Millipore). For quantification purposes, chemiluminescent signals of post-translational modifications were normalized to total protein prior to normalization to β-Tubulin. **For blots of the same molecular weight, two blots were run with the same samples without stripping of blots. All blots were trimmed at the specified molecular weights prior to probing with primary antibodies based on sizing determined from previous literature. Blots were imaged using ECL and X-ray film. For western blotting of irradiated samples, all samples within one blot were X-rayed simultaneously followed by time course harvesting.** The following antibodies were used: YB1

(D299 CST), γH2AX (immunofluorescence: MA1-2022 Thermo Fisher, Immunoblotting/Immunofluorescence: D7T2V CST), H2AX (D17A3 CST), CyclinD2 (sc-56305 SCBT), Chk1(2G1D5 CST), pChk1 Ser317 (D12H3 CST), Chk2 (D9C6 CST), pChk2 Thr68 (C13C1 CST) , β-Tubulin (sc-166729 SCBT), α-Tubulin (#2144 CST), GAPDH (D16H11 CST), p21 (12D1 CST), LaminB1 (D4Q4Z CST), pRb Ser780 (D59B7 CST), Rb (D20 CST), TP53BP1 (A300-273A Bethyl Labs), Rad51 (PC130 Calbiochem), CyclinA (611268 BD Biosciences), RIF1 (A300-569A Bethyl), LaminA/C (4777 CST). Acronyms: CST - Cell Signaling Technology, SCBT - Santa Cruz Biotechnology.

Radiation Dosing

Cell models were irradiated in a cell line dose-dependent manner chosen based on evaluation of IR phenotypic effects up to 48h and beyond 48h. ONS-76 and Daoy were treated with 10Gy for time courses leading up to 48h or 2.5Gy or 5Gy for time points beyond 48h. PZP, D341, and D425 were treated with 2.5Gy and 5Gy for both experiments leading up to 48h and beyond 48h. MBCs were treated with 2Gy for all experiments.

EJ7 NHEJ and DR-GFP assay

Distal EJ without indels assay in HEK293 EJ7 line: HEK293 EEJ7 cells were infected with either shScr or shYB1 lentivirus. Twenty-four hours later, media was removed, and cells were transfected with 3 ug I-SceI and 2 ug of both sgRNA7a and sgRNA7b plasmids. Forty-eight hours later, cells were harvested, washed twice with PBS, resuspended in PBS and subjected to flow cytometry (Aurora Cytek) for GFP fluorescence. To measure cNHEJ efficiency, the percentage of GFP positive cells (c-NHEJ positive) was analyzed using the FlowJo software**.** U20S DR-GFP or

HEK293 DR-GFP cells were plated in 10 cm dishes and the next day transfected with the shRNA of interest. After twenty-four hours, cells were transfected with 5 ug I-SceI plasmid. Seventy-two hours later, cells were harvested, washed twice with PBS, resuspended in PBS and subjected to flow cytometry (Aurora Cytek) for GFP. To measure HR efficiency, percentage of GFP positive cells (HR positive) was analyzed using the FlowJo software. For DR-GFP assay biological replicates are presented separately with three technical replicates each.

Cell Synchronization Experiments

Cells were seeded into 10cm dishes or 24 well dishes for 24h prior to addition of Aphidicolin (Final concentration 10ug/mL) with an incubation time of 24h. Media was replaced 10 minutes prior to irradiation.

Flow Cytometry

Cell cycle analysis was performed using the Click-iT™ EdU Alexa Fluor™ 647 Flow Cytometry Assay Kit (ThermoFisher) according to the manufacturer's protocol. Briefly, cells were incubated with 10 uM EdU for 1 hour prior to trypsinization and staining with LIVE/DEAD™ Fixable Aqua Stain (ThermoFisher). Cells were washed twice with PBS and then fixed and permeabilized using the BD Cytofix/Cytoperm™ (BD Biosciences) kit. Cells were then stained using the ThermoFisher Alexa Fluor™ 647 EdU azide and Propidium Iodide (Biolegend). Samples were analyzed on a Beckman Coulter CytoFLEX flow cytometer. All flow analysis was performed using FlowJo (TreeStar). Doublets were gated out for primary analysis and included as separate information.

Immunofluorescence and Analysis

Cells were fixed for 10 minutes in fresh 4% Formaldehyde (made fresh from PFA) prior to 3x wash with PBS. Cells were permeabilized with 0.3% Triton X-100 and blocked with 0.5% Bovine Serum Albumin and 3% Normal Goat Serum. Primary Antibody was added overnight at 4C and secondary was added for 1h at RT. Cell imaging was performed on the Olympus FV1000 at the Emory University Integrated Cellular Imaging Core. Quantification analysis for all foci was performed using CellProfiler software with one set of parameters for all images specific to each image set. A minimum of three images were acquired per condition for all images presented throughout the paper. For biological replicates data was combined prior to statistical analysis.

Comet Assay

Cells were seeded into a 24 well plate 24h prior to irradiation. Cells were then trypsinized, inactivated with media containing 10% FBS, centrifuged, and resuspended in 0.5% low melt agar prior to aliquoting onto comet slides. Electrophoresis was performed according to the Trevigen Comet Assay kit (cat# 4250-050-K). A minimum of three images were acquired per condition per biological replicate. All conditional pairs (NT, 15min, 6hr) were imaged using the same acquisition parameters (Gain and Exposure time) prior to quantification using Open Comet plugin for ImageJ or Cell Profiler.

Data Availability Statement (Single Cell Sequencing)

Single cell sequencing data was obtained from the UCSC cell browser https://d33sxa6bpqwi51.cloudfront.net/ by searching expression data for *YBX1*.

Statistical Analysis

Statistical comparisons were performed using GraphPad Prism. 2-way ANOVA were used for Flow Experiments, cell count, and doubling time comparisons. 1-way ANOVA was used for β-Galactosidase comparisons. For non-gaussian datasets, including comet assays and foci counts, Kruskal-Wallis test is used. For densitometry, ratio-paired t test was used. Bar graphs plot SEM and box and whisker plots contain data range with Tukey plots where applicable.

Acknowledgements

We thank Drs. David Yu, Jennifer Spangle, Andrew Hong, and Wei Zhou for their assistance and valuable feedback on experimental design and insight. shGFP and shLUC control constructs were gifts of Dr. Andrew Hong. We thank Dr. Eric Raabe for donating D425 cells. We thank Dr. Gaurav Naishadh Joshi for assistance on Confocal Microscopy. This work was supported by NINDS R01NS110386 (AMK), NCI Winship Cancer Institute P30 Center Grant CA138292 (AMK, TJD, CCP), Alex's Lemonade Stand Foundation and CURE Childhood Cancer Foundation (CCP).

Author Contributions: LFM, CP, RHSJ, SKR, and AMK designed and/or executed experiments. LFM wrote the manuscript. VC, TH, AD, JR, GAP helped to execute experiments. All authors read and approved of this manuscript.

Data Availability Statement: The authors confirm that the data supporting the findings of this study are available within the article [and/or] its supplementary materials.

Supplemental Data

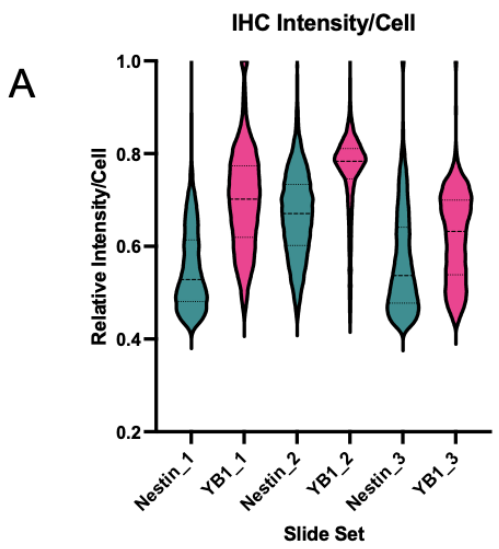

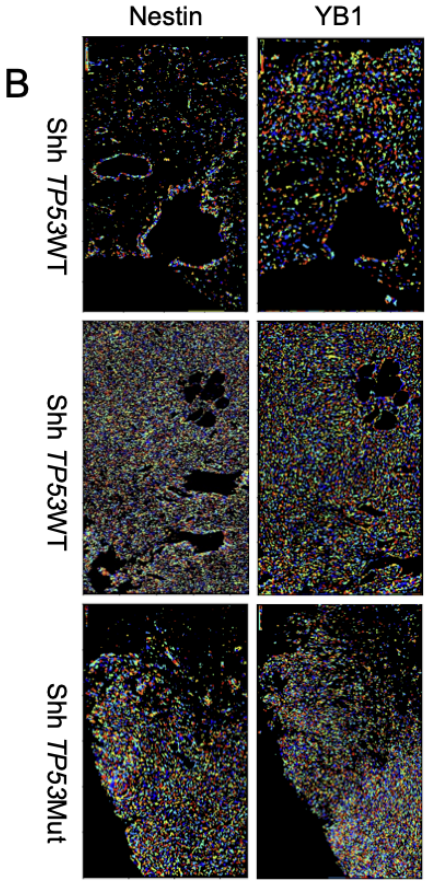

Supplementary Figure 1: (A) Quantification of cell intensity in MB patient IHC samples (Figure 1) using Cell Profiler. Cells above chosen threshold (0.4) are shown in multicolor **(B)**. **(C)** Previously published single cell sequencing of MYC-driven p53 dominant negative Group 3 spontaneous mouse model (GP3-Myc-dnP53) with cell populations corresponding to active cell cycling active cell cycling (MP-A1, -2), progenitor (MP-B1,-B2, -B3), and differentiated neoplastic cell populations (MP-C1, -C2).

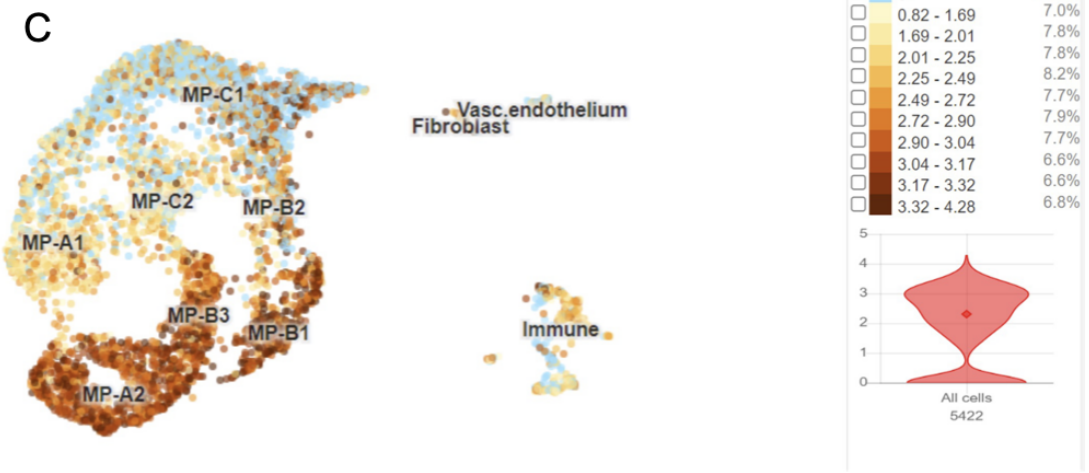

Condition	Sub G1	G0/G1	S	G2/M
shGFP NT	1.46	78.10	9.86	9.87
shYB-1 NT	0.80	77.53	6.01	13.47
shGFP 10 Gy (24 Hours)	1.81	85.33	1.11	9.88
shYB-1 10 Gy (24 Hours)	1.12	80.90	1.39	14.90
shGFP 10 Gy (48 Hours)	4.79	81.07	1.11	11.72
shYB-1 10 Gy (48 Hours)	1.37	81.60	1.87	13.63

Condition	Sub G1	G0/G1	S	G2/M
shGFP NT	0.70	0.89	3.70	2.63
shYB-1 NT	0.47	3.00	3.63	1.70
shGFP 10 Gy (24 Hours)	1.09	10.57	0.61	7.70
shYB-1 10 Gy (24 Hours)	0.79	0.82	0.62	2.14
shGFP 10 Gy (48 Hours)	2.65	6.55	0.78	3.16
shYB-1 10 Gy (48 Hours)	1.20	3.72	1.68	2.83

Comparison	Sub-G1	Doublets
NT	-2.400 to 3.713	-5.030 to 6.230
10 Gy (24 Hours)	-2.366 to 3.746	-2.764 to 8.497
10 Gy (48 Hours)	0.3602 to 6.473	3.303 to 14.56

Supplementary Figure 2: Percent averages across three independent experiments of ONS-76 cell cycle analysis for shGFP and shYB1 cells non-irradiated and irradiated at 10Gy (**Figure 2**). Cell cycle phase on x axis and cell condition on y axis. Mean of cell cycle (**Top**), SD of cell cycle (**Middle**). (**Bottom**) 95% CI for comparisons in Figure 2 C and D.

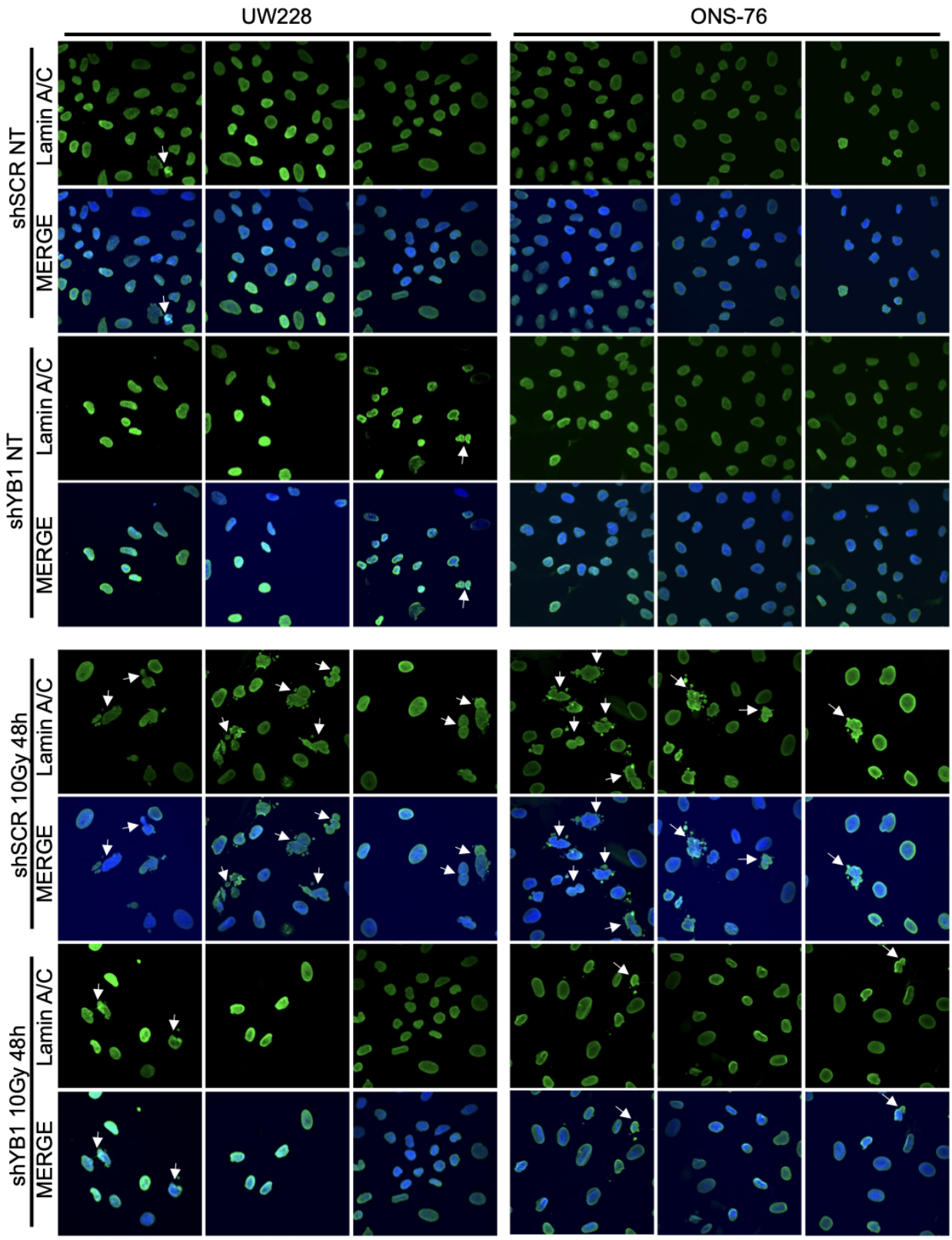
UW228
ONS-76
shSCR NT
Lamin A/C
MERGE
shYB1 NT
Lamin A/C
MERGE
shSCR 10Gy 48h
Lamin A/C
MERGE
shYB1 10Gy 48h
Lamin A/C
MERGE

Supplementary Figure 3: Representative images of nuclear envelope (stained with LaminA/C) in ONS-76 p53wt (**Right**) and UW228 p53Mut (**Left**) following 10Gy irradiation. Following 24 or 48 hours for UW228 and ONS-76, respectively, there is increased aberrations in nuclear morphology in shSCR cells compared to shYB1.

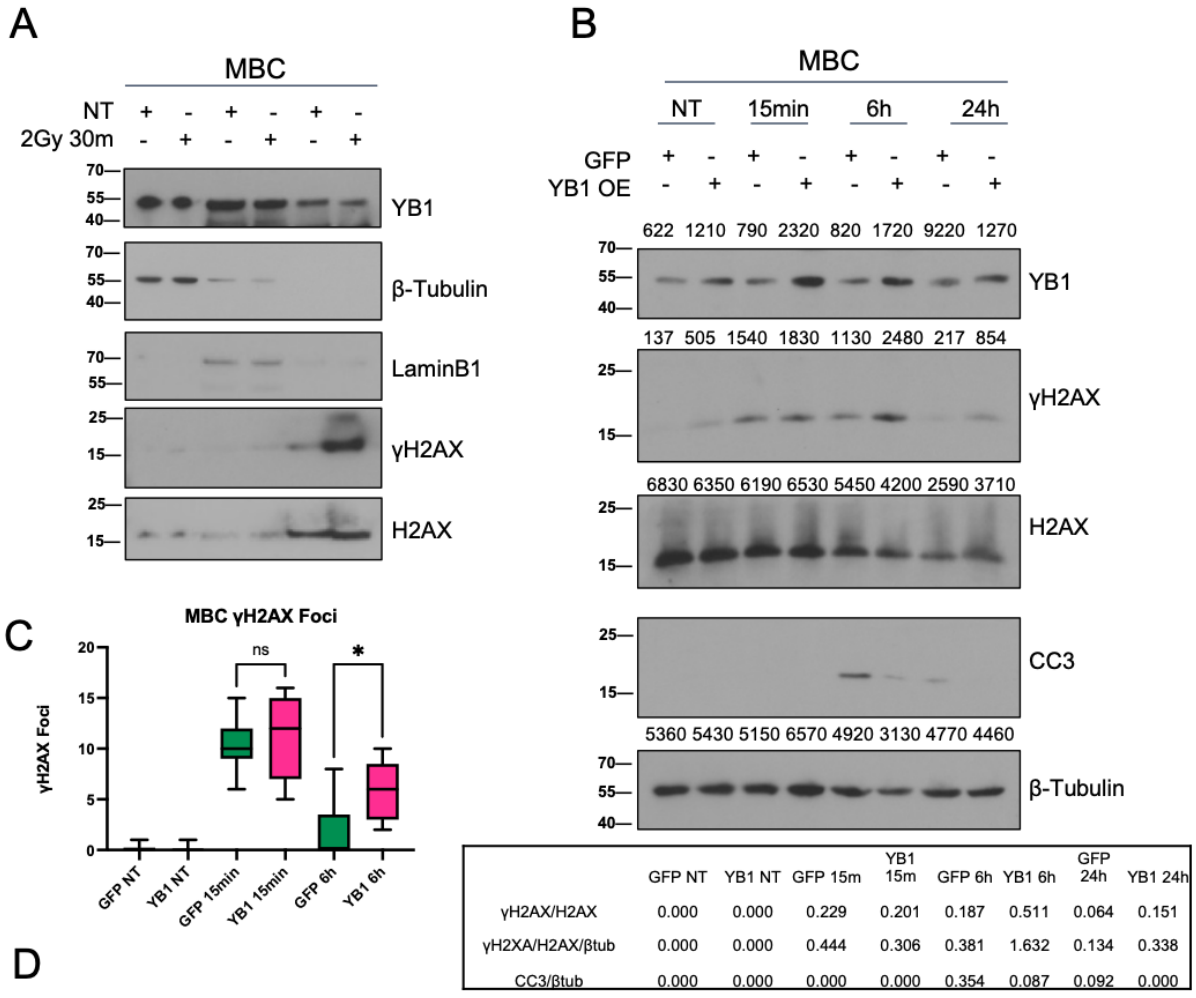

	GFP NT	YB1 NT	GFP 15m	YB1 15m	GFP 6h	YB1 6h	GFP 24h	YB1 24h
γH2AX/H2AX	0.000	0.000	0.229	0.201	0.187	0.511	0.064	0.151
γH2XA/H2AX/βtub	0.000	0.000	0.444	0.306	0.381	1.632	0.134	0.338
CC3/βtub	0.000	0.000	0.000	0.000	0.354	0.087	0.092	0.000

Supplementary Figure 4: (A) Primary MBCs, non-treated and treated with 2Gy 30min following 24h of plating, fractionated into cytoplasmic, nuclear, and chromatin. β-Tubulin (Cytoplasm), LaminB1 (Nucleus), and H2AX (Chromatin), serve as the fraction controls. **(B)** Densitometry of MBC YB1 OE time course at 2Gy (Figure 3) with either normalization to H2AX or H2AX and β-tubulin. NT density was subtracted from each condition within group. **(C)** Representative IF of MBCs irradiated with 2Gy show similar levels of γH2AX foci accumulation at 15min but a difference in resolution at 6h (GFP NT SEM = 0.11, YB1 NT SEM = 0.083, GFP 15min SEM = 0.7519, YB1 15min SEM = 1.16, GFP 6h SEM = 0.72, YB1 6h SEM = 0.78, GFP 6h vs YB1 6h p=0.0354 mean rank diff. = -19.38, Kruskal-Wallis test, n=1). **(D)** Daoy cell time course western blot of YB1 KD cells showing persistence of γH2AX in shGFP at 24 hours following 10Gy radiation.

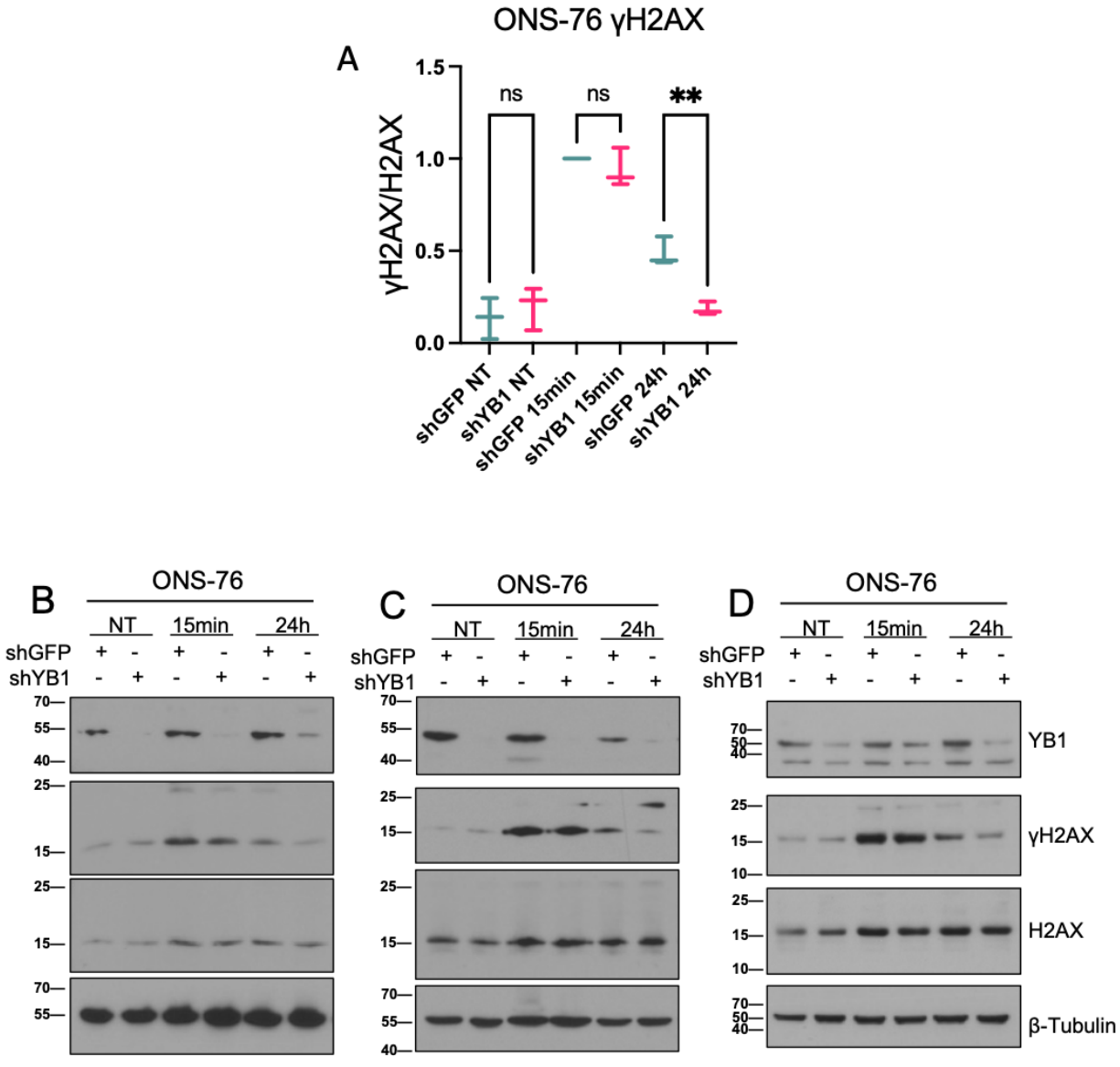

Supplementary figure 5: (A) Densitometry of three biological replicates of ONS-76 time courses for cells treated at 10Gy **(B-D)** normalized to shGFP 15min (shGFP vs shYB1 24h 95% CI = 0.1086-0.4971 p=0.0030, Ordinary one-way ANOVA, n=3).

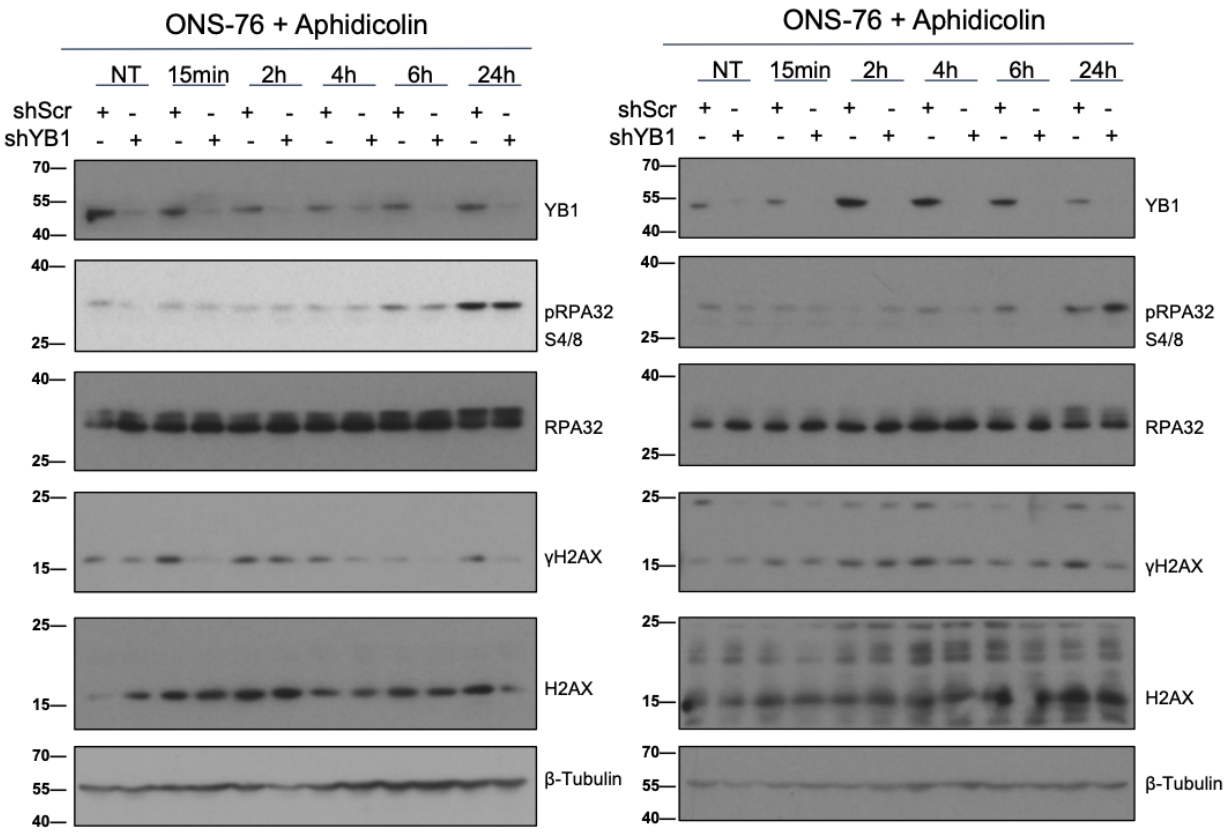

Supplementary Figure 6: (B and C) biological replicates of ONS-76 Aphidicolin experiments for RPA32 Densitometry (Figure 4)

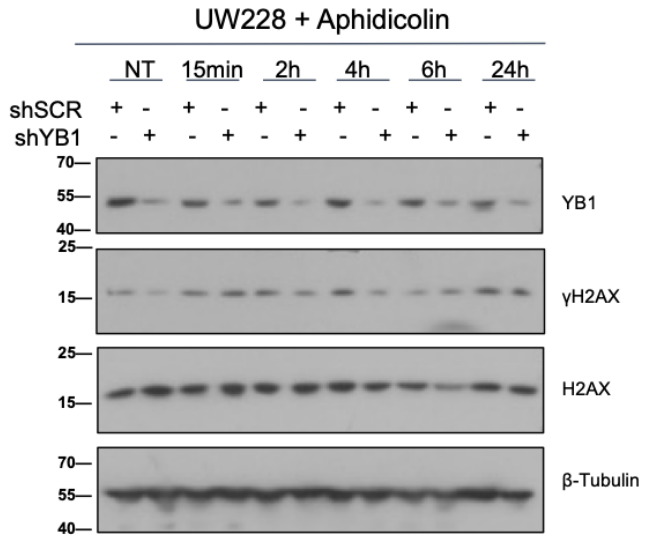

Supplementary Figure 7: 10Gy radiation of UW228 shSCR and shYB1 cells following S-phase synchronization with aphidicolin.

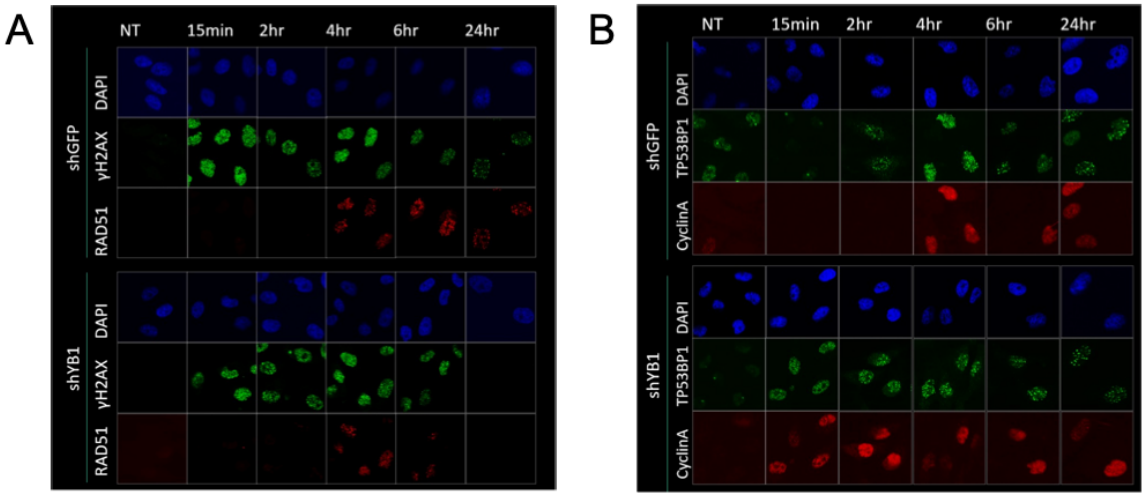

Supplementary Figure 8: (A) Non-Synchronized ONS-76 exposed to 10Gy results in greater TP53BP1 accumulation in shYB1 cells that is sustained until 24h (stats in main paper). **(B)** Non-Synchronized ONS-76 exposed to 10Gy results in reduced RAD51 accumulation in shYB1 cells up to 6h and at 24h (stats in main paper).

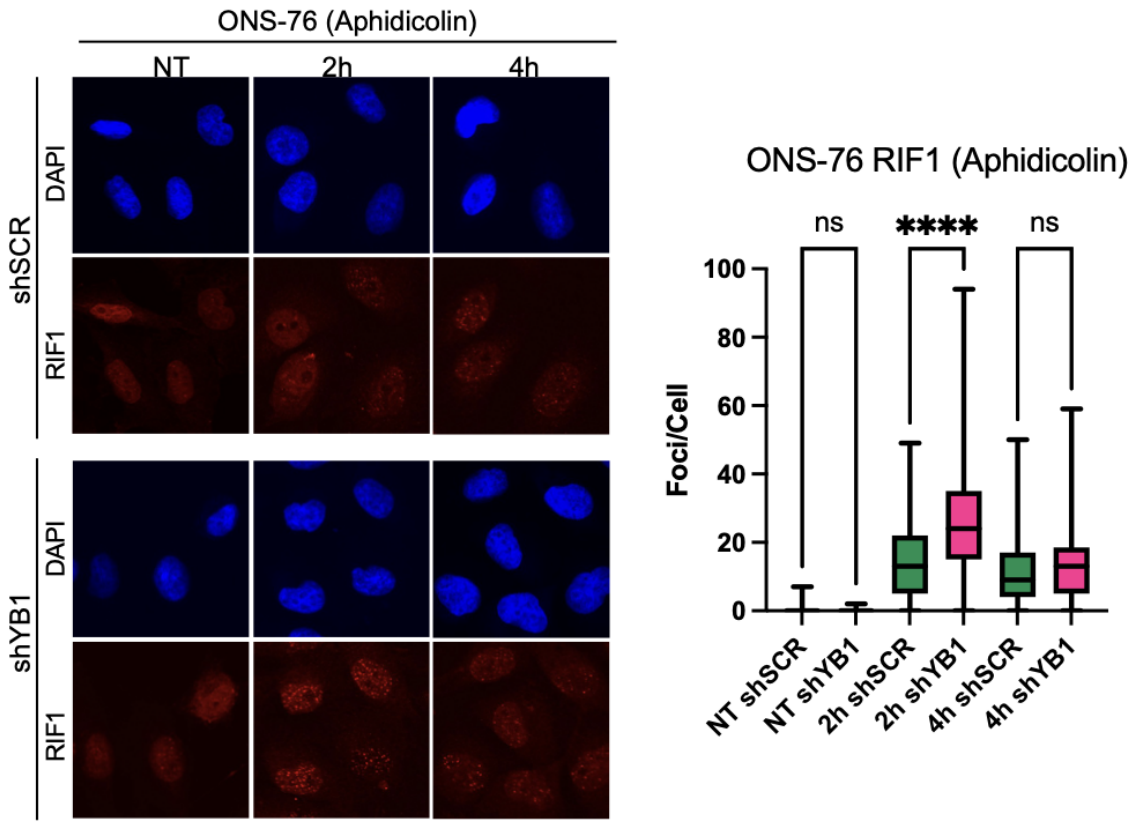

Supplementary Figure 9: 10Gy irradiation of S-phase synchronized ONS-76 shows greater RIF1 foci formation following YB1 depletion at 2 hours compared to control irradiated (2h mean rank diff. = -140.6 $p<0.0001$, 4h mean rank diff. = -47.75 $p=0.2346$, Kruskal-Wallis test n=3).

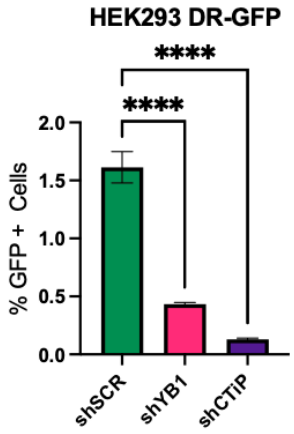

Supplementary Figure 10: (B) Three technical replicates of DR-GFP assay in 293T cells showing reduced induction of GFP in YB1 depleted cells following SCEI mediated cleavage compared to control with shCtIP as a positive control (shSCR vs shYB1 95% CI = 1.02-1.34 $p<0.0001$, shSCR vs shCTiP 95% CI = 1.32-1.65 $p<0.0001$, one-way ANOVA n=1).

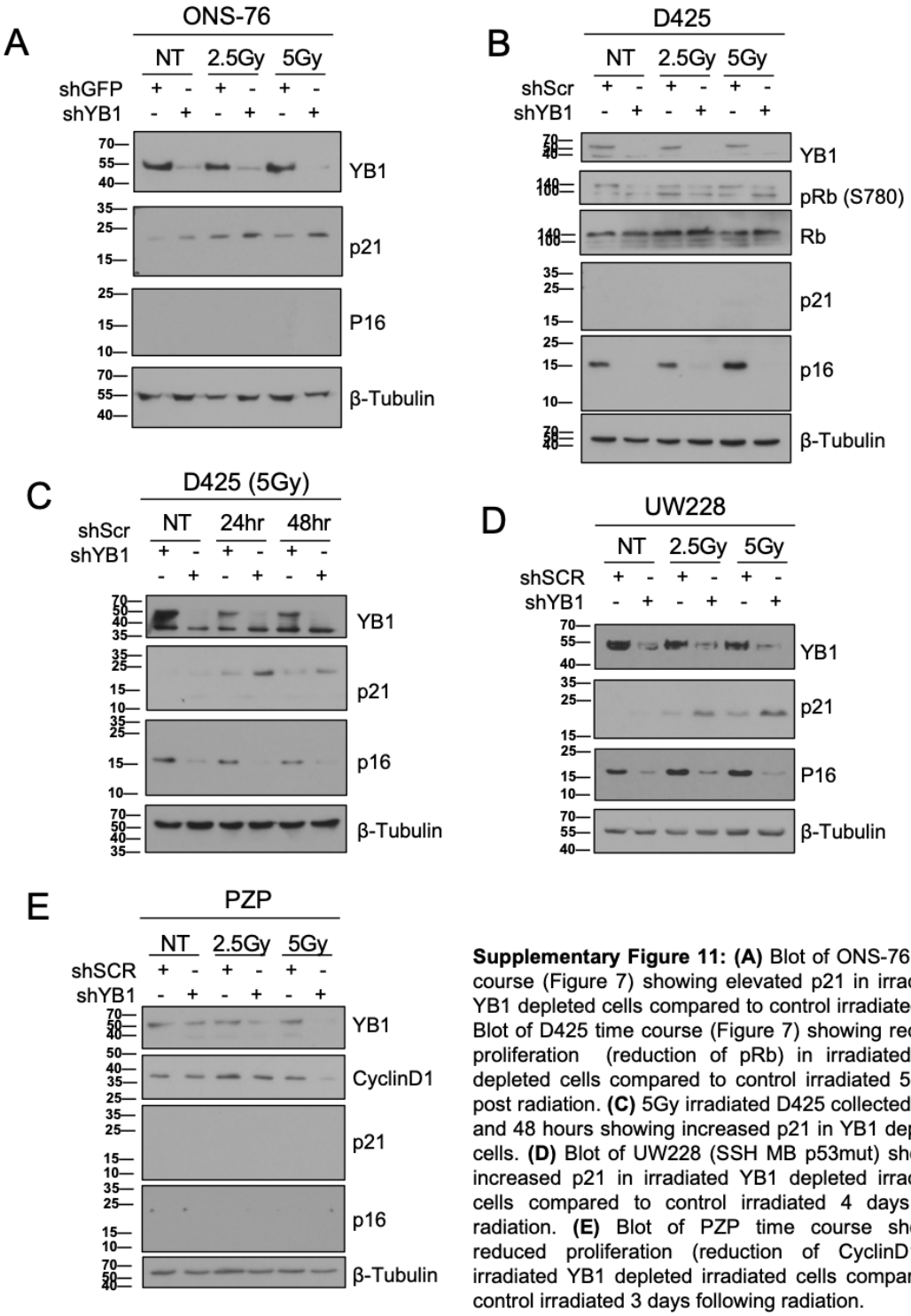

Supplementary Figure 11: (A) Blot of ONS-76 time-course (Figure 7) showing elevated p21 in irradiated YB1 depleted cells compared to control irradiated. **(B)** Blot of D425 time course (Figure 7) showing reduced proliferation (reduction of pRb) in irradiated YB1 depleted cells compared to control irradiated 5 days post radiation. **(C)** 5Gy irradiated D425 collected at 24 and 48 hours showing increased p21 in YB1 depleted cells. **(D)** Blot of UW228 (SSH MB p53mut) showing increased p21 in irradiated YB1 depleted irradiated cells compared to control irradiated 4 days post radiation. **(E)** Blot of PZP time course showing reduced proliferation (reduction of CyclinD1) in irradiated YB1 depleted irradiated cells compared to control irradiated 3 days following radiation.

ONS-76 Growth

Tukey's multiple comparisons test	Mean Diff.	95.00% CI of diff.	Summary	Adjusted P Value
shScr NT vs. shYB1 NT	439583	-43173 to 922340	ns	0.0891
shScr 2.5Gy vs. shYB1 2.5Gy	679167	196410 to 1161923	**	0.0026
shScr 5Gy vs. shYB1 5Gy	531250	48494 to 1014006	*	0.0251

ONS-76 Doubling Time

Tukey's multiple comparisons test	Mean Diff.	95.00% CI of diff.	Summary	Adjusted P Value
NT	-0.6633	-8.577 to 7.250	ns	0.9942
2.5Gy	-2.393	-10.31 to 5.520	ns	0.8034
5Gy	-13.45	-21.36 to -5.533	**	0.0015

PZP Growth

Tukey's multiple comparisons test	Mean Diff.	95.00% CI of diff.	Summary	Adjusted P Value
shScr NT vs. shYB1 NT	1333333	888467 to 1778200	****	<0.0001
shScr 2.5Gy vs. shYB1 2.5Gy	1087917	643050 to 1532783	****	<0.0001
shScr 5Gy vs. shYB1 5Gy	603333	158467 to 1048200	**	0.0039

PZP Doubling Time

Tukey's multiple comparisons test	Mean Diff.	95.00% CI of diff.	Summary	Adjusted P Value
NT	-0.6933	-1.688 to 0.3014	ns	0.2149
2.5Gy	-1.513	-2.508 to -0.5186	**	0.0036
5Gy	-4.11	-5.105 to -3.115	****	<0.0001

D341 Growth

Tukey's multiple comparisons test	Mean Diff.	95.00% CI of diff.	Summary	Adjusted P Value
shScr NT vs. shYB1 NT		0.3291 to 0.9692	*	0.045
shScr 2.5Gy vs. shYB1 2.5Gy		0.6798 to 0.8681	*	0.0114
shScr 5Gy vs. shYB1 5Gy		0.4117 to 0.9521	*	0.0407

D341 Doubling Time

Tukey's multiple comparisons test	Mean Diff.	95.00% CI of diff.	Summary	Adjusted P Value
NT	-11.28	-18.94 to -3.630	**	0.0074
2.5Gy	-20.94	-28.59 to -13.28	***	0.0001

D425 Growth

Tukey's multiple comparisons test	Mean Diff.	95.00% CI of diff.	Summary	Adjusted P Value
shScr NT vs. shYB1 NT	959167	744528 to 1173805	****	<0.0001
shScr 2.5Gy vs. shYB1 2.5Gy	594167	379528 to 808805	****	<0.0001
shScr 5Gy vs. shYB1 5Gy	257500	42862 to 472138	*	0.0124

D425 Doubling Time

Tukey's multiple comparisons test	Mean Diff.	95.00% CI of diff.	Summary	Adjusted P Value
NT	-48.52	-478.8 to 381.8	ns	0.978
2.5Gy	-507.3	-937.6 to -77.03	*	0.025

Supplementary Figure 12: List of all comparisons for Figure 7 showing Mean Difference, 95% confidence interval, and adjusted p value.

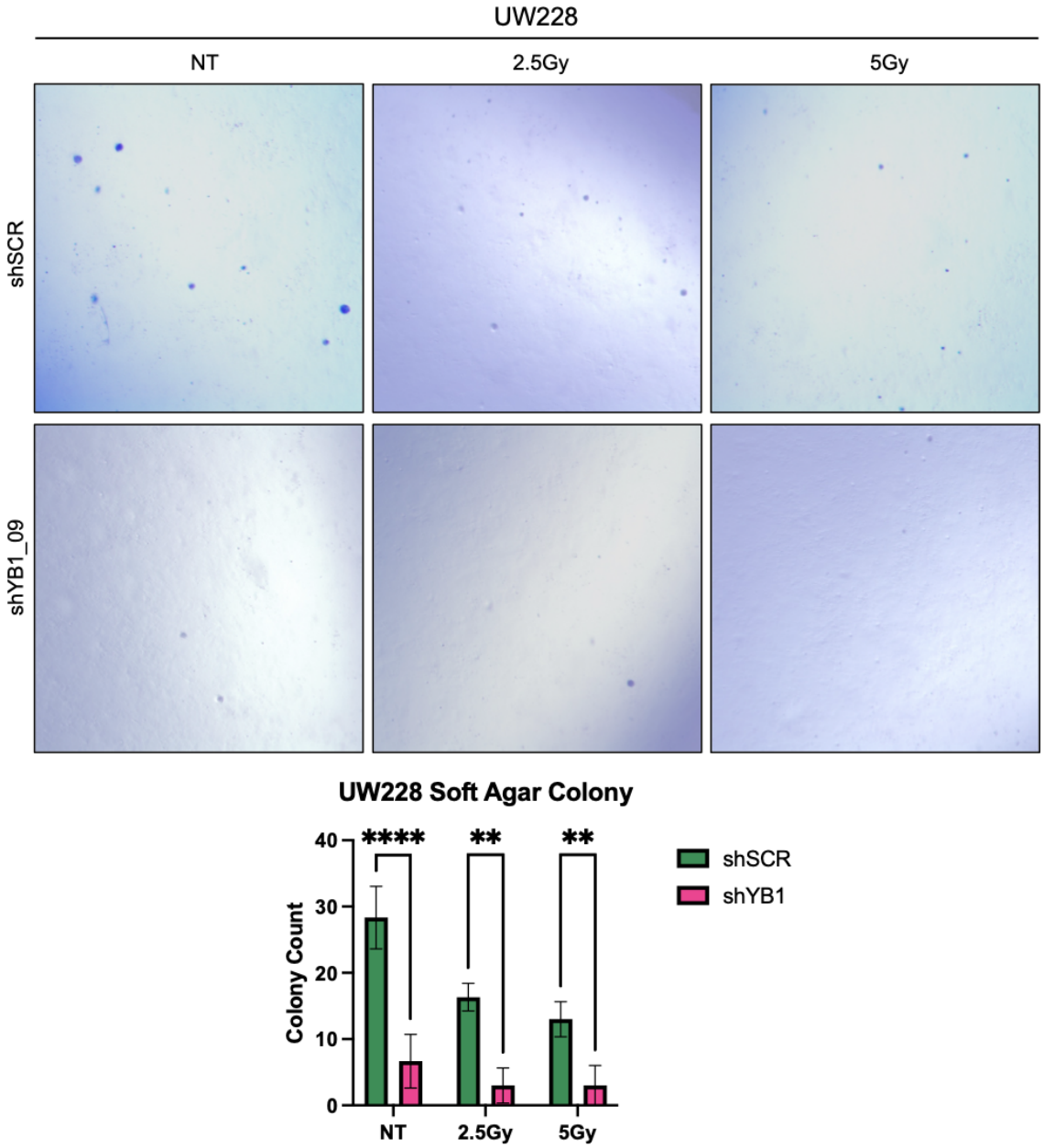

Supplementary Figure 13: Soft Agar Colony Formation assay of UW228 showing differences in colony formation that decreases proportional to the radiation dose (shSCR NT vs shYB1 NT 95% CI = 14.16-29.17 p<0.0001, shSCR vs shYB1 2.5Gy 95% CI = 5.831-20.84 p=0.0011, shSCR vs shYB1 95% CI = 2.498-17.50 p=0.0092 n=3 2-way ANOVA).

Chapter 5

PlexinD1 and Sema3E in Development and Disease

5.1 Abstract

Plexins and Semaphorins are a group of transmembrane and secreted proteins responsible for mediating a range of developmental processes consisting primarily of proliferation and migration. Numerous studies are published on semaphorin-plexin signaling as drivers of axonal and vascular guidance molecules, both promoting and inhibiting cell migration with context dependent downstream signaling. In the developing cortex, PlexinD1 and Sema3E are crucial for appropriate neuron proliferation and axon patterning. Alternatively, retinal developmental vascularization is driven by the repulsive forces resulting from binding of Sema3E to PlexinD1. PlexinD1 can also colocalize with VEGFR2 to modulate endothelial cell proliferation for appropriate vascularization. On the other hand, the switch from repulsion to attraction is complex, and results from a combination of Neuropilin-1 - PlexinD1 colocalization or Sema3E cleavage prior to secretion. Binding of cleaved Sema3E to PlexinD1 or binding of full length Sema3E to an NRP1/PlexinD1 receptor complex can drive the proliferative-metastatic behavior of cancer cells seemingly hijacking developmental programing. Here we review the relevant literature for Sema3E, NRP1, PlexinD1, and VEGFR2 interactions as drivers of development and cancer cell proliferation and migration.

5.2 Discovery and structure of PlexinD1

Authors Tamagnone and Comoglio are pioneers in the search for Plexin family members; and in 1999, the group published a seminal work identifying novel members and their respective sequences. Using RT-PCR for partial known sequences to PlexinB1, PlexinA2, and PlexinA1, the group then utilized the GENIE and HEXON predictive algorithms to identify PlexinD1 and PlexinB3.[296] Shortly thereafter, investigations into the spatio-temporal expression of PlexinD1 laid the foundation for understanding PlexinD1 signaling in the developing central nervous system. Following a 2001 study characterizing expression of PlexinD1 in the endothelial cells and dentate gyrus of developing embryos, Zwaag et al. isolated full length PlexinD1 through Rapid Amplification of cDNA Ends (RACE) PCR,[297,298] from which the group established putative protein domains based on predictive sequences already established in the literature:

> "PLXND1 contains all the domains that are present in plexin family members: a sema-domain, three Met-related sequences (MRS), three glycine/proline-rich motifs, a single transmembrane domain, and two highly conserved intracellular domains together known as the SEX-plexin (SP) domain (Tamagnone et al., 1999). PLXND1 differs from other plexins in the third MRS motif, which contains only six of the eight conserved cysteines normally encountered in a MRS."

The finalized structure of PlexinD1 can be seen in **Figure 1**.[299] PlexinD1 consists of an extracellular region responsible for interacting with dimerized semaphorin proteins, a hydrophobic transmembrane domain, and an intracellular region primarily characterized by the GTPase activating domain which binds activated GTP-bound guanine nucleotide-binding proteins to stimulate their GTPase activity.

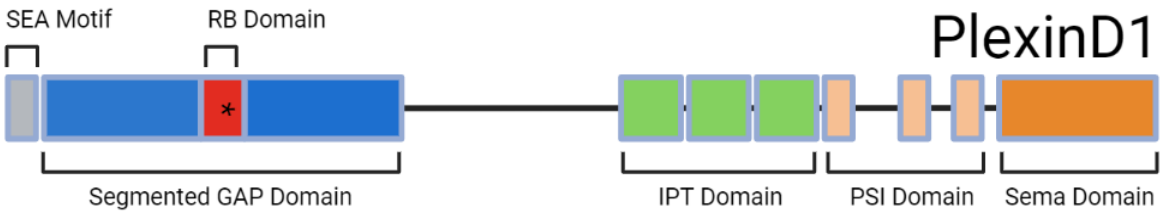

Figure 1: PlexinD1 Structure

PlexinD1 consists of 5 protein domains and 1 motif. The extracellular component of PlexinD1 consists of a Sema-PSI (Plexin-Semaphorin- Integrin) domain that is responsible for binding semaphorin proteins and an IPT (Immunoglobulin-Plexin-Transcription Factor) domain. The intracellular component of PlexinD1 consists of a segmented GAP (GTPase Activating Protein) domain, an RBD (RHO-GTPase Binding Domain), and a SEA (Serine-Glutamine-Alanine) motif.

Following structural characterization of PlexinD1, using *in situ* hybridization, the group laid the foundation for future work by mapping the expression of PlexinD1 RNA in the CNS. PlexinD1 was found to be expressed in neocortex below leptomeninges, cranial and spinal ganglia, striatum, rostral part of the hippocampal area, and the external granular layer of the cerebellum (EGL). Of significance to our studies was the expression of PlexinD1 in the EGL of developing cerebellum, which implicates PlexinD1 as a driver of cerebellar development and, potentially, medulloblastoma.

5.3 PlexinD1-Sema3E during development: attraction and repulsion

One of the predominant PlexinD1 expression patterns observed in the 2001 and 2002 studies mentioned previously is in the endothelial cells of embryonic developing vasculature. This finding extends into numerous other studies investigating the phenotypic consequences of endothelial PlexinD1 expression. Knockdown of PlexinD1 in a zebrafish developmental model results in extensive branching and irregular patterning of fish trunk vasculature.[300] Unlike future findings, the expression of Sema3A was found to modulate the repulsive vascular patterning during zebrafish development. Semaphorin 3E, the more commonly known binding partner of PlexinD1, was initially found to bind and modulate PlexinD1 activity in the mouse retina model for studying angiogenesis, when vessels sprout from pre-existing vasculature.[301,302] In this model, VEGF drives PlexinD1 expression, and Sema3E-PlexinD1 signaling regulates VEGF induced Notch signaling, resulting in less branching and an uneven growth front. Interestingly, Sema3E is expressed ubiquitously in the developing eye, however; it is the spatio-temporal expression of PlexinD1 which regulates vascularization, a phenotype conserved during avian ocular development.[303] In the same vein, while PlexinD1 is the predominant signaling receptor for Sema3E, it does not act alone. Both Neuropilin-1 and VEGFR2 colocalize and signal through PlexinD1 to switch signaling between repulsion and attraction. Colocalization of PlexinD1 with these co-receptors in the presence of full-length semaphorins typically results in a pro-migratory phenotype, however, this semaphorin isoform dependent (**Figure 2**). Tamagnone et al. published a similar signaling paradigm in the same year establishing a relationship between VEGF and PlexinD1 showing that Notch, whose expression can be regulated by VEGF, drives PlexinD1 expression through promoter binding. This would imply a VEGF → Notch → PlexinD1 signaling axis potentially stymied by inhibiting VEGF signaling (e.g. Bevacizumab) or Notch signaling (e.g. RIN1, CB103, and Furin Inhibitors).[304,305]

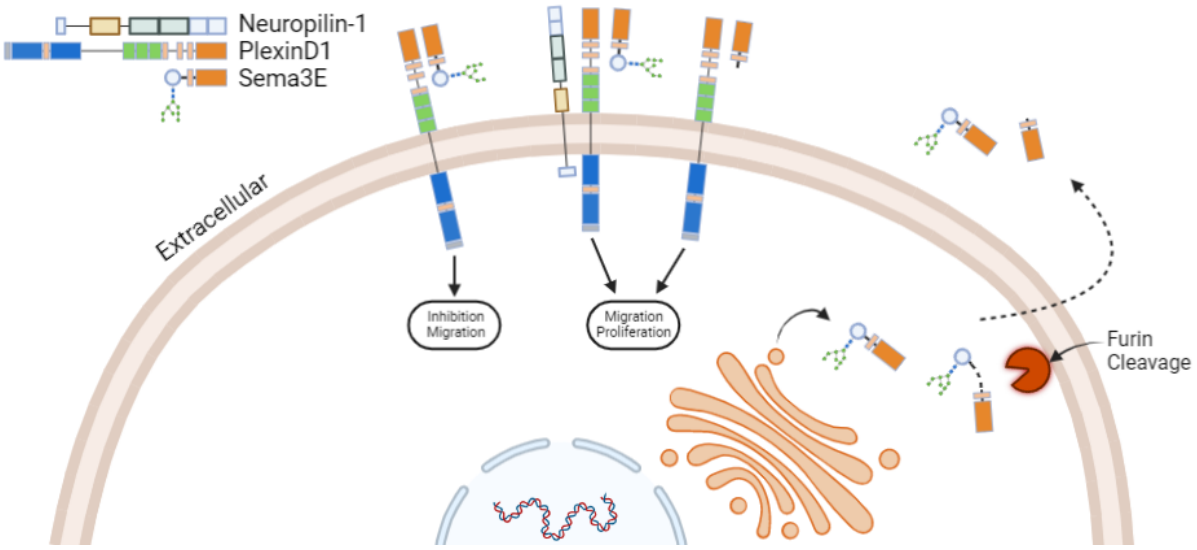

Figure 2 Functional interactions between PlexinD1, NRP1, and Sema3E

When full-length Sema3E binds PlexinD1 in isolation, the result is typically a repulsive or migration inhibitory effect. Binding to a PlexinD1/NRP1 complex can result in a migratory phenotype. Sema3E can be cleaved by Furin to produce a 62kDa and 25kDa fragment which can also be glycosylated in the golgi prior to secretion. Binding of the cleaved form to PlexinD1 in isolation is sufficient to induce migration. VEGFR2 can also colocalize with PlexinD1 to facilitate VEGFR2 signaling even in the absence of VEGF (Not Shown).

On the contrary, in the setting of retinopathy Sema3C can signal through NRP1 and PlexinD1 to disrupt endothelial tip cell formation and vascular branching.[306] The combinatorial effects of receptor colocalization and semaphorin isoform presence can give rise to seemingly contradictory phenotypes and, as mentioned previously, developmental guidance by PlexinD1 is not limited to vasculature. PlexinD1 mRNA is ever-present during axonal patterning of the CNS, as exemplified by early *in situ* hybridization studies. Even from very early stages of neuronal migration from

birthplace to final destination, PlexinD1 downregulation results in reduction of somal translocation and an increase in filopodial protrusions.[307] PlexinD1/NRP1/VEGFR2 colocalization is another common theme in the developing CNS. In corticofugal neurons between cortex and subcortex and striatonigral neurons of the striatum, Sema3E acts as a repellent when binding PlexinD1 in the absence of NRP1. Upon colocalization in subicular neurons, however, Sema3E acts as an attractant.[308] Furthermore, when VEGFR2 colocalizes with NRP1 and PlexinD1 in subicular neurons of the developing forebrain, once Sema3E is added, VEGFR2 becomes tyrosine phosphorylated leading to the activation of AKT.[309] These data would support the previous finding whereby spatial colocalization of VEGFR2/NRP1/PlexinD1 followed by Sema3E binding impacts switching between repulsion and attraction independent of the VEGF ligand. While the exogenously applied Sema3E in these studies does not appear to be cleaved, which would result in a repulsive behavior when bound to isolated PlexinD1, the cleavage status of Sema3E endogenous to the subiculum or cortex is unclear. Moreover, Sema3E cleavage appears to play a more prominent role in cancer where cells may hijack developmental signaling to mediate migration and metastasis through these signaling axes.

5.4 PlexinD1-Sema3E in cancer

The sometimes paradoxical phenotypes resulting from PlexinD1-Sema3E signaling that are so crucial to development also manifest in cancer. Not only can the migratory and proliferative phenotypes associated with Sema3E depletion diverge, many of the studies interrogating the PlexinD1 signaling axes do not present sufficient data on the Sema3E cleavage variant expressed

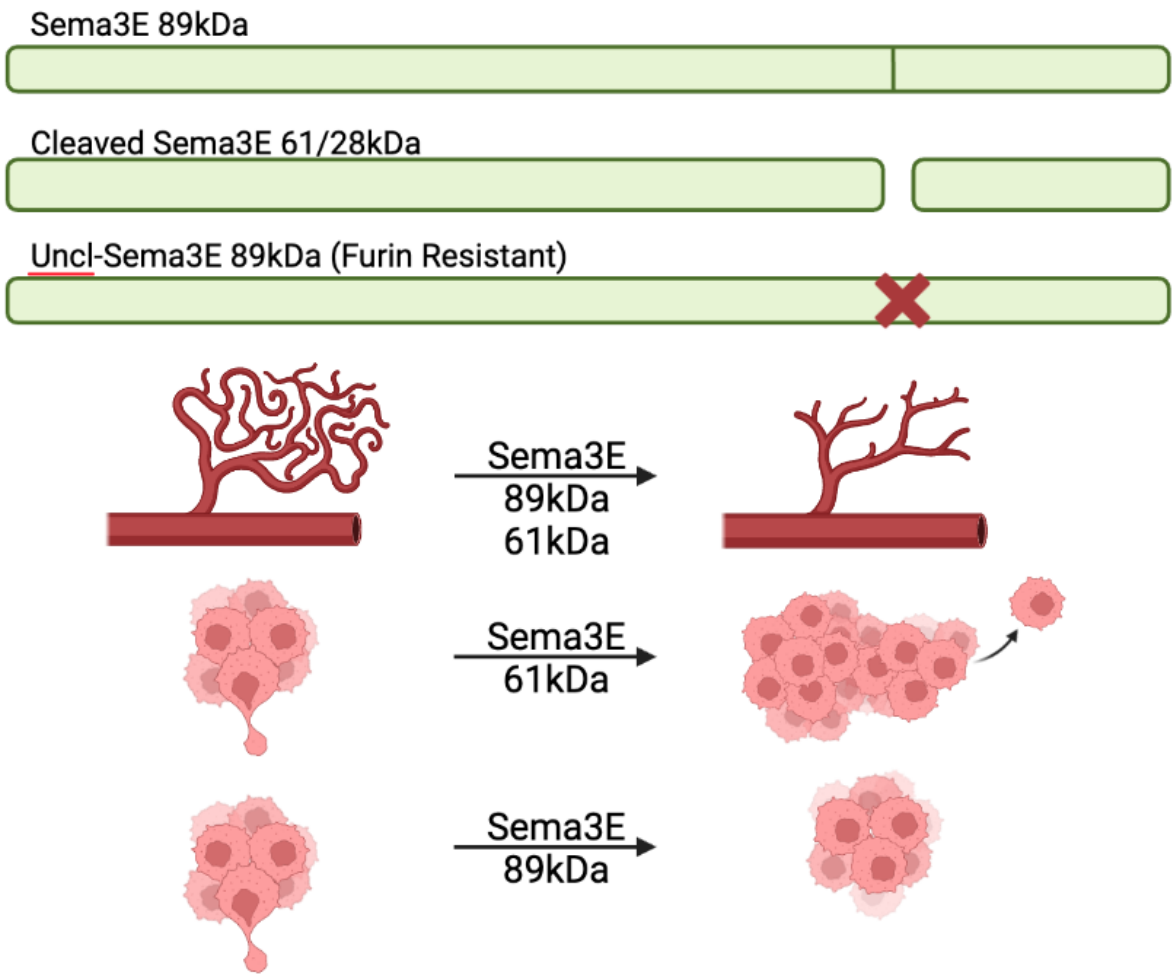

Figure 3: Sema3E Cleavage Sites and Cleavage Phenotype Model

Sema3E protein is detected on immunoblots between 28-100kDa. Furin cleavage resistance results in full length Sema3E either at 89 or 100kDa, indicating glycosylation for cell secretion. In epithelial cells Sema3E inhibits vascular density and cell migration. In cancer cells, p61 Sema3E promotes migration while full length Sema3E inhibits migration and proliferation.

in their tumor models (**Figure 3**). Additionally, early studies on PlexinD1 expression in development and cancer rely heavily on mRNA levels which we demonstrate in chapter 6 to not necessarily be correlative with protein levels due to translational regulation of PlexinD1 by YB1.

In 2010, the Tamagnone group, who discovered PlexinD1, observed a positive correlation between PlexinD1 and Sema3E mRNA and metastasis by comparing mRNA levels between non-metastatic and metastatic positive melanoma patients and their metastases.[310] For this study, the majority of Sema3E was expressed at ~61kDa (p61) with Sema3E or PlexinD1 depletion reducing metastases while having little to no impact on tumor growth. PlexinD1 expression was also required for implantation of UV administered tumor cells. On the other hand, ectopic Sema3E expression reduced vascular density in tumors and reduced tunneling and proliferation of HUVECs, which is more in line with angiogenic phenotypes seen during development. A positive correlation between tumor grade and sema3E expression was also shown in ovarian endometrioid cancer.[311] From this study, cells with higher levels of Sema3E mRNA exhibited faster wound closure and transwell migration while inhibition of the Furin protease, responsible for cleaving Sema3E, resulted in reduced migratory distance. Sema3E high cells were also found to have elevated phosphorylation of AKT and ERK1/2 with migratory phenotype in Sema3E high cells abrogated by Wortmanin or PD98059, inhibitors of PI3K and ERK1/2, respectively.

In the case of endothelial cells, Sema3E binding induces activation of PIP5K1β resulting in PIP2 production, activation of GEP100, exchange of GDP for GTP in Arf6, and the disassembly of F-actin resulting in cytoskeletal collapse regardless of Sema3E cleavage.[312,313] In cancer cells, however, p61 Sema3E promotes the migration of cancer cells by signaling through PI3K/AKT and ERK1/2, while full length Sema3E inhibits cancer cell migration (**Figure3**). The Tamagnone group progressed this narrative by developing a furin resistant Sema3E, called Uncl-Sema3E.[314] Following Uncl-Sem3E exposure in HUVECs, phosphorylation of FAK and ERK1/2 and F-actin assembly are reduced, while exposure in breast or lung cancer cells results in reduced pERK and

migration. Of significance, the effect of p61 on tumor proliferation was highly variable across cell lines with some experiencing a reduction in metastasis and proliferation. Interestingly, in our own cell lines, depletion of full length Sema3E still results in a reduction of wound closure with inconsistencies in EMT shift (Chapter 6). This phenotypic variability across cancer types could be attributed to differences in NRP1 or VEGFR2 binding with PlexinD1 which can alter the effect of full length Sema3E on migration. Unfortunately, the expression and colocalization characteristics of PlexinD1 and its binding partners are neglected in many studies, preventing any meaningful conclusions. Cancer cell secretion of Sema3E and induction of EC collapse concomitant with an increase in migration and metastasis of cancer cells is unexpected and contradictory. However, hypoxia induction caused by endothelial cell collapse could be driving cancer cell migration as HRE-containing genes, particularly HIF1α, are activated.[315]

An additional PlexinD1 binding partner not present in developmental literature, TGFβRII, can dimerize with PlexinD1 to activate cell proliferation and migration. In Hepatocellular carcinoma, double positive IHC for PlexinD1 and TGFβRII is correlative with worse overall survival compared to only TGFβRII high only, PlexinD1 high only, or PlexinD1/TGFβRII double negative which had the best overall survival.[316] In PDAC, Co-IP of PlexinD1 shows TGFβPII binding and depletion of PlexinD1 abrogates TGFβ mediated Smad3 phosphorylation which is required for TGFβRII signaling.[317] More importantly, a PlexinD1 binding peptide engineered to disrupt PlexinD1/TGFβRII signaling followed from this study and showed potent anti-proliferative properties. The anti-migratory, anti-proliferative effects of this peptide are conserved in our studies (chapter 6). Following peptide binding, there is a potential to disrupt all interactions between

PlexinD1 and its known binding partners, TGFβRII, NRP1, and VEGFR2. This presents a clinically translational option for targeting PlexinD1.

5.5 Discussion

From angiogenic and neuronal guidance to migration and EMT, PlexinD1 boasts a range of developmental and oncogenic phenotypes that are only further complicated by differences in binding partners, including NRP1, VEGFR2, TGFβRII, and its canonical ligands Sema4A and Sema3E. Sema3E, the only secreted semaphorin, creates a microenvironment more prone to hypoxia through paracrine signaling between tumor and epithelial cells. The autocrine effect of Sema3E amongst tumor cells reinforces the migratory phenotypes associated with hypoxia responsive genes resulting from epithelial cell collapse and vascular regression. While binding peptides for disruption PlexinD1 signaling are promising for ameliorating these pro-oncogenic phenotypes, implementation of anti-metastatic drugs into the clinic remains challenging due to mets already being present when patients seek treatment. In the case of medulloblastoma, however, administration of anti-metastatic drugs as part of the standard of care could drastically improve outcomes for patients who relapse with mets, which typically results in a dismal prognosis (Chapter 1).

Chapter 6

YB1 Regulates PLXND1 Translation to Modulate Migration and EMT in SHH Medulloblastoma

Author's Contribution and Acknowledgment of Reproduction

This chapter is reproduced with edits from an unpublished manuscript in progress.

LFM and AMK contributed to the conception, design, and methodology of the study. AMK sponsored the study. LFM, VC, and GZ performed experiments.

6.1 Abstract

Y-Box Binding Protein 1 (YB1) is a pleiotropic oncogene capable of DNA and RNA binding through a cold shock domain (CSD) allowing it to function as a transcription factor and RNA binding protein. By performing RNA Binding protein immunoprecipitation sequencing (RIPseq) on RNAs bound by YB1 followed by YB1 silencing, we found PlexinD1 to be bound and positively translationally regulated. Plexins and Semaphorins are a group of membrane bound and secreted proteins implicated in cell migration and proliferation, regulating developmental programs such as axonal guidance and angiogenesis. MB cells are capable of hematogenous and cerebral spinal fluid (CSF) mediated metastasis and patients who present with metastasis faire substantially worse, regardless of subgroup. Here we show that upon silencing YB1, PlexinD1 protein levels decrease without changes in mRNA levels, and PlexinD1 protein levels are highly elevated in the tumor tissue of NeuroD2-SmoA1 mice. Additionally, silencing PlexinD1 leads to changes in epithelial to mesenchymal (EMT) programming and a reduction in migration potential. We then show that Sema3E, a secreted semaphorin capable of binding PlexinD1, is also preferentially expressed in tumor tissue and binds to Neuropilin-1 and PlexinD1 to mediate a migratory and proliferative phenotype. Upon Sema3E silencing, cells have reduced migration and proliferation. Thus, we have uncovered a novel YB1 → PlexinD1 signaling axis activated by NRP1 and Sema3E binding in the setting of Medulloblastoma.

6.2 Introduction

Medulloblastoma (MB), a tumor of the cerebellum, accounts for nearly 20% of all childhood brain tumors with a 75%-90% survival rate for standard and low risk patients following standard of care, which includes resection, radiation, and chemotherapy.[10] Unfortunately, patients who relapse with metastasis have a fairly dismal prognosis with an overall survival of less than 1 year.[20] In the past, we found YB1 to drive cerebellar granular neural precursor cell (CGNP) and Sonic Hedgehog (SHH) MB cell proliferation, implicating YB1 in cerebellar development and SHH MB tumor progression, respectively.[201] Y-box binding protein 1 is a multifaceted oncogene driving tumor initiation, growth, and therapeutic resistance in multiple brain tumors.[262] The cold-shock domain gives YB1 the ability to bind DNA and facilitate transcription or DNA repair or to bind RNAs either to stabilize itself or regulate translation.[318] YB1 was shown to regulate its own translation in addition to transcripts crucial to disease progression and metastasis, such as HIF1α.[191,223] Here we nominate PlexinD1 as a novel target for YB1 to regulate post-transcriptionally, with developmental and oncogenic implications.

PlexinD1 is a single pass transmembrane protein that binds in trans or cis to a number of other proteins including co-receptors NRP1, VEGFR2, and TGFβRII or its canonical ligands Sema4A and Sema3E.[299,317] In development, PlexinD1 is robustly expressed throughout the central nervous system and modulates the guidance of neurons, particularly in the cortex.[307] In corticofugal and striatonigral neurons, Sema3E is a repellant while in subicular neurons it is an attractant due to differences in co-receptor expression.[308,309] In developing vasculature of the eye and zebrafish, Sema3E provides repulsive cues and in HUVECs drives cytoskeletal collapse.[302,303,310] The secretion of Sema3E paired with preferential expression of PlexinD1 can create a complex,

hypoxic microenvironment that promotes tumor cell migration. In its cleaved ~61kDa form, Sema3E can promote cell migration in breast, colon, and ovarian cancer, while in its full length 89-100kDa form, Sema3E inhibits tumor cell migration.[310,311] Furthermore, a furin protease inhibitor resistant form of Sema3E, Uncl-Sema3E, was found to inhibit tumor cell proliferation and migration, creating a potential therapeutic window.[314]

Here we investigate a YB1 → PlexinD1 signaling axis responsible for mediating SHH MB migration through the post-transcriptional regulation of PlexinD1 mRNA. We characterize the published PlexinD1 binding partners and Sema3E cleavage variants in our models and integrate a recently developed PlexinD1 binding peptide to inhibit PlexinD1 migratory and proliferative signaling.[317]

6.3 Results

6.3.1 PlexinD1 is enriched in YB1 RIPseq of primary murine SHH MB cells

To understand what RNAs YB1 may regulate from the MB transcriptome through RNA binding we performed three independent RNA Binding Protein Immunoprecipitations (RIP) of primary cells derived from NeuroD2-SmoA1 SHH mouse model tumors. Cells were plated for 24 hours prior to RIP, RNA cleanup, and subsequent sequencing. Differential expression analysis was performed between RIP input RNA and RIP enriched RNA and plotted as a partial volcano plot showing RNA fold change over input, with only positively enriched RNAs plotted for a total of 1198 significantly enriched RNAs (**Figure 1c**). YB1 was chosen as a positive control to ensure successful RIPseq due to auto-binding and translational regulation. Indeed, YB1 is the second most

enriched target in the RIPseq with a Log2 fold change of 1.16 and adjusted p value of 9.44e-10. We also performed Gene Set Enrichment Analysis on input alone to assess the health and identity of primary cells once isolated (**Figure 1b**). Even upon isolation, primary MB cells show enriched Sonic Hedgehog signaling. Because of recent interest in Plexin-Semaphorin and Plexin-Neuropilin signaling in tumor biology and the role of PlexinB2 in cerebellar development, we chose to investigate PlexinD1, which ranked 9th on the scale of most significantly enriched with a fold change of 1.22 and an adjusted p value of 1.61e-7.[319] We then validated our RIPseq using standard PCR of cDNA generated from RIP to avoid amplification and detection of non-specific SYBR green signal with primers directed to YB1, PlexinD1, and Actin as a control (**Figure 1d**). YB1 and PlexinD1 bands are clearly enriched over input with little to no amplification in IgG IP controls. These data show numerous RNAs to be bound by YB1 at levels higher than cytoplasmic steady state and that YB1 may regulate migration and proliferation through PlexinD1.

Figure 1: PlexinD1 mRNA is enriched in SHH MB RIPseq

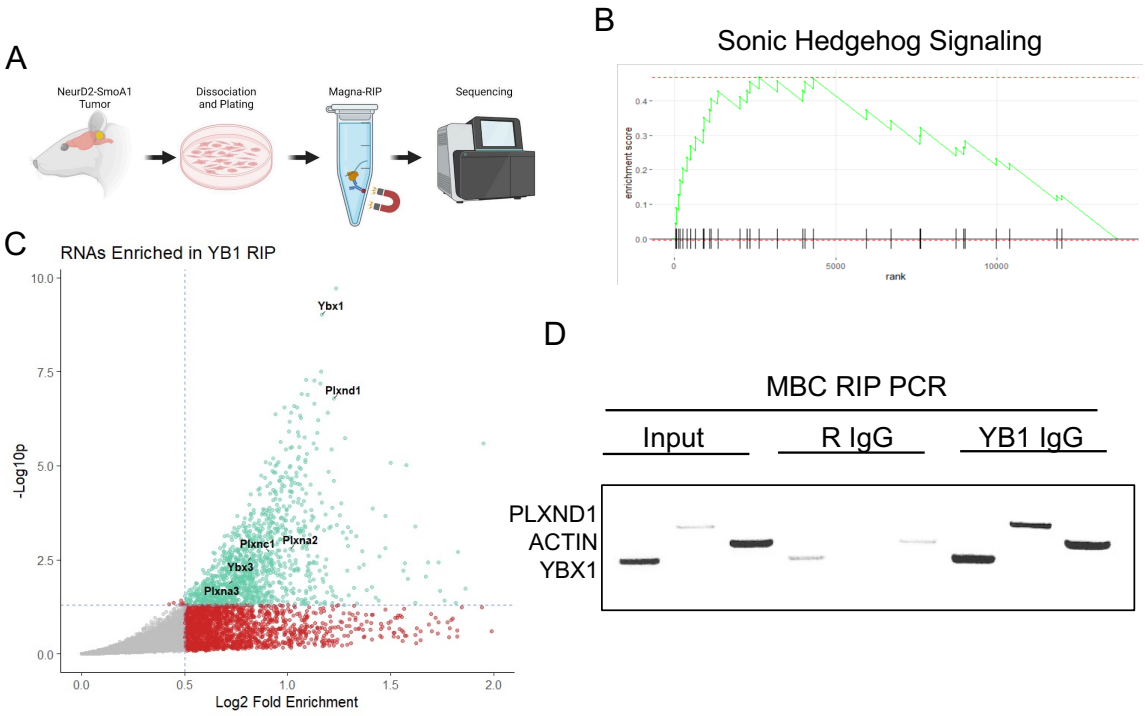

Figure 1: PlexinD1 is enriched in YB1 RIPseq and PlexinD1 is expressed in SHH MB

(A) Diagram of primary cell RIPseq workflow. **(B)** GSEA of RIPseq input with enrichment of SHH signaling, p=0.0012. **(C)** Volcano plot of RNAs enriched in YB1 RIPseq. Differential expression analysis compares YB1 bound RNAs to input RNAs. YB1 log2 fold change=1.16 p=9.44e-10, PlexinD1 log2 fold change=1.03 p=2.62e-7, p value adjusted. **(D)** PCR of YB1 RIPseq with product run on agarose with YB1 as a positive control.

6.3.2 PlexinD1 is expressed in SHH MB and Membrane PlexinD1 is expressed and colocalizes with NRP1 and Sema3E in SHH MB cells

We next investigated the relative levels of protein and RNA of PlexinD1 following YB1 depletion through shRNA in numerous models to determine the direction of RNA regulation and whether there may be compensation by YB3.[320] In the NeurD2-SmoA1 model, we previously demonstrated YB1 to be significantly upregulated in tumor tissue compared to matched normal cerebellum.[201] Here we show that, concomitant with YB1 expression, PlexinD1 is also enriched in tumor tissue compared to matched control (**Figure 2a-b and Supp Fig 1a**). Comparatively, the RNA levels of YB1 are significantly elevated, correlative with protein, while PlexinD1 RNA levels are non-significantly decreased (**Figure 2c**). These data show that PlexinD1 protein is not only significantly upregulated in tumor tissue, but that PlexinD1 RNA levels are not a reliable indication of PlexinD1 protein levels in this model. We also mined microarray data which shows enrichement of PlexinD1 mRNA in SHH MB patients over other subgroups (**Figure 2c**). Finally, to understand what binding partners may be signaling through PlexinD1 in our cells, we probed for NRP1 and Sema3E in non-permeabilized SHH MB cells, including PZPs and MBCs derived from NeuroD2-SmoA1 (**Figure 2d).** Indeed, NRP1 and Sema3E appear to colocalize in the membrane of these cells indicated by fluorophore overlap. Altogether, these data indicate that PlexinD1 protein but not mRNA are enriched in tumor but not matched non-tumor of SHH MB which suggests a post-transcriptional mechanism of regulation. Additionally, Sema3E is expressed in the tumor region indicating an autocrine mechanism of PlexinD1 activation and PlexinD1 colocalizes with Sema3E and NRP1 in the membrane of SHH MB cells.

Figure 2: PlexinD1 protein and binding partners are expressed in SHH MB

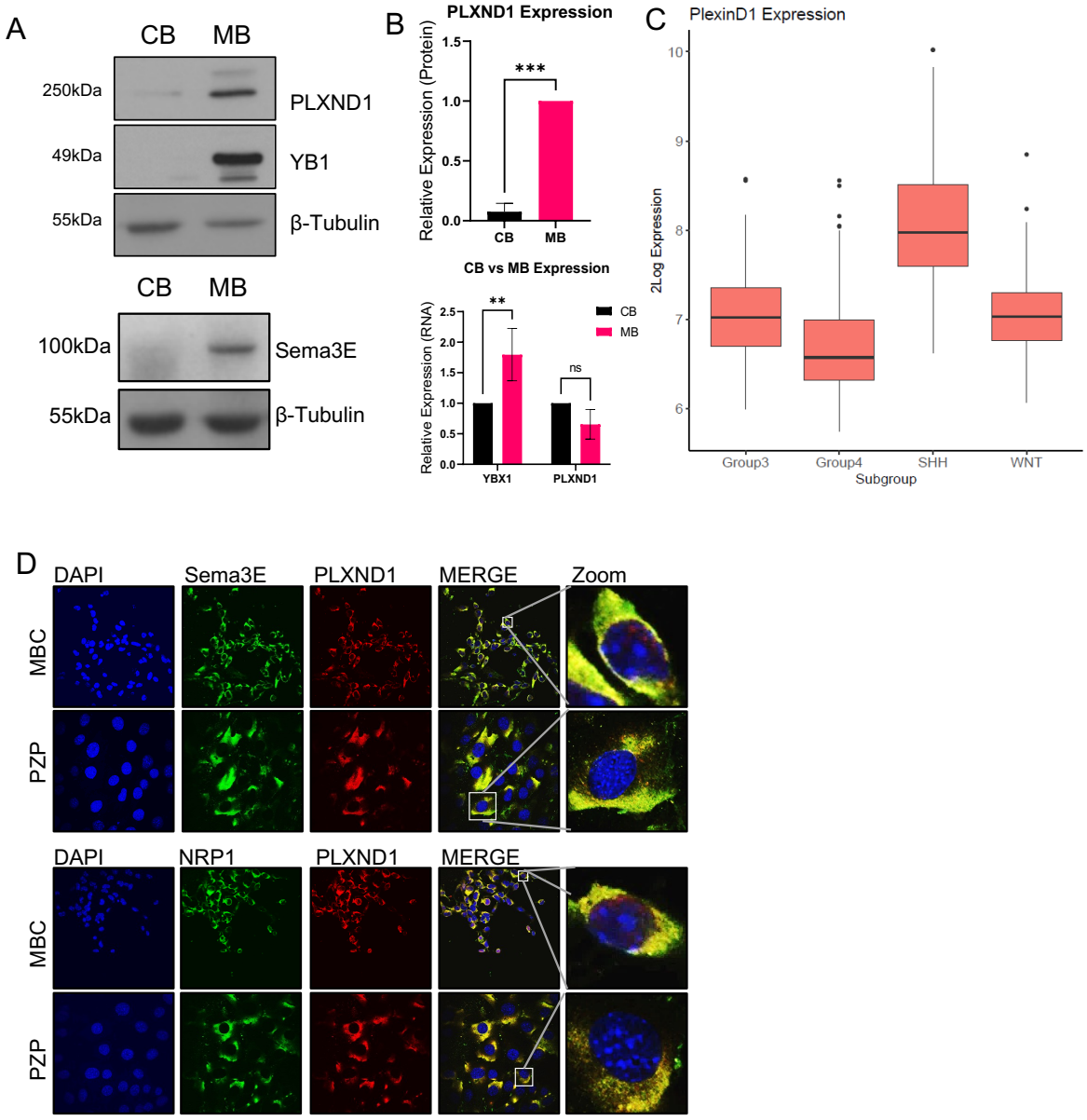

Figure 2: Figure 2: PlexinD1 protein and binding partners are expressed in SHH MB

(A) Samples taken from NeuroD2-SmoA1 SHH MB mouse model for PlexinD1 and YB1 enrichment in MB (tumor) over CB (matched non-tumor) (**Top**) and Sema3E enrichment in in MB (tumor) over CB (matched non-tumor) (**Bottom**). **(B)** PlexinD1 densitometry of NeuroD2-SmoA1 mice CB vs MB p=0.0001, paired t-test n=4 (**Top)** and RT-qPCR of YB1 (CB vs MB p=0.0013)

and PlexinD1 (CB vs MB p=0.0906) of NeuroD2-SmoA1 mice, n=3 (**Bottom**). **(C)** Microarray data mining for PlexinD1 expression across MB subgroups. (**D**) Immunofluorescence of PlexinD1 binding partners Sema3E and Neuropilin-1 in MBC primary SmoA1 cells and PZP cells.

6.3.3 YB1 Positively Regulates PlexinD1 Translation in Human and Mouse SHH Models

We then investigated whether YB1 is required for PlexinD1 translation by measuring PlexinD1 protein and RNA levels following YB1 depletion. In PZP and ONS-76 cells we see a similar trend to the tumor tissue (**Figure 2a-e and Supp Figure 2b).** Following YB1 silencing across three independent replicates we see a decrease in PlexinD1 protein levels across models with non-significant changes in PlexinD1 RNA levels. Similarly, when we knockdown YB1 in the NeuroD2-SmoA1 primary mouse cells we see a decrease in PlexinD1 protein and, similarly, upon YB1 overexpression we see an increase in PlexinD1 protein (**Supp Fig 2c**). Finally, to investigate whether PlexinD1 protein levels are decreasing due to increased proteasomal degradation, we treated UW228 and PZP cells with MG132 (**Figure 3 e,f).** Following proteasomal inhibition, PlexinD1 levels are increased in YB1 intact cells while YB1 depleted cells have unchanged or decreased PlexinD1. These data support a model whereby YB1 is capable of binding and facilitating the translation of PlexinD1 in the absence of transcriptional differences. We also concluded that YB3 may not compensate as an RNA Binding Protein upon YB1 silencing in our models given the sustained PlexinD1 protein decrease upon stable YB1 depletion. In order to understand the functional importance of this increased translation, we then investigated the effects of PlexinD1 depletion in our cells.

Figure 3: YB1 regulates PlexinD1 protein levels post-transcriptionally

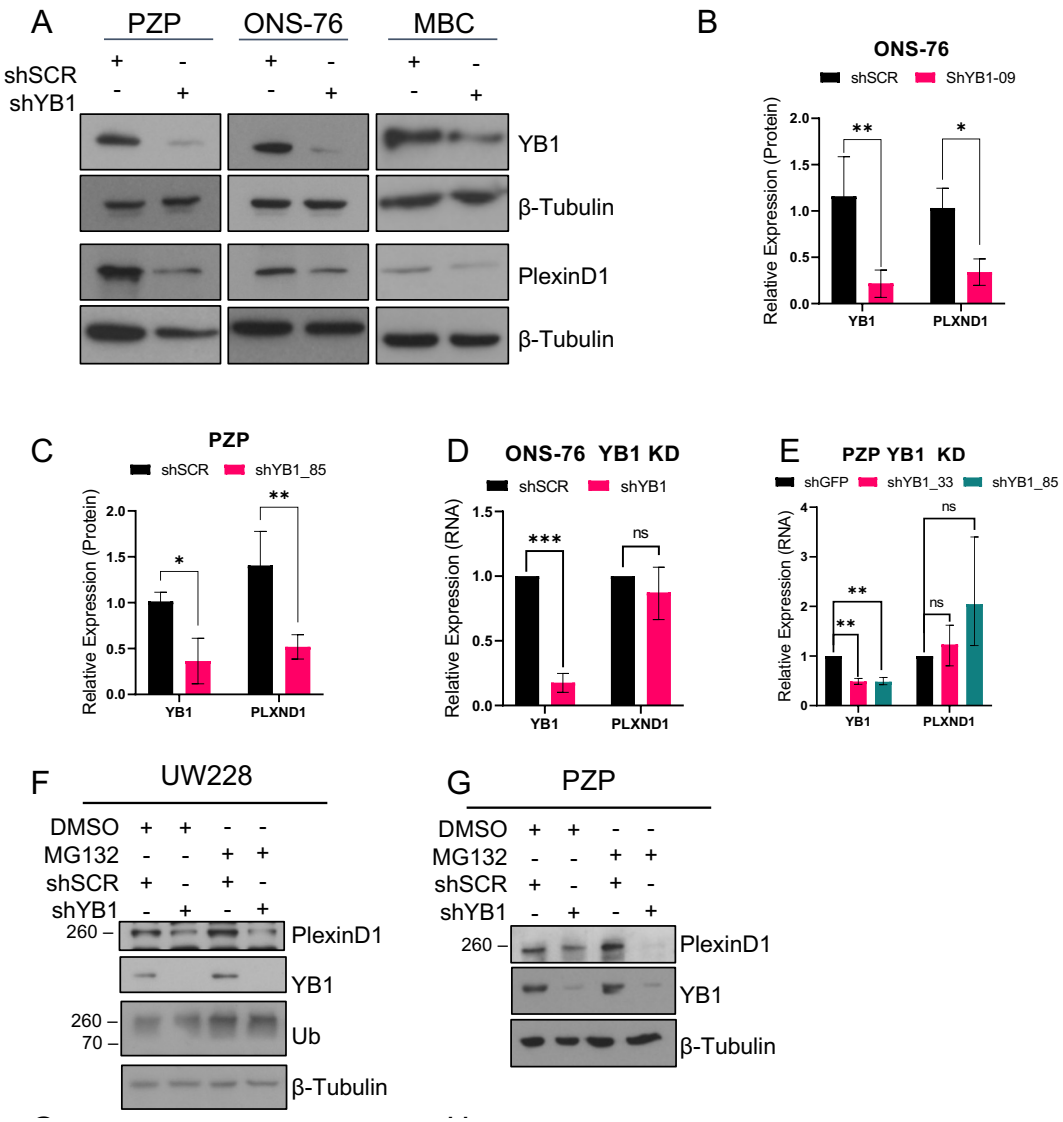

Figure 3: YB1 positively regulates PlexinD1 translation in SHH MB ((A) Western blotting of PlexinD1 following YB1 KD in 2 SHH MB cells lines and primary MBCs. **(B)** Densitometry of ONS-76 following YB1 KD for YB1 (shSCR vs shYB1 p=0.0024) and PlexinD1 (shSCR vs shYB1 p=0.0137) n=3. **(C)** Densitometry of PZP following YB1 KD for YB1 (shSCR vs shYB1 p=0.018) and PlexinD1 (shSCR vs shYB1 p=0.0031) n=3. **(G)** RT-qPCR of ONS-76 following

YB1 KD for YB1 (shSCR vs shYB1 p=0.0026) and PlexinD1 (shSCR vs shYB1 p=0.40) n=3. **(D)** RT-qPCR of PZP following YB1 KD (shSCR vs shYB1_33, YB1 p=0.009, PlexinD1 p=0.5) (shSCR vs shYB1_85, YB1 p=0.015, PlexinD1 p=0.19), n=3. **(E)** Inhibition of protein degradation (MG132) showing PlexinD1 decrease maintenance following YB1 KD in PZPs. **(F)** Inhibition of protein degradation (MG132) showing PlexinD1 decrease maintenance following YB1 KD in UW228. (G) Inhibition of protein degradation (MG132) showing PlexinD1 decrease maintenance following YB1 KD in PZP.

6.3.4 PlexinD1 and Sema3E Regulate SHH MB Cell Migration

PlexinD1 is implicated in regulating angiogenesis and cell migration in the setting of both development and cancer; thus, we chose to investigate what role PlexinD1 may play in cell migration and EMT in SHH MB. Using PZP, UW228, and ONS-76 cells, we performed scratch assays in low growth factor media over the course of 16, 24, and 48 hours on sh scramble and PlexinD1 depleted cells (**Figure 4a**). In all models, silencing of PlexinD1 results in significantly decreased wound closure times and ONS-76 and PZP cells experience a shift in N-Cadherin and β-Catenin (**Figure 4c-f and Supp Fig 3**). Additionally, while silencing of Sema3E also results in reduced migration, the rate of closure is faster than PlexinD1 depleted cells (**Figure 4g-i).** These data indicate a role for both PlexinD1 and its ligand, Sema3E, in regulating the migration and, potentially, proliferation of SHH MB cells.

Figure 4: PlexinD1 and Sema3E Regulate Migration and EMT

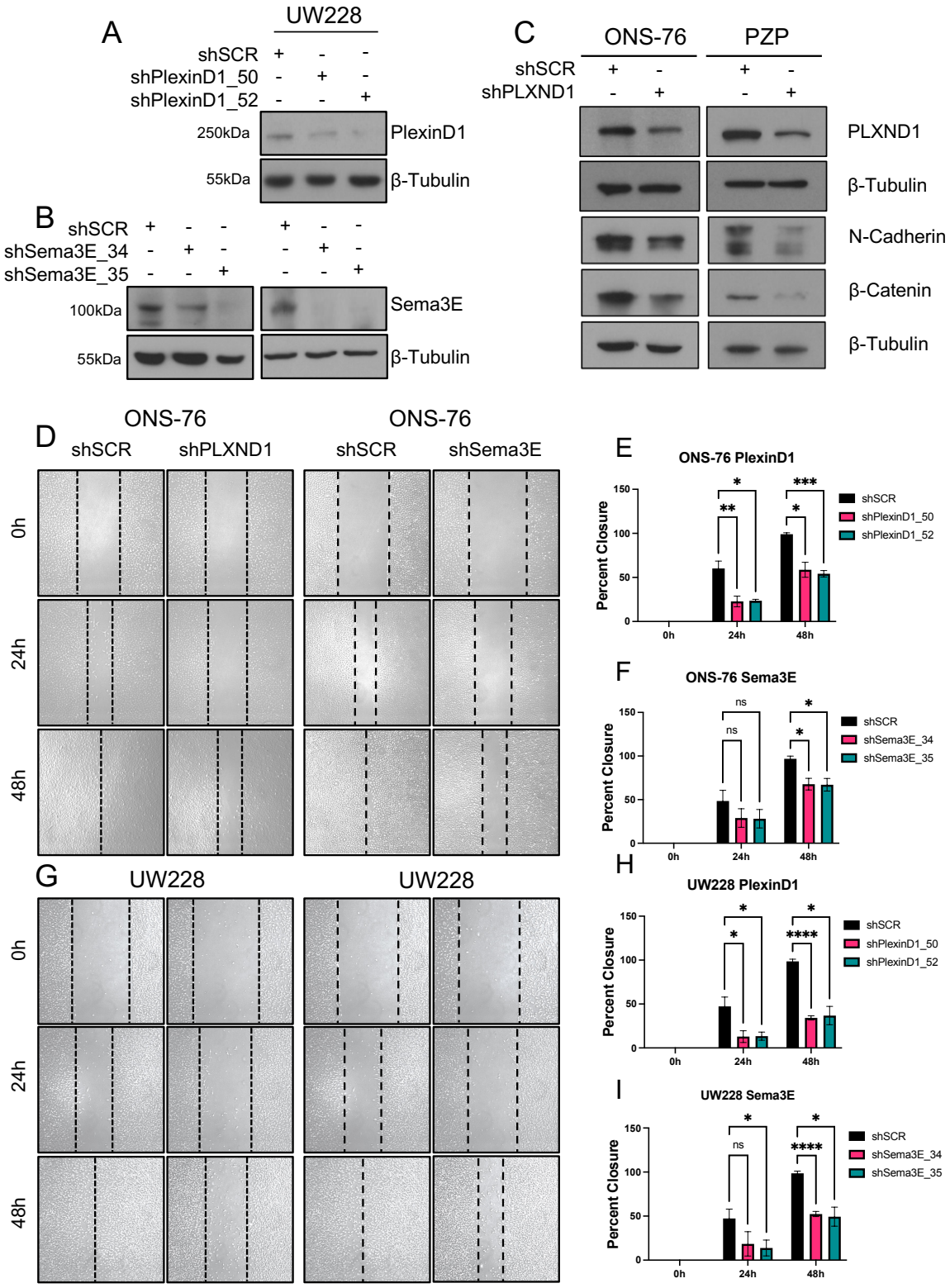

Figure 4: PlexinD1 and Sema3E Regulate Migration (A) PlexinD1 knockdown in UW228. **(B)** Sema3E knockdown in ONS-76 (left) and UW228 (right). **(C)** PlexinD1 depletion in ONS-76 and PZP cells with shift in EMT markers. **(D)** Scratch assay of ONS-76 (left) and UW228 (right) scramble and PlexinD1 depleted cells. **(E)** Percent closure calculations for scramble and PlexinD1 depleted ONS-76 cells. **(F)** Percent closure calculations for scramble and PlexinD1 depleted UW228 cells. **(G)** Scratch assay of ONS-76 (left) and UW228 (right) scramble and Sema3E depleted cells. **(H)** Percent closure of scramble and Sema3E depleted ONS-76 cells. **(I)** Percent closure of scramble and Sema3E depleted UW228. Scratch assay statistics in supplement.

6.3.5 Peptide inhibition of PlexinD1 reduces proliferation and migration

In order to validate effects of PlexinD1 depletion on migration and EMT and interrogate the potential for clinically translational inhibition of PlexinD1, we next employ a recently developed anti-PlexinD1 peptide.[317] PlexinD1 targeted peptide inhibition of proliferation indicates an IC50 of 160.2μM for ONS-76, 125.2μM for PZP, and 96.8μM for MBC cells (**Figure 5a-c**). We then performed immunoblotting of SHH MB cells following peptide treatment for select EMT markers. In MBCs exposed to peptide for 24 hours, PlexinD1 targeted cells show decreased β-Catenin and Slug compared to scramble peptide control (**Figure 5d**). Alternatively, ONS-76 and PZP cells exposed to peptide for 24 hours show consistency in reduced snail but no other markers (**Figure 5e**). We then performed sphere on Matrigel assays to assess migratory inhibition up to 24 hours. MBCs and PZPs were cultured in neurobasal media under low attachment conditions until they formed spheres and were subsequently plated onto Matrigel in media supplemented with either scramble or PlexinD1 targeted peptide. In both MBCs and PZPs, cell migration out of spheres and

onto Matrigel is significantly reduced in a dose dependent manner (**Figure 5f,h**). Together these data indicate PlexinD1 can be pharmacologically inhibited to shift EMT and reduce cell migration.

Figure 5: PlexinD1 binding peptide reduces proliferation, EMT, and Migration

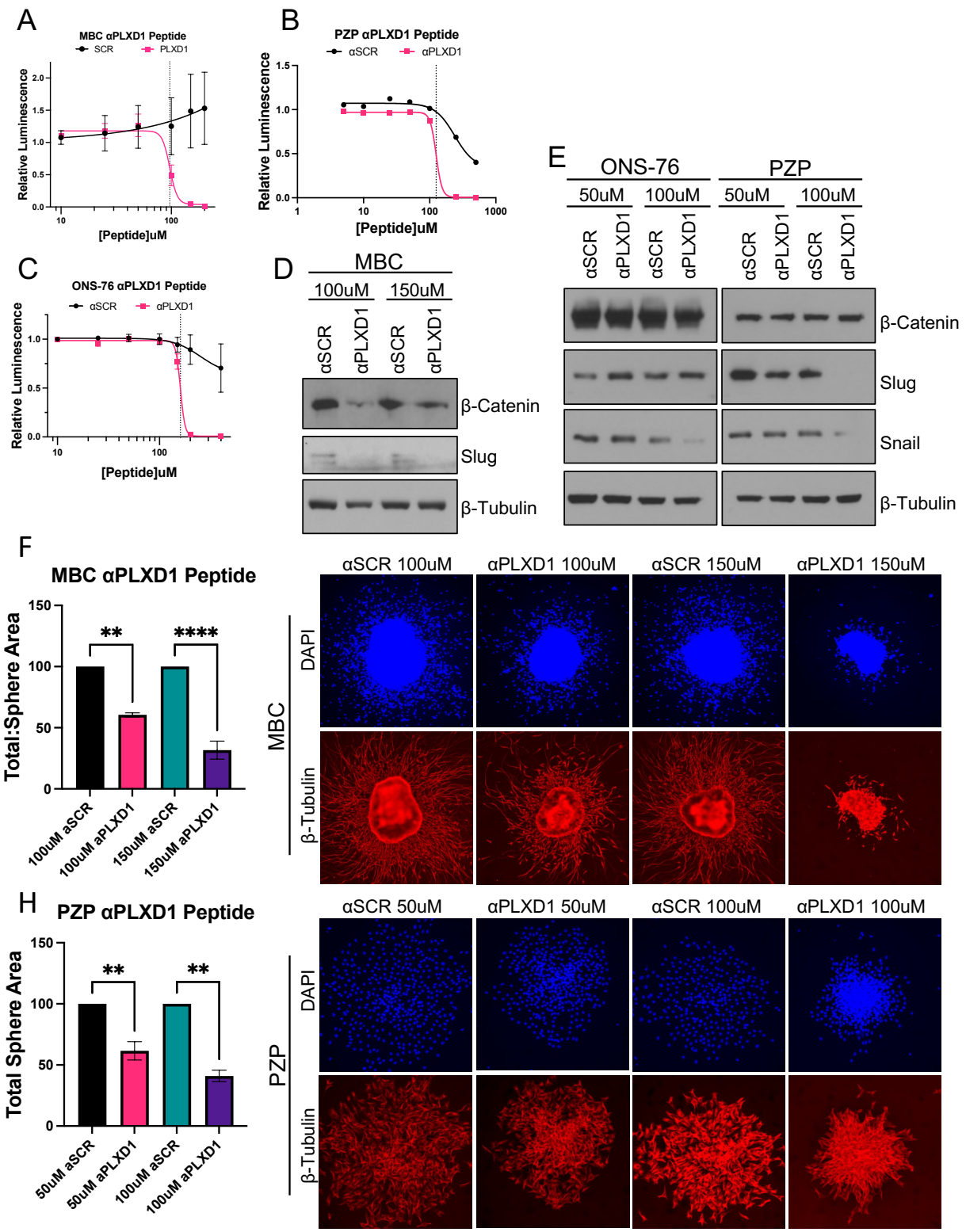

Figure 5: Peptide inhibition of PlexinD1 reduces migration. (A) IC50 curve following 72h treatment of MBCs with scramble or PlexinD1 inhibitory peptide (IC50 αSCR=unstable, IC50 αPlexinD1= 96.82uM), n=2. **(B)** IC50 curve following 72h treatment of PZP cells with scramble or PlexinD1 inhibitory peptide (IC50 αSCR = 238.9uM, IC50 αPlexinD1=125.2uM), n=1 (**C**) IC50 curve following 72h treatment of ONS-76 cells with scramble or PlexinD1 inhibitory peptide (IC50 αSCR = 252uM, IC50 αPlexinD1=160.2uM), n=2. (**D**) Immunoblotting of MBCs following 24h peptide treatment. (**E**) Immunoblotting of ONS-76 (left) and PZP (right) following 24h peptide treatment. (**F**) Sphere on Matrigel assay for MBCs indicating reduction in migration of cells from sphere (SCR vs PLXD1 100uM p=0.0036, SCR vs PLXD1 150uM p<0.0001), Ordinary one-way ANOVA, n=3. (**G**) Sphere on Matrigel assay for PZPs indicating reduction in migration of cells from sphere (SCR vs PLXD1 50uM p=0.0072, SCR vs PLXD1 100uM p=0.0014), Ordinary one-way ANOVA, n=2.

6.4 Discussion

Metastasis in medulloblastoma patients continues to present the greatest clinical challenges, and patients who relapse with metastasis have an overall survival of less than 1 year.[20] Additionally, incidence of metastasis is informed by subgroup, with Group 3 patients presenting the most frequently and SHH group incidence being ~11%.[23] While some recent studies have implicated ATOH1 and LDHA in driving leptomeningeal spread, the primary site of MB metastasis, more studies are needed to identify clinically actionable metastatic drivers and to understand molecular mechanisms regulating leptomeningeal dissemination.

Here we present a mechanism by which YB1, an oncogene crucial for CGNP and SHH MB cell proliferation, can promote migration through the translational upregulation of PlexinD1.

Interestingly, we find that Sema3E, the primary secreted ligand responsible for binding and activating PlexinD1 signaling, is secreted from SHH MB cells. This indicates a potential autocrine feedback mechanism to promote migration. Interestingly, we primarily observe full length, glycosylated Sema3E secretion in our SHH MB cells, which would suggest an autocrine inhibitory effect given several studies of furin protease inhibitor resistant Sema3E inhibition of tumor cells migration.[314] Contrary to this, we observe decreases in migration and EMT changes with PlexinD1 depletion and a decrease in migration alone with Sema3E depletion. This indicates a divergence from published paradigms for Sema3E, which could be a result of NRP1 co-localization in our cells as this can alter the phenotypic effects of Sema3E binding.[309]

The secretion of Sema3E by SHH MB cells raises the potential for paracrine signaling between tumor cells and endothelial cells. Sema3E, regardless of cleavage, induces HUVAC and endothelial cell collapse and regression and tumors expressing Sema3E have worse vascularization.[312,313] In theory, intertumoral hypoxia resulting from vascular collapse may drive hypoxia response element promoter binding and transcriptional changes related to migration and EMT.[315] Therefore, Sema3E signaling may simultaneously promote migration of tumor cells through intracellular signaling of PlexinD1 as well as secondary effects of a hypoxic microenvironment. Alternatively, Sema3E could be secreted into the cerebrospinal fluid, promoting ventricular migration and leptomeningeal dissemination.

While targeting PlexinD1 with a peptide presents the potential for clinical relevance, there are observed differences between peptide inhibition and shRNA mediated depletion, primarily differences in EMT marker shift, and other cells in the body may still express PlexinD1, presenting

on target off tumor effects. Depletion of PlexinD1 does not allow for any persistence of intracellular signaling that may occur with internalized blocking peptide bound PlexinD1 and the blocking peptide was designed to displace TGFβRII from PlexinD1 resulting in disruption of signaling and not necessarily target it for degradation. Preliminarily, however, there is a clear decrease in migratory potential upon PlexinD1 depletion and PlexinD1 may be involved in cerebellar development given SHH MB is a disease of cerebellar development and SHH signaling dysfunction. Altogether, a YB1 → PlexinD1 signaling axis appears to be responsible for migration of SHH MB and could be disrupted through PlexinD1 targeted peptides to ameliorate further metastasis or standard of care induced metastasis; however, more studies are needed to assess *in vivo* efficacy.

6.5 Materials and methods

NeuroD2-SmoA1 primary cell culture:

MBCs were isolated from NeuroD2-SmoA1 mouse tumors and cultured as described previously.[294,295] Cells were seeded on Matrigel (Corning) coated plates with Neurobasal medium containing penicillin/streptomycin, 1 mmol/L sodium pyruvate, 1x B27 supplement, and 2 mmol/L L-glutamine. Primary MBCs were cultured for 4 hours with 10% FBS prior to media change to No FBS at which point Lentivirus or Adenovirus were added with an incubation time of 48 hours prior to experiment initiation or 24 hours prior to re-implantation into BL6 mice.All primary cells were infected with 5 viral particles/cell and incubated for 48-72 hours prior to harvesting. Virus for primary cells was ultra-centrifuged and quantified with a p24 ELISA from Takara Bio prior to infection.

RIPseq and Analysis

Three independent NeuroD2-SmoA1 mice were sacrificed and cells plated for 24 hours prior to RNA binding protein immunoprecipitation (**RIP**) with approximately 10e6 cells per plate. RIP was performed according to the manufacturer's instructions for Magna RIP kit (catalog: 17-700) with YB1 CST Antibody (D2A11 #9744) and Rabbit IgG CST control. All samples were cleaned using the RNA clean up kit from ZYMO. Samples were sequenced through CD Genomics and analyzed using STAR genome aligner on an AWS server and processed locally in R using DEseq. Differential expression was assessed based on RIP enrichment over input control for each sample. YB1 served as a positive control and Actin as a negative control. GSEA was performed on the input to ensure cells were healthy. Results were validated with a standard PCR using qPCR primers to ensure signal detection excluded background primer amplification due to the large number of cycles required. R Code is available upon request. RNA counts are available on NCBI.

Cell Lines:

Mouse MB cell line Pzp53Med (p53 null, murine derived[269]) was a generous gift from Dr. Matthew Scott (Stanford). Human MB cell line ONS76 (p53 wildtype) was obtained from ATCC. For the purposes of this study Pzp53Med and ONS76 is SHH. ONS-76 and Pzp53Med cells were cultured in DMEM/F12 with 10% FBS. Control shRNA constructs consisted of shscramble (shscr). Knockdown shRNA constructs were purchased from mission sigma. YBX1 knockdown in human cell lines was performed using TRCN0000315309 (referred to as shYB1_09) or TRCN0000315307 (referred to as shYB1_07) and knockdown in mouse cells was performed using TRCN0000333885 (referred to as shYB1_85) or TRCN0000077210 (referred to as shYB1_10).

PLXND1 knockdown in human cells was performed using TRCN0000061550 (referred to as shPLXND1_50) and TRCN0000061552 (referred to as shPLXND1_52). PLXND1 knockdown in mouse cells was performed using TRCN0000078775 (referred to as shPLXND1_75) and TRCN0000078777 (referred to as shPLXND1_77). All shRNA infected immortalized cells were passaged twice with Puro before experimentation in the absence of puro.

Western Blotting

For all non-PLXND1 blots, cells were lysed in RIPA with protease and phosphatase inhibitors followed by sonication and quantification with BCA. For PLXND1 blots, cells were lysed in RIPA with 2% SDS followed by sonication, quantification with BCA, and warming with DTT at 37C (boiling was avoided to prevent hydrophobic protein aggregation and precipitation) or lysed using RIPA supplemented with IGEPAL and prepped through standard procedure. Proteins were run on a 6-8% SDS-PAGE gel and transferred for 1hr at 250mAmps with a large protein transfer buffer containing SDS and 10% Methanol. Tubulin controls were probed separately for standard RIPA and RIPA + 2% SDS. For all blots, 15ug of protein was loaded per lane of an SDS-PAGE gel and transferred onto 0.45um millipore PVDF membrane.

RT-qPCR

RNA was isolated from tissue or cell samples using 1mL TRIzol followed by RNA purification according to the manufacturer's protocol (Thermo Scientific). Reverse transcription was performed on 500ng-2µg RNA per 20µL RT reaction according to the manufacturer's instructions using a High-Capacity cDNA Reverse Transcription Kit (Applied Biosystems). qPCR was performed using either BioRad 2X SYBR master mix or Applied Biosystems 2X SYBR master mix. 25-200ng of cDNA was utilized per qPCR reaction and primers were validated based on non-template

controls and melt-curve analyses. For quantification purposes, Ct values were normalized to β-Actin. Relative expression was calculated using the ΔΔCt method. The following primer pairs were used:

Species	Target	Forward Primer	Reverse Primer
Human	β-Actin	5’ AGA GCT ACG AGC TGC CTG AC 3’	5’ AGC ACT GTG TTG GCG TAC AG 3’
	PLXND1	(BioRad qHsaCID0007287)	(BioRad qHsaCID0007287)
	YBX1	5’ CCC CAG GAA GTA CCT TCG C 3’	5’ GTT CCT TCC TCG GAT GGT CAG 3’
Mouse	β-Actin	5’ CCA GTT GGT AAC AAT GCC ATG 3’	5’ GGC TGT ATT CCC CTC CAT CG 3’
	PLXND1	5’ CGC AAC CGT AGC CTA GAA GAC 3’	5’ GGT TAA GGT CGA AGG TGA AGA G 3’
	YBX1	5’ CAG ACC GTA ACC ATT ATA GAC GC 3’	5’ ATC CCT CGT TCT TTT CCC CAC 3’

Immunofluorescence

Cells were fixed for 10 minutes in fresh 4% ParaFormaldehyde prior to 3x wash with PBS. For intracellular staining cells were permeabilized with 0.3% Triton X-100 and blocked with 5% Bovine Serum Albumin, 3% Normal Goat Serum, and 3% Donkey Serum. For surface staining cells were not permeabilized but blocked with 5% Bovine Serum Albumin, 3% Normal Goat Serum, and 3% Donkey Serum. For secondary only controls cells were blocked and incubated with PBS while paired samples were incubated with primary antibody. Primary antibody was added

overnight at 4C and secondary was added for 1 hour at RT. Cell imaging was performed on the Olympus FV1000 at the Emory University Integrated Cellular Imaging Core.

Cell Migration and Invasion Assay

Cell migration was measured using in vitro wound-healing assay and 3D colony formation/matrigel invasion assay. For scratch assays cells were seeded with 2.5% FBS and grown to ~70-80% confluence before scratching with a sterile P1000 pipette tip. Wound closure was photographed at 0, 16, 24, and 48 hours post-scratch. Wound closure area was measured using ImageJ software. Cell invasion was measured using 3D colony formation assays in Matrigel (Corning). Cells were embedded in 50% Matrigel and incubated with media replacement every 3 to 4 days. Colony formation was photographed at 14 days post plating. Spheres were counted based on presence or absence of sphere projections.

Statistical Analysis

Statistical comparisons were performed using GraphPad Prism. One-way analysis of variance (ANOVA) was used for western blotting densitometry, and two-way ANOVA was used for wound-healing analyses. Paired t-tests were used for RT-qPCR analyses. All error bars represent data range. A significance threshold of $p < 0.05$ was used in all analyses.

Supp Figure 1

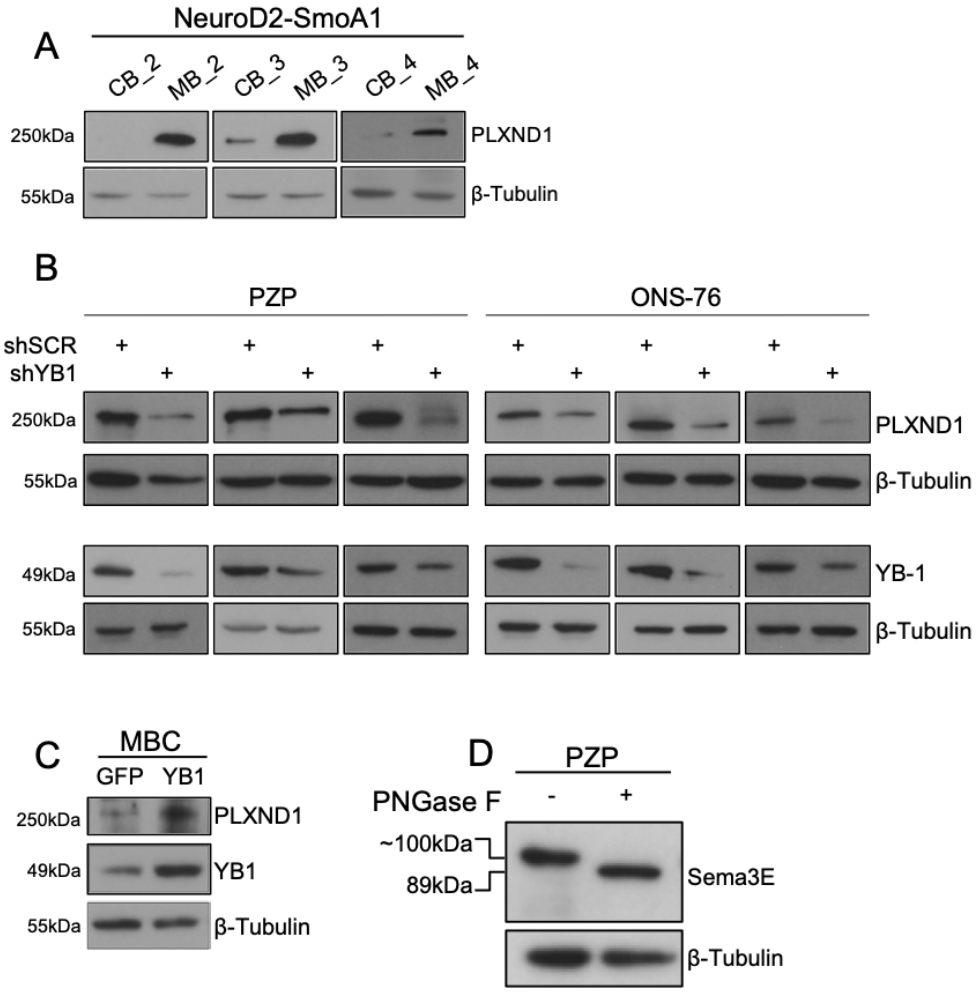

Supplementary Figure 1: (A) 3 additional biological replicates of NeuroD2-SmoA1 mouse tumors divided into non-tumor (CB) and tumor (MB) corresponding to figure 3. **(B)** biological triplicates of YB1 KD with concomitant decrease in PlexinD1 corresponding to figure 3. **(C)** Overexpression of YB1 in MBCs derived from NeuroD2-SmoA1 mice showing increased PlexinD1. **(D)** PNGase F treatment of PZP cell lysate indicating a shift in in 100kDa Sema3E to 89kDa, the full length isoform.

Supp Figure 2

Comparison	Mean Diff.	95.00% CI of diff.	Below threshold?	Summary	Adjusted P Value
ONS-76 shPlexinD1					
24h					
shSCR vs. shPlexinD1_50	37.37	16.51 to 58.23	Yes	**	0.008
shSCR vs. shPlexinD1_52	36.6	11.52 to 61.69	Yes	*	0.0231
48h					
shSCR vs. shPlexinD1_50	40.37	15.23 to 65.51	Yes	*	0.0189
shSCR vs. shPlexinD1_52	44.86	35.49 to 54.23	Yes	***	0.0008
ONS-76 shSema3E					
24h					
shSCR vs. shSema3E_34	19.55	-11.65 to 50.75	No	ns	0.1726
shSCR vs. shSema3E_35	20.41	-10.72 to 51.55	No	ns	0.1555
48h					
shSCR vs. shSema3E_34	29.11	11.82 to 46.40	Yes	*	0.013
shSCR vs. shSema3E_35	29.79	11.11 to 48.47	Yes	*	0.0155
UW228 shPlexinD1					
24h					
shSCR vs. shPlexinD1_50	34.35	7.998 to 60.71	Yes	*	0.0234
shSCR vs. shPlexinD1_52	33.81	6.039 to 61.57	Yes	*	0.0308
48h					
shSCR vs. shPlexinD1_50	64.36	57.66 to 71.06	Yes	****	<0.0001
shSCR vs. shPlexinD1_52	61.68	31.54 to 91.81	Yes	*	0.0108
UW228 shSema3E					
24h					
shSCR vs. shSema3E_34	28.9	-5.525 to 63.32	No	ns	0.082
shSCR vs. shSema3E_35	33.41	6.325 to 60.49	Yes	*	0.0259
48h					
shSCR vs. shSema3E_34	46.3	38.73 to 53.86	Yes	****	<0.0001
shSCR vs. shSema3E_35	49.16	17.76 to 80.56	Yes	*	0.0194

Supplementary Figure 2: Statistical analysis of scratch assays corresponding to figure 4

Supp Figure 3

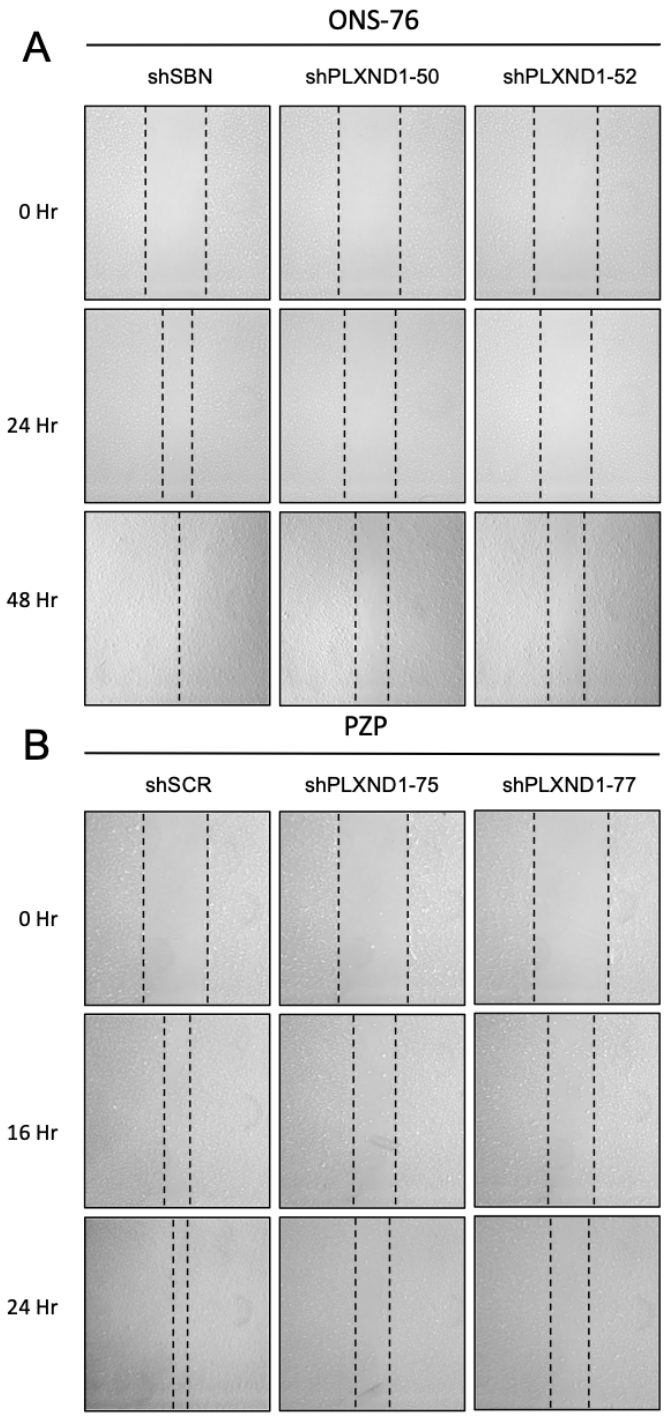

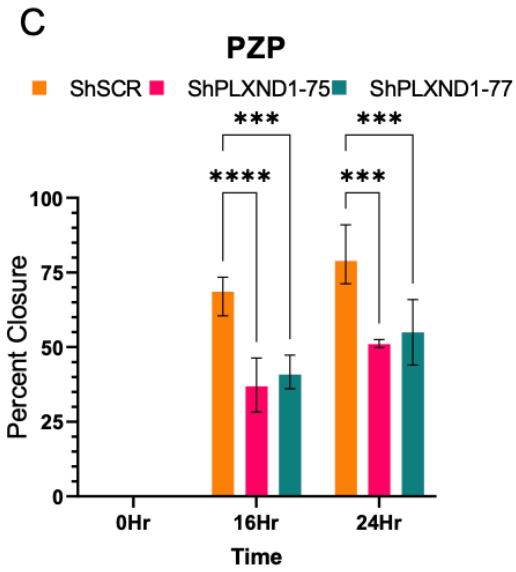

Supplementary Figure 3: (A) Additional images for ONS-76 scratch assay following PlexinD1 depletion corresponding to figure 4. **(B)** Scratch assay of PZP cells following PlexinD1 depletion. **(C)** Analysis of percent closure of PZP cells (B).

Chapter 7

Conclusions and Future Directions

Medulloblastoma is a disease of development originating in the cerebellum. SHH MB, for example, is emblematic of SHH activated cerebellar granular neural precursor cells during post-natal cerebellar development up until cell migration into the granular layer. Persistence of this signaling resulting from mutations to SHH signaling in the CGNPs, for example, keeps these cells in the progenitor state. A similar narrative is true for Group3 MB as well whereby CD133+ stem cells are thought to experience some genomic alterations resulting in continued proliferation and self-renewal leading to tumor development. The genetic and transcriptomic differences between patients resulting from these origin events as well as the group specific accumulation of additional driver mutations leads to 4 distinct subgroups of which SHH is the primary focus of this dissertation. And while there have been great strides in improving overall survival of patients since the 1970s, stress from cranio-spinal radiation and chemotherapy can result in intellectual deficits and secondary malignancies in developing children and adolescents. Additionally, these modalities may induce metastasis, a major cause of recurrence and mortality, and they may not eliminate stem cell compartments, a major source of recurrence. The goal of this dissertation is to improve standard of care response, reduce incidence of recurrence and mortality, and reduce side effects and secondary malignancies from standard of care. I provided support for this through research to understand YB1 targetability for sensitizing cells to radiation and establishing a role for YB1 in MB cell migration.

YB1 is an excellent therapeutic candidate for a number of reasons. The nucleotide binding domain of YB1 allows it to function in two crucial aspect of tumor biology: promoter binding for gene transcription and DNA repair. Not only can YB1 bind modified or broken DNA to facilitate repair, reducing the efficacy of radiation and chemotherapy, it can also drive expression of efflux proteins (MDR1), anti-apoptotic proteins (BCL2), or cell cycle proteins (Cyclins), again making the cells more resistant to standard of care. Additionally, YB1 can purportedly bind and inhibit p53 to suppress pro-apoptotic cell response. This could make cells even more resistant to cell death or senescence induced by radiation and chemotherapy, potentially even accelerating driver mutation acquisition. As discussed in chapter 2, eliminating p53 rescues many developmentally lethal genetic alterations such as ATR ablation, and apoptotic inhibition under genomic stress can result in gene amplification, such as with MYC. YB1 can drive these phenotypes which makes it such an important therapeutic consideration. Here we show that depletion of YB1 from SHH and group 3 and 4 MB results in reduced proliferation and in some cases increased p21 and β-Gal staining, indications of increased senescence. Many aspects of DNA repair and cell cycling dynamics we observed were contradictory to this, however. For example, in many experiments, H2AX phosphorylation is still present in YB1 intact cells 24 hours after radiation while YB1 depleted cells appear to have resolved their DNA damage. This was consistent with Edu incorporation assays indicating a greater sub-G1 population and lower viability in irradiated YB1 intact ONS-76 cells compared to irradiated YB1 depleted cells. This data was also consistent with LaminA/C staining indicating severe nuclear fractionation at 24 and 48 hours in both irradiated YB1 intact UW228 and ONS-76 cells, which were present as doublets in cell cycle flow. Hypothetically, a small population of YB1 high cells may experience mitotic catastrophe resulting in nuclear fractionation, γH2AX re-accumulation, and cell death, while the majority re-populate and

potentially carry novel driver mutations. As the Dunn group observed in their studies, some YB1 high breast cancer cells may experience cell cycle checkpoint slippage and cell death, while others experience HER2 gene amplification. It seems possible that in response to radiation the mechanisms of repair may be what drives the previously mentioned observations, which we chose to investigate based on published interactions between YB1 and γH2AX and the MRN complex. When cells were examined for Rad51 and TP53BP1, YB1 intact cells accumulate greater Rad51 and lower TP53BP1 nuclear foci. Given Rad51 is critical for the strand invasion during homologous recombination and TP53BP1 blocks the early stages of end resection and subsequently homologous recombination; I supposed that YB1 may drive HR and that in the absence of YB1 cells commit to NHEJ. Indeed, in YB1 depleted U2OS DR-GFP and HEK-EJ7-NHEJ cells we observe less HR and more NHEJ. Together the data suggests that YB1 high cells commit to HR and bypass cell cycle checkpoints with a portion of the population experiencing mitotic catastrophe because of checkpoint slippage while many recover and continue proliferating in a state maintained by apoptotic and senescence inhibition, potentially through p53. These suppositions raise many unanswered questions about the anti-proliferative phenotype of irradiated YB1 depleted cells that can only be answered by further experimentation.

In order to make a firm conclusion about whether YB1 depletion increases mutational burden I propose the following: Sky probe and whole genome sequencing of YB1 intact and depleted cells following radiation. By labeling a metaphase spread of YB1 depleted cells with Sky probes and looking at variant calling for point mutations, we may find that the reason for decreased proliferation and increased senescence of irradiated YB1 depleted cells is a result of strong mutational burden and gross chromosomal rearrangements that would affect cell proliferation and

viability. However, in the case that the mutational burden is of equivalent detriment between YB1 intact and depleted cells, I may then assume that YB1 depleted cells are undergoing apoptosis and senescence as a result of YB1's known role in regulating p53 or BCL2. I would then propose the following experiments to compare irradiated YB1 intact and YB1 depleted cells: transient YB1 depletion and irradiation or no depletion and irradiation. We may either inhibit YB1 with SU056 prior to and 24 hours after radiation, transiently depleting YB1 with a dox inducible short hairpin against YB1, or transfecting with siRNA to transiently deplete YB1, the latter two being more logistically challenging. Following the initial repair and a recover period of several days, cells would then be assessed for proliferative capacity or lysed for western blotting to probe for p53, p21, and BCL2. If the decreased proliferation is not a result of differences in repair mechanism but instead the result of YB1 acting on p53 and BCL2, we would anticipate there to be no difference in proliferation and similar levels of p53, p21, and BCL2 between YB1 intact and YB1 depleted cell populations. However, if YB1 driven NHEJ does result in greater mutational burden, over time YB1 inhibition of p53 and promotion of BCL2 may not be sufficient to maintain cell viability while p53 and p21 may continue to rise higher than cells that had functional YB1 during the repair period. While these additional experiments may shed light on mechanistic drivers of reduced proliferation, the translatability of these in vitro findings are also lacking. As of 2023 there are no studies describing the blood brain barrier penetrability of SU056; however, in pre-liminary studies not presented here, MB cells are amenable to the drug with IC50s lower than those published by Tailer et al. in 2021. Therefore, to investigate the feasibility of targeting YB1 pharmacologically, I would administer SU056 to tumor naïve mice followed by HPLC on brain tissue. If BBB penetrance is successful, we may then consider administering SU056 with or without radiation to assess impact on survival of $PTCH^{fl/fl}$ tumors or NSGs implanted with UW228,

ONS-76, D341, or D425. One of the greatest challenges of translating a drug like SU056 into the clinic is potentially catastrophic side effects on the developing body. Because we are considering a tumor of development and given YB1 is implicated in regulating fetal development we would need to administer SU056 to early post-natal mice to assess potential on target off tumor effects of the drug on CGNPs and other active progenitor populations that may express YB1. These data are crucial to understanding when YB1 inhibition is optimal and whether there is clinical feasibility.

While we may have established a role for YB1 in the DNA damage response to ionizing radiation in an attempt to sensitize to standard of care, YB1 may also regulate another driver of recurrence and mortality. Metastasis, either when patients present or following standard of care, poses challenges to clinicians and surgeons. As discussed in chapter one, molecular mechanisms of metastasis and how to eliminate metastatic populations remains poorly understood. For this reason we investigated a role for YB1 in metastasis through post-transcriptional regulation of translation. As the Sorenson group has established, YB1 can promote HIF1α translation to drive cell migration and osteosarcoma metastasis and other groups have shown YB1 to bind Snail RNA, an EMT transcription factor. Therefore, we performed RIPseq on YB1 bound RNAs from which we extracted several Plexin isoforms. Plexins are a class of transmembrane proteins that can regulate migration through binding of their canonical ligands, semaphorins, or through transactivation of RTKs (VEGFR2, TGFBRII, and HER2). Plexins and Semaphorins are well established as key regulators of neuronal and endothelial cell migration and the already demonstrated roles for PlexinA2 and PlexinB2 in cerebellar development make PlexinD1 a great candidate to explore for both cerebellar development and as a mediator of medulloblastoma cell migration. There were

concerns about the sustained reduction in protein levels of proteins whose RNAs are bound by YB1 following YB1 depletion due to published reports by the Ovchinnikov group for YB3 to compensate for YB1 in global RNA binding. However, when we knockdown YB1 in primary, immortalized, and patient derived SHH MB cells we find a sustained decrease in PlexinD1 protein levels without a decrease in mRNA levels. Subsequently, when we inhibit proteasomal degradation with MG132 we do not see rescue of PlexinD1 protein in YB1 depleted cells. These data are strong indications of a post-transcriptional mechanism whereby YB1 positively regulates PlexinD1 translational; however, this does not indicate a role for PlexinD1 in cell migration. Depletion of PlexinD1 or targeting of PlexinD1 with a peptide developed to disrupt PlexinD1 interactions with co-receptors, results in decreased migration in both scratch and sphere on Matrigel assays and a shift to an epithelial phenotype. These data provide strong support for a YB1 → PlexinD1 → Pro-migration signaling axis in SHH MB. However, there remain several unanswered questions including whether (a) YB1 depletion shifts PlexinD1 mRNA away from the polysome fractions, (b) PlexinD1 is signaling through RTKs or TGFBRII, (c) YB1 depletion will also reduce migration, (d) PlexinD1 re-expression in YB1 depleted cells rescues YB1 mediated cell migration, and (e) whether depleting or inhibiting YB1 or PlexinD1 *in vivo* will result in reduced incidence of metastasis prior to and during the treatment period.

While a decrease in PlexinD1 protein levels concomitant with no changes in mRNA levels alongside proteasome inhibition studies provide a strong case for post—transcriptional regulation of PlexinD1 translation, polysome profiling is still an important consideration. mRNAs that are actively translated in cells tend to be bound to ribosomes and can be found in polysomes with a greater number of bound ribosomes indicating a more active translation. By taking YB1 depleted

cells and performing polysome profiling, consisting of running RNAs bound by ribosomes inhibited by cycloheximide on a sucrose gradient, we expect to see a shift in PlexinD1 RNA away from the polysome fraction which would support the hypothesis that YB1 facilitates ribosomal loading and translation of PlexinD1. In addition to this, we might also consider the mechanism of translation such as either 5'Cap or IRES mediated translation. To investigate this, we could overexpress YB1 and inhibit mTOR, a regulator of 5'Cap translation initiation, through Torin1 or 2 and investigate whether PlexinD1 protein levels decrease. If we see no decrease in PlexinD1 protein with mTOR inhibition and assuming YB1 is also not reliant on 5'Cap translation initiation, we may conclude that PlexinD1 translation is not 5'Cap dependent. However, if we do see a reduction in PlexinD1 protein with YB1 over expression and mTOR inhibition this may indicate two possible interpretations: (a) YB1 is not sufficient to overcome mTOR inhibition and (b) YB1 regulation of PlexinD1 translation is 5'Cap dependent.

Secondary to this, it is still unclear whether YB1 depletion is sufficient to reduce migration of SHH MB cells and whether PlexinD1 is the only migratory regulator. Given we see sustained decreases in PlexinD1 protein levels after YB1 depletion using shRNA and puromycin selection, there is a strong likelihood that YB1 depletion will reduce migratory potential. However, it is very unlikely that PlexinD1 is the only protein affected by YB1 depletion as numerous Plexins are bound and potentially regulated by YB1. Rescuing YB1 depleted cells with PlexinD1 may achieve some degree of migration restoration; however, there are likely many migratory proteins that are reduced due to not only RNA binding but also transcriptional regulation by YB1. If we would like to further investigate whether PlexinD1 is solely responsible for YB1 mediated migration we would need to perform mass spec on YB1 depleted samples and correlate them with RIPseq results.

If PlexinD1 does not act alone we will see changes in other proteins bound by YB1 in RIPseq which we could then deplete to understand their effects on the cell. It is likely that PlexinB2 is also regulated by YB1 and responsible for YB1 mediated migration of cells.

Thirdly, understanding PlexinD1 transactivation of transmembrane binding partners is important for elucidating the switch to pro-migratory phenotype of PlexinD1 signaling. In the absence of binding partners, binding of Sema3E to PlexinD1 will activate it's GAP domain and turn off migratory signaling. However, the presence of TGFBRII, VEGFR, or ERBB2 has been shown to over-ride PlexinD1 GAP activity resulting in activation of Smad proteins and/or the PI3K/AKT signaling axis. Given the reduction in migration when we deplete PlexinD1 or Sema3E from our cells, we would anticipate a reduction in phosopho-Smad or phospho-Akt when we deplete PlexinD1 or Sema3E. To strengthen the hypothesis that a reduction in phosopho-Smad or phospho-Akt is a result of an interaction between PlexinD1 and these other co-receptors, we may also perform a Co-IP of PlexinD1 followed by western blotting for these co-receptors.

Finally, while many of the findings already established in our system are very promising, whether YB1 or PlexinD1 facilitate metastasis prior to or following standard of care cannot be effectively answered without *in vivo* work. In theory, YB1 inhibition by SU056 should abolish RNA binding and translational regulation resulting in a similar reduction in PlexinD1 protein levels that we have observed following YB1 depletion. In order to investigate whether YB1 and PlexinD1 are crucial for migration and metastasis, we may treat $PTCH^{fl/fl}$ mice or NSG mice implanted with UW228 or ONS-76 with SU056 or perform stable KD in UW228 or ONS-76 of YB1 or PlexinD1. If PlexinD1

is required for metastasis, we should observe a reduction in spinal metastasis with inhibition or depletion of YB1 or depletion of PlexinD1.

Overall, these studies are a step forward in understanding how to sensitize MB patients to standard of care, treating metastatic cell populations, reducing treatment induced metastasis, and potentially ameliorate the need for harsh treatment methods like radiation and chemotherapy. Targeting YB1 with either SU056 or siRNA carrying nanoparticles delivered through focused ultrasound with or without radiation and chemotherapy could improve patient survival dramatically and ultimately improve quality of life.

References

1. Ostrom, Q. T. *et al.* CBTRUS Statistical Report: Primary Brain and Other Central Nervous System Tumors Diagnosed in the United States in 2013–2017. *Neuro. Oncol.* **22**, iv1–iv96 (2020).
2. Kool, M. *et al.* Molecular subgroups of medulloblastoma: an international meta-analysis of transcriptome, genetic aberrations, and clinical data of WNT, SHH, Group 3, and Group 4 medulloblastomas. *Acta Neuropathologica* vol. 123 473–484 Preprint at https://doi.org/10.1007/s00401-012-0958-8 (2012).
3. Northcott, P. A., Dubuc, A. M., Pfister, S. & Taylor, M. D. Molecular subgroups of medulloblastoma. *Expert Rev. Neurother.* **12**, 871–884 (2012).
4. Taylor, M. D. *et al.* Molecular subgroups of medulloblastoma: the current consensus. *Acta Neuropathol.* **123**, 465–472 (2012).
5. Juraschka, K. & Taylor, M. D. Medulloblastoma in the age of molecular subgroups: a review: JNSPG 75th Anniversary Invited Review Article. *J. Neurosurg. Pediatr.* **24**, 353–363 (2019).
6. Dhanyamraju, P. K., Patel, T. N. & Dovat, S. Medulloblastoma: 'Onset of the molecular era'. *Molecular Biology Reports* vol. 47 9931–9937 Preprint at https://doi.org/10.1007/s11033-020-05971-w (2020).
7. Hill, R. M. *et al.* Combined MYC and P53 defects emerge at medulloblastoma relapse and define rapidly progressive, therapeutically targetable disease. *Cancer Cell* **27**, 72–84 (2015).
8. Roussel, M. F. & Robinson, G. W. Role of MYC in Medulloblastoma. *Cold Spring Harb. Perspect. Med.* **3**, (2013).
9. Cavalli, F. M. G. *et al.* Intertumoral Heterogeneity within Medulloblastoma Subgroups. *Cancer Cell* **31**, 737–754.e6 (2017).
10. Ramaswamy, V. *et al.* Risk stratification of childhood medulloblastoma in the molecular era: the current consensus. *Acta Neuropathol.* **131**, 821–831 (2016).
11. Wefers, A. K. *et al.* Subgroup-specific localization of human medulloblastoma based on pre-operative MRI. *Acta Neuropathol.* **127**, 931–933 (2014).
12. Northcott, P. A. *et al.* Medulloblastoma. *Nat Rev Dis Primers* **5**, 11 (2019).
13. Paterson, E. & Farr, R. F. Cerebellar Medulloblastoma: Treatment by Irradiation of the Whole Central Nervous System. *Acta Radiologica* vol. 39 323–336 Preprint at https://doi.org/10.3109/00016925309136718 (1953).
14. Rutka, J. T. & Hoffman, H. J. Medulloblastoma: a historical perspective and overview. *J. Neurooncol.* **29**, 1–7 (1996).
15. Leary, S. *et al.* MBCL-16. EFFICACY OF CARBOPLATIN GIVEN CONCOMITANTLY WITH RADIATION AND ISOTRETINOIN AS A PRO-APOPTOTIC AGENT IN MAINTENANCE THERAPY IN HIGH-RISK MEDULLOBLASTOMA: A REPORT FROM THE CHILDREN'S ONCOLOGY GROUP. *Neuro-Oncology* vol. 22 iii391–iii391 Preprint at https://doi.org/10.1093/neuonc/noaa222.492 (2020).
16. Yuan, X., Larsson, C. & Xu, D. Mechanisms underlying the activation of TERT transcription and telomerase activity in human cancer: old actors and new players. *Oncogene* **38**, 6172–6183 (2019).
17. Northcott, P. A. *et al.* The whole-genome landscape of medulloblastoma subtypes. *Nature* **547**, 311–317 (2017).
18. Tamayo-Orrego, L. & Charron, F. Recent advances in SHH medulloblastoma progression:

tumor suppressor mechanisms and the tumor microenvironment. *F1000Res.* **8**, (2019).
19. Riemondy, K. A. *et al.* Neoplastic and immune single cell transcriptomics define subgroup-specific intra-tumoral heterogeneity of childhood medulloblastoma. *Neuro. Oncol.* (2021) doi:10.1093/neuonc/noab135.
20. Hsieh, P.-C. *et al.* The clinical experience of medulloblastoma treatment and the significance of time sequence for development of leptomeningeal metastasis. *Childs. Nerv. Syst.* **24**, 1463–1467 (2008).
21. MacDonald, T. J. *et al.* Expression profiling of medulloblastoma: PDGFRA and the RAS/MAPK pathway as therapeutic targets for metastatic disease. *Nat. Genet.* **29**, 143–152 (2001).
22. Korenberg, M. J. On predicting medulloblastoma metastasis by gene expression profiling. *J. Proteome Res.* **3**, 91–96 (2004).
23. Singh, M., Bakhshinyan, D., Venugopal, C. & Singh, S. K. Preclinical Modeling and Therapeutic Avenues for Cancer Metastasis to the Central Nervous System. *Frontiers in Oncology* vol. 7 Preprint at https://doi.org/10.3389/fonc.2017.00220 (2017).
24. Cerebellar tentorium. https://en.wikipedia.org/wiki/Cerebellar_tentorium (2005).
25. Zapotocky, M. *et al.* Differential patterns of metastatic dissemination across medulloblastoma subgroups. *J. Neurosurg. Pediatr.* **21**, 145–152 (2018).
26. Hernan, R. *et al.* ERBB2 up-regulates S100A4 and several other prometastatic genes in medulloblastoma. *Cancer Res.* **63**, 140–148 (2003).
27. Herrlinger, U. *et al.* Vascular endothelial growth factor (VEGF) in leptomeningeal metastasis: diagnostic and prognostic value. *Br. J. Cancer* **91**, 219–224 (2004).
28. Davare, M. A. *et al.* Secreted meningeal chemokines, but not VEGFA, modulate the migratory properties of medulloblastoma cells. *Biochem. Biophys. Res. Commun.* **450**, 555–560 (2014).
29. Nalla, A. K. *et al.* Suppression of uPAR retards radiation-induced invasion and migration mediated by integrin β1/FAK signaling in medulloblastoma. *PLoS One* **5**, e13006 (2010).
30. Grausam, K. B. *et al.* ATOH1 Promotes Leptomeningeal Dissemination and Metastasis of Sonic Hedgehog Subgroup Medulloblastomas. *Cancer Res.* **77**, 3766–3777 (2017).
31. Qin, N. *et al.* Intratumoral heterogeneity of MYC drives medulloblastoma metastasis and angiogenesis. *Neuro. Oncol.* **24**, 1509–1523 (2022).
32. Packer, R. J. *et al.* Phase III study of craniospinal radiation therapy followed by adjuvant chemotherapy for newly diagnosed average-risk medulloblastoma. *J. Clin. Oncol.* **24**, 4202–4208 (2006).
33. Friedman, H. S. & Schold, S. C., Jr. Rational approaches to the chemotherapy of medulloblastoma. *Neurol. Clin.* **3**, 843–853 (1985).
34. Merchant, T. E. *et al.* Multi-institution prospective trial of reduced-dose craniospinal irradiation (23.4 Gy) followed by conformal posterior fossa (36 Gy) and primary site irradiation (55.8 Gy) and dose-intensive chemotherapy for average-risk medulloblastoma. *Int. J. Radiat. Oncol. Biol. Phys.* **70**, 782–787 (2008).
35. Ruggiero, A. *et al.* Platinum compounds in children with cancer: toxicity and clinical management. *Anticancer Drugs* **24**, 1007–1019 (2013).
36. Sadoughi, F. *et al.* The role of DNA damage response in chemo- and radio-resistance of cancer cells: Can DDR inhibitors sole the problem? *DNA Repair* **101**, 103074 (2021).
37. Santivasi, W. L. & Xia, F. Ionizing radiation-induced DNA damage, response, and repair. *Antioxid. Redox Signal.* **21**, 251–259 (2014).

38. Goldstein, M. & Kastan, M. B. The DNA damage response: implications for tumor responses to radiation and chemotherapy. *Annu. Rev. Med.* **66**, 129–143 (2015).
39. Hong, B.-J. *et al.* Tumor hypoxia and reoxygenation: the yin and yang for radiotherapy. *Radiat. Oncol. J.* **34**, 239–249 (2016).
40. Basu, A., Broyde, S., Iwai, S. & Kisker, C. DNA damage, mutagenesis, and DNA repair. *J. Nucleic Acids* **2010**, 182894 (2010).
41. Bartek, J. & Lukas, J. Chk1 and Chk2 kinases in checkpoint control and cancer. *Cancer Cell* **3**, 421–429 (2003).
42. Prince, E. W. *et al.* Checkpoint kinase 1 expression is an adverse prognostic marker and therapeutic target in MYC-driven medulloblastoma. *Oncotarget* **7**, 53881–53894 (2016).
43. Pazzaglia, S. *et al.* High incidence of medulloblastoma following X-ray-irradiation of newborn Ptc1 heterozygous mice. *Oncogene* **21**, 7580–7584 (2002).
44. Pazzaglia, S. *et al.* Two-hit model for progression of medulloblastoma preneoplasia in Patched heterozygous mice. *Oncogene* **25**, 5575–5580 (2006).
45. Leonard, J. M., Ye, H., Wetmore, C. & Karnitz, L. M. Sonic Hedgehog signaling impairs ionizing radiation–induced checkpoint activation and induces genomic instability. *J. Cell Biol.* **183**, 385–391 (2008).
46. Lang, P. Y. *et al.* ATR maintains chromosomal integrity during postnatal cerebellar neurogenesis and is required for medulloblastoma formation. *Development* **143**, 4038–4052 (2016).
47. Petroni, M. & Giannini, G. A MYCN-MRN complex axis controls replication stress for the safe expansion of neuroprogenitor cells. *Mol Cell Oncol* **3**, e1079673 (2016).
48. Kuzyk, A. & Mai, S. c-MYC-induced genomic instability. *Cold Spring Harb. Perspect. Med.* **4**, a014373 (2014).
49. Campaner, S. & Amati, B. Two sides of the Myc-induced DNA damage response: from tumor suppression to tumor maintenance. *Cell Div.* **7**, 6 (2012).
50. Kenney, A. M., Cole, M. D. & Rowitch, D. H. Nmyc upregulation by sonic hedgehog signaling promotes proliferation in developing cerebellar granule neuron precursors. *Development* **130**, 15–28 (2003).
51. Frappart, P.-O. *et al.* Recurrent genomic alterations characterize medulloblastoma arising from DNA double-strand break repair deficiency. *Proc. Natl. Acad. Sci. U. S. A.* **106**, 1880–1885 (2009).
52. Wolpaw, A. J. *et al.* Drugging the 'Undruggable' MYCN Oncogenic Transcription Factor: Overcoming Previous Obstacles to Impact Childhood Cancers. *Cancer Res.* **81**, 1627–1632 (2021).
53. Moreira, D. C. *et al.* Targeting MYC-driven replication stress in medulloblastoma with AZD1775 and gemcitabine. *J. Neurooncol.* **147**, 531–545 (2020).
54. Krüger, K. *et al.* Multiple DNA damage-dependent and DNA damage-independent stress responses define the outcome of ATR/Chk1 targeting in medulloblastoma cells. *Cancer Lett.* **430**, 34–46 (2018).
55. Endersby, R. *et al.* Small-molecule screen reveals synergy of cell cycle checkpoint kinase inhibitors with DNA-damaging chemotherapies in medulloblastoma. *Sci. Transl. Med.* **13**, (2021).
56. Ray Chaudhuri, A. & Nussenzweig, A. The multifaceted roles of PARP1 in DNA repair and chromatin remodelling. *Nat. Rev. Mol. Cell Biol.* **18**, 610–621 (2017).
57. Chan, C. Y., Tan, K. V. & Cornelissen, B. PARP Inhibitors in Cancer Diagnosis and

Therapy. *Clin. Cancer Res.* (2020) doi:10.1158/1078-0432.CCR-20-2766.
58. Parmar, K. *et al.* The CHK1 Inhibitor Prexasertib Exhibits Monotherapy Activity in High-Grade Serous Ovarian Cancer Models and Sensitizes to PARP Inhibition. *Clin. Cancer Res.* **25**, 6127–6140 (2019).
59. McGrail, D. J. *et al.* Improved prediction of PARP inhibitor response and identification of synergizing agents through use of a novel gene expression signature generation algorithm. *NPJ Syst Biol Appl* **3**, 8 (2017).
60. Tong, W.-M. *et al.* Null Mutation of DNA Strand Break-Binding Molecule Poly(ADP-ribose) Polymerase Causes Medulloblastomas in p53−/− Mice. *The American Journal of Pathology* vol. 162 343–352 Preprint at https://doi.org/10.1016/s0002-9440(10)63825-4 (2003).
61. Marino, S., Vooijs, M., van Der Gulden, H., Jonkers, J. & Berns, A. Induction of medulloblastomas in p53-null mutant mice by somatic inactivation of Rb in the external granular layer cells of the cerebellum. *Genes Dev.* **14**, 994–1004 (2000).
62. Tanori, M. *et al.* PARP-1 cooperates with Ptc1 to suppress medulloblastoma and basal cell carcinoma. *Carcinogenesis* **29**, 1911–1919 (2008).
63. van Vuurden, D. G. *et al.* PARP inhibition sensitizes childhood high grade glioma, medulloblastoma and ependymoma to radiation. *Oncotarget* **2**, 984–996 (2011).
64. Carruthers, R. & Chalmers, A. J. The potential of PARP inhibitors in neuro-oncology. *CNS Oncol* **1**, 85–97 (2012).
65. Ning, J.-F. *et al.* Myc targeted CDK18 promotes ATR and homologous recombination to mediate PARP inhibitor resistance in glioblastoma. *Nat. Commun.* **10**, 2910 (2019).
66. Morales, J. *et al.* Review of poly (ADP-ribose) polymerase (PARP) mechanisms of action and rationale for targeting in cancer and other diseases. *Crit. Rev. Eukaryot. Gene Expr.* **24**, 15–28 (2014).
67. Kondo, N., Takahashi, A., Ono, K. & Ohnishi, T. DNA Damage Induced by Alkylating Agents and Repair Pathways. *Journal of Nucleic Acids* vol. 2010 1–7 Preprint at https://doi.org/10.4061/2010/543531 (2010).
68. Reardon, J. T., Vaisman, A., Chaney, S. G. & Sancar, A. Efficient nucleotide excision repair of cisplatin, oxaliplatin, and Bis-aceto-ammine-dichloro-cyclohexylamine-platinum(IV) (JM216) platinum intrastrand DNA diadducts. *Cancer Res.* **59**, 3968–3971 (1999).
69. Kummar, S. *et al.* Randomized phase II trial of cyclophosphamide and the oral poly (ADP-ribose) polymerase inhibitor veliparib in patients with recurrent, advanced triple-negative breast cancer. *Invest. New Drugs* **34**, 355–363 (2016).
70. McQuade, R. M., Stojanovska, V., Bornstein, J. C. & Nurgali, K. PARP inhibition in platinum-based chemotherapy: Chemopotentiation and neuroprotection. *Pharmacol. Res.* **137**, 104–113 (2018).
71. Murai, J. *et al.* Rationale for poly(ADP-ribose) polymerase (PARP) inhibitors in combination therapy with camptothecins or temozolomide based on PARP trapping versus catalytic inhibition. *J. Pharmacol. Exp. Ther.* **349**, 408–416 (2014).
72. Cefalo, G. *et al.* Temozolomide is an active agent in children with recurrent medulloblastoma/primitive neuroectodermal tumor: an Italian multi-institutional phase II trial. *Neuro. Oncol.* **16**, 748–753 (2014).
73. Bautista, F. *et al.* Medulloblastoma in children and adolescents: a systematic review of contemporary phase I and II clinical trials and biology update. *Cancer Med.* **6**, 2606–2624

(2017).
74. Le Teuff, G. *et al.* Phase II study of temozolomide and topotecan (TOTEM) in children with relapsed or refractory extracranial and central nervous system tumors including medulloblastoma with post hoc Bayesian analysis: A European ITCC study. *Pediatr. Blood Cancer* **67**, e28032 (2020).
75. Daniel, R. A. *et al.* Central nervous system penetration and enhancement of temozolomide activity in childhood medulloblastoma models by poly(ADP-ribose) polymerase inhibitor AG-014699. *British Journal of Cancer* vol. 103 1588–1596 Preprint at https://doi.org/10.1038/sj.bjc.6605946 (2010).
76. Murai, J. *et al.* Stereospecific PARP trapping by BMN 673 and comparison with olaparib and rucaparib. *Mol. Cancer Ther.* **13**, 433–443 (2014).
77. Tell, G., Quadrifoglio, F., Tiribelli, C. & Kelley, M. R. The many functions of APE1/Ref-1: not only a DNA repair enzyme. *Antioxid. Redox Signal.* **11**, 601–620 (2009).
78. Thakur, S. *et al.* APE1/Ref-1 as an emerging therapeutic target for various human diseases: phytochemical modulation of its functions. *Exp. Mol. Med.* **46**, e106 (2014).
79. Demple, B. & Harrison, L. Repair of oxidative damage to DNA: enzymology and biology. *Annu. Rev. Biochem.* **63**, 915–948 (1994).
80. Loeb, L. A. & Preston, B. D. Mutagenesis by apurinic/apyrimidinic sites. *Annu. Rev. Genet.* **20**, 201–230 (1986).
81. Boiteux, S. & Guillet, M. Abasic sites in DNA: repair and biological consequences in Saccharomyces cerevisiae. *DNA Repair* **3**, 1–12 (2004).
82. Li, H. *et al.* PARP inhibitor resistance: the underlying mechanisms and clinical implications. *Mol. Cancer* **19**, 107 (2020).
83. Dumitrache, L. C. *et al.* Apurinic endonuclease-1 preserves neural genome integrity to maintain homeostasis and thermoregulation and prevent brain tumors. *Proc. Natl. Acad. Sci. U. S. A.* **115**, E12285–E12294 (2018).
84. Bobola, M. S. *et al.* Apurinic endonuclease activity in adult gliomas and time to tumor progression after alkylating agent-based chemotherapy and after radiotherapy. *Clin. Cancer Res.* **10**, 7875–7883 (2004).
85. Silber, J. R. *et al.* The apurinic/apyrimidinic endonuclease activity of Ape1/Ref-1 contributes to human glioma cell resistance to alkylating agents and is elevated by oxidative stress. *Clin. Cancer Res.* **8**, 3008–3018 (2002).
86. Bobola, M. S., Blank, A., Berger, M. S., Stevens, B. A. & Silber, J. R. Apurinic/apyrimidinic endonuclease activity is elevated in human adult gliomas. *Clin. Cancer Res.* **7**, 3510–3518 (2001).
87. Bobola, M. S. *et al.* Apurinic/apyrimidinic endonuclease activity is associated with response to radiation and chemotherapy in medulloblastoma and primitive neuroectodermal tumors. *Clin. Cancer Res.* **11**, 7405–7414 (2005).
88. Saeedi, M., Eslamifar, M., Khezri, K. & Dizaj, S. M. Applications of nanotechnology in drug delivery to the central nervous system. *Biomedicine & Pharmacotherapy* vol. 111 666–675 Preprint at https://doi.org/10.1016/j.biopha.2018.12.133 (2019).
89. Kievit, F. M. *et al.* Nanoparticle mediated silencing of DNA repair sensitizes pediatric brain tumor cells to γ-irradiation. *Mol. Oncol.* **9**, 1071–1080 (2015).
90. Long, K. *et al.* Small-molecule inhibition of APE1 induces apoptosis, pyroptosis, and necroptosis in non-small cell lung cancer. *Cell Death Dis.* **12**, 503 (2021).
91. Borgo, C. & Ruzzene, M. Role of protein kinase CK2 in antitumor drug resistance. *J. Exp.*

Clin. Cancer Res. **38**, 287 (2019).
92. Fritz, G. & Kaina, B. Phosphorylation of the DNA repair protein APE/REF-1 by CKII affects redox regulation of AP-1. *Oncogene* **18**, 1033–1040 (1999).
93. Carter, R. J. & Parsons, J. L. Base Excision Repair, a Pathway Regulated by Posttranslational Modifications. *Mol. Cell. Biol.* **36**, 1426–1437 (2016).
94. Nitta, R. T. *et al.* Casein kinase 2 inhibition sensitizes medulloblastoma to temozolomide. *Oncogene* **38**, 6867–6879 (2019).
95. Gerson, S. L. MGMT: its role in cancer aetiology and cancer therapeutics. *Nat. Rev. Cancer* **4**, 296–307 (2004).
96. Rao, A. M., Quddusi, A. & Shamim, M. S. The significance of MGMT methylation in Glioblastoma Multiforme prognosis. *J. Pak. Med. Assoc.* **68**, 1137–1139 (2018).
97. Zheng, Y. *et al.* Targeting protein kinase CK2 suppresses prosurvival signaling pathways and growth of glioblastoma. *Clin. Cancer Res.* **19**, 6484–6494 (2013).
98. Pierre, F. *et al.* Discovery and SAR of 5-(3-Chlorophenylamino)benzo[c][2,6]naphthyridine-8-carboxylic Acid (CX-4945), the First Clinical Stage Inhibitor of Protein Kinase CK2 for the Treatment of Cancer. *Journal of Medicinal Chemistry* vol. 54 635–654 Preprint at https://doi.org/10.1021/jm101251q (2011).
99. Rabalski, A. J., Gyenis, L. & Litchfield, D. W. Molecular Pathways: Emergence of Protein Kinase CK2 (CSNK2) as a Potential Target to Inhibit Survival and DNA Damage Response and Repair Pathways in Cancer Cells. *Clin. Cancer Res.* **22**, 2840–2847 (2016).
100. Jia, H. *et al.* Casein kinase 2 promotes Hedgehog signaling by regulating both smoothened and Cubitus interruptus. *J. Biol. Chem.* **285**, 37218–37226 (2010).
101. Purzner, T. *et al.* Developmental phosphoproteomics identifies the kinase CK2 as a driver of Hedgehog signaling and a therapeutic target in medulloblastoma. *Sci. Signal.* **11**, (2018).
102. Leroux, A. E., Schulze, J. O. & Biondi, R. M. AGC kinases, mechanisms of regulation and innovative drug development. *Semin. Cancer Biol.* **48**, 1–17 (2018).
103. Manning, B. D. & Cantley, L. C. AKT/PKB signaling: navigating downstream. *Cell* **129**, 1261–1274 (2007).
104. Liu, W. *et al.* A prognostic analysis of pediatrics central nervous system small cell tumors: evaluation of EGFR family gene amplification and overexpression. *Diagn. Pathol.* **9**, 132 (2014).
105. Slongo, M. L. *et al.* Functional VEGF and VEGF receptors are expressed in human medulloblastomas. *Neuro. Oncol.* **9**, 384–392 (2007).
106. Svalina, M. N. *et al.* IGF1R as a Key Target in High Risk, Metastatic Medulloblastoma. *Sci. Rep.* **6**, 27012 (2016).
107. Blom, T. *et al.* Amplification and overexpression of KIT, PDGFRA, and VEGFR2 in medulloblastomas and primitive neuroectodermal tumors. *J. Neurooncol.* **97**, 217–224 (2010).
108. Black, P., Carroll, R. & Glowacka, D. Expression of platelet-derived growth factor transcripts in medulloblastomas and ependymomas. *Pediatr. Neurosurg.* **24**, 74–78 (1996).
109. Hoxhaj, G. & Manning, B. D. The PI3K-AKT network at the interface of oncogenic signalling and cancer metabolism. *Nat. Rev. Cancer* **20**, 74–88 (2020).
110. Manning, B. D. & Toker, A. AKT/PKB Signaling: Navigating the Network. *Cell* **169**, 381–405 (2017).
111. Dangelmaier, C. *et al.* PDK1 selectively phosphorylates Thr(308) on Akt and contributes to

human platelet functional responses. *Thromb. Haemost.* **111**, 508–517 (2014).
112. Xu, F., Na, L., Li, Y. & Chen, L. Roles of the PI3K/AKT/mTOR signalling pathways in neurodegenerative diseases and tumours. *Cell Biosci.* **10**, 54 (2020).
113. Liu, Q., Turner, K. M., Alfred Yung, W. K., Chen, K. & Zhang, W. Role of AKT signaling in DNA repair and clinical response to cancer therapy. *Neuro. Oncol.* **16**, 1313–1323 (2014).
114. Xu, N., Lao, Y., Zhang, Y. & Gillespie, D. A. Akt: a double-edged sword in cell proliferation and genome stability. *J. Oncol.* **2012**, 951724 (2012).
115. Benson, E. K. *et al.* p53-dependent gene repression through p21 is mediated by recruitment of E2F4 repression complexes. *Oncogene* **33**, 3959–3969 (2014).
116. Woods, D. & Turchi, J. J. Chemotherapy induced DNA damage response: convergence of drugs and pathways. *Cancer Biol. Ther.* **14**, 379–389 (2013).
117. Iyama, T. & Wilson, D. M., 3rd. DNA repair mechanisms in dividing and non-dividing cells. *DNA Repair* **12**, 620–636 (2013).
118. Fraser, M. *et al.* MRE11 promotes AKT phosphorylation in direct response to DNA double-strand breaks. *Cell Cycle* **10**, 2218–2232 (2011).
119. Plo, I. *et al.* AKT1 inhibits homologous recombination by inducing cytoplasmic retention of BRCA1 and RAD51. *Cancer Res.* **68**, 9404–9412 (2008).
120. Liu, R. *et al.* PI3K/AKT pathway as a key link modulates the multidrug resistance of cancers. *Cell Death Dis.* **11**, 797 (2020).
121. Roussel, M. F. & Hatten, M. E. Cerebellum development and medulloblastoma. *Curr. Top. Dev. Biol.* **94**, 235–282 (2011).
122. Pazzaglia, S. *et al.* Linking DNA damage to medulloblastoma tumorigenesis in patched heterozygous knockout mice. *Oncogene* **25**, 1165–1173 (2006).
123. Kool, M. *et al.* Genome sequencing of SHH medulloblastoma predicts genotype-related response to smoothened inhibition. *Cancer Cell* **25**, 393–405 (2014).
124. Chaturvedi, N. K. *et al.* Improved therapy for medulloblastoma: targeting hedgehog and PI3K-mTOR signaling pathways in combination with chemotherapy. *Oncotarget* **9**, 16619–16633 (2018).
125. Baryawno, N. *et al.* Small-molecule inhibitors of phosphatidylinositol 3-kinase/Akt signaling inhibit Wnt/beta-catenin pathway cross-talk and suppress medulloblastoma growth. *Cancer Res.* **70**, 266–276 (2010).
126. Guerreiro, A. S. *et al.* Targeting the PI3K p110α Isoform Inhibits Medulloblastoma Proliferation, Chemoresistance, and Migration. *Clin. Cancer Res.* **14**, 6761–6769 (2008).
127. Craveiro, R. B. *et al.* The anti-neoplastic activity of Vandetanib against high-risk medulloblastoma variants is profoundly enhanced by additional PI3K inhibition. *Oncotarget* **8**, 46915–46927 (2017).
128. Charles, N. & Holland, E. C. The perivascular niche microenvironment in brain tumor progression. *Cell Cycle* **9**, 3012–3021 (2010).
129. Eckerdt, F. *et al.* Pharmacological mTOR targeting enhances the antineoplastic effects of selective PI3Kα inhibition in medulloblastoma. *Sci. Rep.* **9**, 12822 (2019).
130. Crespo, S., Kind, M. & Arcaro, A. The role of the PI3K/AKT/mTOR pathway in brain tumor metastasis. *J. Cancer Metastasis Treat.* **2**, 80 (2016).
131. Hambardzumyan, D. *et al.* PI3K pathway regulates survival of cancer stem cells residing in the perivascular niche following radiation in medulloblastoma in vivo. *Genes Dev.* **22**, 436–448 (2008).

132. Shariati, M. & Meric-Bernstam, F. Targeting AKT for cancer therapy. *Expert Opin. Investig. Drugs* **28**, 977–988 (2019).
133. Martorana, F. *et al.* AKT Inhibitors: New Weapons in the Fight Against Breast Cancer? *Front. Pharmacol.* **12**, 662232 (2021).
134. Machl, A. *et al.* M2698 is a potent dual-inhibitor of p70S6K and Akt that affects tumor growth in mouse models of cancer and crosses the blood-brain barrier. *Am. J. Cancer Res.* **6**, 806–818 (2016).
135. Badiali, M. *et al.* p53 gene mutations in medulloblastoma. Immunohistochemistry, gel shift analysis, and sequencing. *Diagn. Mol. Pathol.* **2**, 23–28 (1993).
136. Pomeroy, S. L. The p53 tumor suppressor gene and pediatric brain tumors. *Curr. Opin. Pediatr.* **6**, 632–635 (1994).
137. Dee, S., Haas-Kogan, D. A. & Israel, M. A. Inactivation of p53 is associated with decreased levels of radiation-induced apoptosis in medulloblastoma cell lines. *Cell Death Differ.* **2**, 267–275 (1995).
138. Lu, X. *et al.* The Wip1 Phosphatase acts as a gatekeeper in the p53-Mdm2 autoregulatory loop. *Cancer Cell* **12**, 342–354 (2007).
139. Chao, C. C.-K. Mechanisms of p53 degradation. *Clin. Chim. Acta* **438**, 139–147 (2015).
140. Woodburn, R. T., Azzarelli, B., Montebello, J. F. & Goss, I. E. Intense p53 staining is a valuable prognostic indicator for poor prognosis in medulloblastoma/central nervous system primitive neuroectodermal tumors. *J. Neurooncol.* **52**, 57–62 (2001).
141. Adesina, A. M., Nalbantoglu, J. & Cavenee, W. K. p53 gene mutation and mdm2 gene amplification are uncommon in medulloblastoma. *Cancer Res.* **54**, 5649–5651 (1994).
142. Saylors, R. L., 3rd *et al.* Infrequent p53 gene mutations in medulloblastomas. *Cancer Res.* **51**, 4721–4723 (1991).
143. Giordana, M. T. *et al.* MDM2 overexpression is associated with short survival in adults with medulloblastoma. *Neuro. Oncol.* **4**, 115–122 (2002).
144. Harris, S. L. & Levine, A. J. The p53 pathway: positive and negative feedback loops. *Oncogene* **24**, 2899–2908 (2005).
145. Dharia, N. V. *et al.* A first-generation pediatric cancer dependency map. *Nat. Genet.* **53**, 529–538 (2021).
146. Zenvirt, S., Kravchenko-Balasha, N. & Levitzki, A. Status of p53 in human cancer cells does not predict efficacy of CHK1 kinase inhibitors combined with chemotherapeutic agents. *Oncogene* **29**, 6149–6159 (2010).
147. Williams, A. B. & Schumacher, B. p53 in the DNA-Damage-Repair Process. *Cold Spring Harb. Perspect. Med.* **6**, (2016).
148. Joerger, A. C. & Fersht, A. R. The p53 Pathway: Origins, Inactivation in Cancer, and Emerging Therapeutic Approaches. *Annu. Rev. Biochem.* **85**, 375–404 (2016).
149. Zhulyn, O., Nieuwenhuis, E., Liu, Y. C., Angers, S. & Hui, C.-C. Ptch2 shares overlapping functions with Ptch1 in Smo regulation and limb development. *Dev. Biol.* **397**, 191–202 (2015).
150. Shakhova, O., Leung, C., van Montfort, E., Berns, A. & Marino, S. Lack of Rb and p53 delays cerebellar development and predisposes to large cell anaplastic medulloblastoma through amplification of N-Myc and Ptch2. *Cancer Res.* **66**, 5190–5200 (2006).
151. Uziel, T. *et al.* The tumor suppressors Ink4c and p53 collaborate independently with Patched to suppress medulloblastoma formation. *Genes Dev.* **19**, 2656–2667 (2005).
152. Holcomb, V. B., Vogel, H., Marple, T., Kornegay, R. W. & Hasty, P. Ku80 and p53

suppress medulloblastoma that arise independent of Rag-1-induced DSBs. *Oncogene* **25**, 7159–7165 (2006).
153. Lee, Y. & McKinnon, P. J. DNA ligase IV suppresses medulloblastoma formation. *Cancer Res.* **62**, 6395–6399 (2002).
154. Orii, K. E., Lee, Y., Kondo, N. & McKinnon, P. J. Selective utilization of nonhomologous end-joining and homologous recombination DNA repair pathways during nervous system development. *Proc. Natl. Acad. Sci. U. S. A.* **103**, 10017–10022 (2006).
155. Chun, J., Buechelmaier, E. S. & Powell, S. N. Rad51 paralog complexes BCDX2 and CX3 act at different stages in the BRCA1-BRCA2-dependent homologous recombination pathway. *Mol. Cell. Biol.* **33**, 387–395 (2013).
156. Kim, J., Kim, J. & Lee, Y. DNA polymerase β deficiency in the p53 null cerebellum leads to medulloblastoma formation. *Biochem. Biophys. Res. Commun.* **505**, 548–553 (2018).
157. Konopleva, M. *et al.* MDM2 inhibition: an important step forward in cancer therapy. *Leukemia* **34**, 2858–2874 (2020).
158. Malek, R., Matta, J., Taylor, N., Perry, M. E. & Mendrysa, S. M. The p53 inhibitor MDM2 facilitates Sonic Hedgehog-mediated tumorigenesis and influences cerebellar foliation. *PLoS One* **6**, e17884 (2011).
159. Van Maerken, T. *et al.* Pharmacologic activation of wild-type p53 by nutlin therapy in childhood cancer. *Cancer Lett.* **344**, 157–165 (2014).
160. Künkele, A. *et al.* Pharmacological activation of the p53 pathway by nutlin-3 exerts anti-tumoral effects in medulloblastomas. *Neuro. Oncol.* **14**, 859–869 (2012).
161. Ghassemifar, S. & Mendrysa, S. M. MDM2 antagonism by nutlin-3 induces death in human medulloblastoma cells. *Neurosci. Lett.* **513**, 106–110 (2012).
162. Nishimori, H. *et al.* A novel brain-specific p53-target gene, BAI1, containing thrombospondin type 1 repeats inhibits experimental angiogenesis. *Oncogene* vol. 15 2145–2150 Preprint at https://doi.org/10.1038/sj.onc.1201542 (1997).
163. Zhu, D. *et al.* BAI1 Suppresses Medulloblastoma Formation by Protecting p53 from Mdm2-Mediated Degradation. *Cancer Cell* **33**, 1004–1016.e5 (2018).
164. Zhang, H. *et al.* EZH2 targeting reduces medulloblastoma growth through epigenetic reactivation of the BAI1/p53 tumor suppressor pathway. *Oncogene* **39**, 1041–1048 (2020).
165. Wei, Y. *et al.* p53 Function Is Compromised by Inhibitor 2 of Phosphatase 2A in Sonic Hedgehog Medulloblastoma. *Mol. Cancer Res.* **17**, 186–198 (2019).
166. Pecháčková, S., Burdová, K. & Macurek, L. WIP1 phosphatase as pharmacological target in cancer therapy. *J. Mol. Med.* **95**, 589–599 (2017).
167. Fiscella, M. *et al.* Wip1, a novel human protein phosphatase that is induced in response to ionizing radiation in a p53-dependent manner. *Proc. Natl. Acad. Sci. U. S. A.* **94**, 6048–6053 (1997).
168. Castellino, R. C. *et al.* Medulloblastomas overexpress the p53-inactivating oncogene WIP1/PPM1D. *J. Neurooncol.* **86**, 245–256 (2008).
169. Akamandisa, M. P., Nie, K., Nahta, R., Hambardzumyan, D. & Castellino, R. C. Inhibition of mutant PPM1D enhances DNA damage response and growth suppressive effects of ionizing radiation in diffuse intrinsic pontine glioma. *Neuro. Oncol.* **21**, 786–799 (2019).
170. Doucette, T. A. *et al.* WIP1 Enhances Tumor Formation in a Sonic Hedgehog–Dependent Model of Medulloblastoma. *Neurosurgery* vol. 70 1003–1010 Preprint at https://doi.org/10.1227/neu.0b013e31823e5332 (2012).
171. Wen, J. *et al.* WIP1 modulates responsiveness to Sonic Hedgehog signaling in neuronal

precursor cells and medulloblastoma. *Oncogene* **35**, 5552–5564 (2016).
172. Yi, M. *et al.* Advances and perspectives of PARP inhibitors. *Exp. Hematol. Oncol.* **8**, 29 (2019).
173. Burgess, A. *et al.* Clinical Overview of MDM2/X-Targeted Therapies. *Front. Oncol.* **6**, 7 (2016).
174. Qiu, Z., Oleinick, N. L. & Zhang, J. ATR/CHK1 inhibitors and cancer therapy. *Radiother. Oncol.* **126**, 450–464 (2018).
175. Didier, D. K., Schiffenbauer, J., Woulfe, S. L., Zacheis, M. & Schwartz, B. D. Characterization of the cDNA encoding a protein binding to the major histocompatibility complex class II Y box. *Proc. Natl. Acad. Sci. U. S. A.* **85**, 7322–7326 (1988).
176. Sutherland, B. W. *et al.* Akt phosphorylates the Y-box binding protein 1 at Ser102 located in the cold shock domain and affects the anchorage-independent growth of breast cancer cells. *Oncogene* **24**, 4281–4292 (2005).
177. Evdokimova, V. *et al.* Akt-mediated YB-1 phosphorylation activates translation of silent mRNA species. *Mol. Cell. Biol.* **26**, 277–292 (2006).
178. Bader, A. G. & Vogt, P. K. Phosphorylation by Akt disables the anti-oncogenic activity of YB-1. *Oncogene* **27**, 1179–1182 (2008).
179. Coles, L. S. *et al.* Phosphorylation of cold shock domain/Y-box proteins by ERK2 and GSK3beta and repression of the human VEGF promoter. *FEBS Lett.* **579**, 5372–5378 (2005).
180. Stratford, A. L. *et al.* Y-box binding protein-1 serine 102 is a downstream target of p90 ribosomal S6 kinase in basal-like breast cancer cells. *Breast Cancer Res.* **10**, R99 (2008).
181. Miao, X. *et al.* Y-box-binding protein-1 (YB-1) promotes cell proliferation, adhesion and drug resistance in diffuse large B-cell lymphoma. *Exp. Cell Res.* **346**, 157–166 (2016).
182. Tiwari, A. *et al.* Stress-Induced Phosphorylation of Nuclear YB-1 Depends on Nuclear Trafficking of p90 Ribosomal S6 Kinase. *Int. J. Mol. Sci.* **19**, (2018).
183. Gieseler-Halbach, S. *et al.* RSK-mediated nuclear accumulation of the cold-shock Y-box protein-1 controls proliferation of T cells and T-ALL blasts. *Cell Death Differ.* **24**, 371–383 (2017).
184. El-Naggar, A. M. *et al.* Class I HDAC inhibitors enhance YB-1 acetylation and oxidative stress to block sarcoma metastasis. *EMBO Rep.* **20**, e48375 (2019).
185. Liu, Q. *et al.* Hyper-O-GlcNAcylation of YB-1 affects Ser102 phosphorylation and promotes cell proliferation in hepatocellular carcinoma. *Exp. Cell Res.* **349**, 230–238 (2016).
186. Chen, L. *et al.* O-GlcNAcylation promotes cerebellum development and medulloblastoma oncogenesis via SHH signaling. *Proc. Natl. Acad. Sci. U. S. A.* **119**, e2202821119 (2022).
187. Alemasova, E. E. *et al.* Poly(ADP-ribosyl)ation as a new posttranslational modification of YB-1. *Biochimie* **119**, 36–44 (2015).
188. Naumenko, K. N. *et al.* The C-Terminal Domain of Y-Box Binding Protein 1 Exhibits Structure-Specific Binding to Poly(ADP-Ribose), Which Regulates PARP1 Activity. *Front Cell Dev Biol* **10**, 831741 (2022).
189. Su, W. *et al.* Silencing of Long Noncoding RNA Triggers Cell Survival/Death Signaling via Oncogenes YBX1, MET, and p21 in Lung Cancer. *Cancer Res.* **78**, 3207–3219 (2018).
190. Skabkina, O. V. *et al.* Poly(A)-binding protein positively affects YB-1 mRNA translation through specific interaction with YB-1 mRNA. *J. Biol. Chem.* **278**, 18191–18198 (2003).
191. Skabkina, O. V., Lyabin, D. N., Skabkin, M. A. & Ovchinnikov, L. P. YB-1 autoregulates

translation of its own mRNA at or prior to the step of 40S ribosomal subunit joining. *Mol. Cell. Biol.* **25**, 3317–3323 (2005).
192. Lyabin, D. N., Eliseeva, I. A. & Ovchinnikov, L. P. YB-1 synthesis is regulated by mTOR signaling pathway. *PLoS One* **7**, e52527 (2012).
193. Lyabin, D. N. & Ovchinnikov, L. P. Selective regulation of YB-1 mRNA translation by the mTOR signaling pathway is not mediated by 4E-binding protein. *Sci. Rep.* **6**, 22502 (2016).
194. Lyabin, D. N., Nigmatullina, L. F., Doronin, A. N., Eliseeva, I. A. & Ovchinnikov, L. P. Identification of proteins specifically interacting with YB-1 mRNA 3' UTR and the effect of hnRNP Q on YB-1 mRNA translation. *Biochemistry* **78**, 651–659 (2013).
195. Pelengaris, S., Khan, M. & Evan, G. c-MYC: more than just a matter of life and death. *Nat. Rev. Cancer* **2**, 764–776 (2002).
196. Uramoto, H. *et al.* p73 Interacts with c-Myc to regulate Y-box-binding protein-1 expression. *J. Biol. Chem.* **277**, 31694–31702 (2002).
197. Ohashi, S., Fukumura, R., Higuchi, T. & Kobayashi, S. YB-1 transcription in the postnatal brain is regulated by a bHLH transcription factor Math2 through an E-box sequence in the 5'-UTR of the gene. *Mol. Cell. Biochem.* **327**, 267–275 (2009).
198. McCormick, M. B. *et al.* NeuroD2 and neuroD3: distinct expression patterns and transcriptional activation potentials within the neuroD gene family. *Mol. Cell. Biol.* **16**, 5792–5800 (1996).
199. Olson, J. M. *et al.* NeuroD2 is necessary for development and survival of central nervous system neurons. *Dev. Biol.* **234**, 174–187 (2001).
200. Pieper, A. *et al.* NeuroD2 controls inhibitory circuit formation in the molecular layer of the cerebellum. *Sci. Rep.* **9**, 1448 (2019).
201. Dey, A. *et al.* YB-1 is elevated in medulloblastoma and drives proliferation in Sonic hedgehog-dependent cerebellar granule neuron progenitor cells and medulloblastoma cells. *Oncogene* **35**, 4256–4268 (2016).
202. Lu, Z. H., Books, J. T. & Ley, T. J. YB-1 is important for late-stage embryonic development, optimal cellular stress responses, and the prevention of premature senescence. *Mol. Cell. Biol.* **25**, 4625–4637 (2005).
203. Uchiumi, T. *et al.* YB-1 is important for an early stage embryonic development: neural tube formation and cell proliferation. *J. Biol. Chem.* **281**, 40440–40449 (2006).
204. Kotake, Y. *et al.* YB1 binds to and represses the p16 tumor suppressor gene. *Genes Cells* **18**, 999–1006 (2013).
205. Bergmann, S. *et al.* YB-1 provokes breast cancer through the induction of chromosomal instability that emerges from mitotic failure and centrosome amplification. *Cancer Res.* **65**, 4078–4087 (2005).
206. Davies, A. H. *et al.* YB-1 evokes susceptibility to cancer through cytokinesis failure, mitotic dysfunction and HER2 amplification. *Oncogene* **30**, 3649–3660 (2011).
207. Fotovati, A. *et al.* YB-1 bridges neural stem cells and brain tumor-initiating cells via its roles in differentiation and cell growth. *Cancer Res.* **71**, 5569–5578 (2011).
208. Jurchott, K. *et al.* YB-1 as a cell cycle-regulated transcription factor facilitating cyclin A and cyclin B1 gene expression. *J. Biol. Chem.* **278**, 27988–27996 (2003).
209. Liu, Z. *et al.* Overexpression of YBX1 Promotes Pancreatic Ductal Adenocarcinoma Growth via the GSK3B/Cyclin D1/Cyclin E1 Pathway. *Mol Ther Oncolytics* **17**, 21–30 (2020).
210. Harada, M. *et al.* YB-1 promotes transcription of cyclin D1 in human non-small-cell lung

cancers. *Genes Cells* **19**, 504–516 (2014).
211. Chao, H.-M. *et al.* Y-box binding protein-1 promotes hepatocellular carcinoma-initiating cell progression and tumorigenesis via Wnt/β-catenin pathway. *Oncotarget* **8**, 2604–2616 (2017).
212. En-Nia, A. *et al.* Transcription factor YB-1 mediates DNA polymerase alpha gene expression. *J. Biol. Chem.* **280**, 7702–7711 (2005).
213. Wu, J. *et al.* Disruption of the Y-box binding protein-1 results in suppression of the epidermal growth factor receptor and HER-2. *Cancer Res.* **66**, 4872–4879 (2006).
214. Ou, Y. *et al.* Kindlin-2 interacts with β-catenin and YB-1 to enhance EGFR transcription during glioma progression. *Oncotarget* **7**, 74872–74885 (2016).
215. Delicato, A., Montuori, E., Angrisano, T., Pollice, A. & Calabrò, V. YB-1 Oncoprotein Controls PI3K/Akt Pathway by Reducing Pten Protein Level. *Genes* **12**, (2021).
216. Di Costanzo, A. *et al.* The p63 protein isoform ΔNp63α modulates Y-box binding protein 1 in its subcellular distribution and regulation of cell survival and motility genes. *J. Biol. Chem.* **287**, 30170–30180 (2012).
217. Sinnberg, T. *et al.* MAPK and PI3K/AKT mediated YB-1 activation promotes melanoma cell proliferation which is counteracted by an autoregulatory loop. *Exp. Dermatol.* **21**, 265–270 (2012).
218. Imada, K. *et al.* Mutual regulation between Raf/MEK/ERK signaling and Y-box-binding protein-1 promotes prostate cancer progression. *Clin. Cancer Res.* **19**, 4638–4650 (2013).
219. Frye, B. C. *et al.* Y-box protein-1 is actively secreted through a non-classical pathway and acts as an extracellular mitogen. *EMBO Rep.* **10**, 783–789 (2009).
220. Kosnopfel, C. *et al.* Tumour Progression Stage-Dependent Secretion of YB-1 Stimulates Melanoma Cell Migration and Invasion. *Cancers* **12**, (2020).
221. Evdokimova, V. *et al.* Translational activation of snail1 and other developmentally regulated transcription factors by YB-1 promotes an epithelial-mesenchymal transition. *Cancer Cell* **15**, 402–415 (2009).
222. Pang, T. *et al.* Y Box-Binding Protein 1 Promotes Epithelial-Mesenchymal Transition, Invasion, and Metastasis of Cervical Cancer via Enhancing the Expressions of Snail. *Int. J. Gynecol. Cancer* **27**, 1753–1760 (2017).
223. El-Naggar, A. M. *et al.* Translational Activation of HIF1α by YB-1 Promotes Sarcoma Metastasis. *Cancer Cell* **27**, 682–697 (2015).
224. Quintero-Fabián, S. *et al.* Role of Matrix Metalloproteinases in Angiogenesis and Cancer. *Front. Oncol.* **9**, 1370 (2019).
225. Shinkai, K. *et al.* Nuclear expression of Y-box binding protein-1 is associated with poor prognosis in patients with pancreatic cancer and its knockdown inhibits tumor growth and metastasis in mice tumor models. *Int. J. Cancer* **139**, 433–445 (2016).
226. Lim, J. P. *et al.* Silencing Y-box binding protein-1 inhibits triple-negative breast cancer cell invasiveness via regulation of MMP1 and beta-catenin expression. *Cancer Lett.* **452**, 119–131 (2019).
227. Guo, T. *et al.* Transcriptional activation of NANOG by YBX1 promotes lung cancer stem-like properties and metastasis. *Biochem. Biophys. Res. Commun.* **487**, 153–159 (2017).
228. Zhang, H. *et al.* Prostaglandin E2 promotes hepatocellular carcinoma cell invasion through upregulation of YB-1 protein expression. *Int. J. Oncol.* **44**, 769–780 (2014).
229. Guo, T. T., Yu, Y. N., Yip, G. W. C., Matsumoto, K. & Bay, B. H. Silencing the YB-1 gene inhibits cell migration in gastric cancer in vitro. *Anat. Rec.* **296**, 891–898 (2013).

230. Ha, B., Lee, E. B., Cui, J., Kim, Y. & Jang, H. H. YB-1 overexpression promotes a TGF-β1-induced epithelial-mesenchymal transition via Akt activation. *Biochem. Biophys. Res. Commun.* **458**, 347–351 (2015).
231. Ohga, T. *et al.* Role of the human Y box-binding protein YB-1 in cellular sensitivity to the DNA-damaging agents cisplatin, mitomycin C, and ultraviolet light. *Cancer Res.* **56**, 4224–4228 (1996).
232. Shibahara, K. *et al.* Targeted disruption of one allele of the Y-box binding protein-1 (YB-1) gene in mouse embryonic stem cells and increased sensitivity to cisplatin and mitomycin C. *Cancer Sci.* **95**, 348–353 (2004).
233. Gaudreault, I., Guay, D. & Lebel, M. YB-1 promotes strand separation in vitro of duplex DNA containing either mispaired bases or cisplatin modifications, exhibits endonucleolytic activities and binds several DNA repair proteins. *Nucleic Acids Res.* **32**, 316–327 (2004).
234. Pestryakov, P. *et al.* Effect of the multifunctional proteins RPA, YB-1, and XPC repair factor on AP site cleavage by DNA glycosylase NEIL1. *J. Mol. Recognit.* **25**, 224–233 (2012).
235. Alemasova, E. E. *et al.* Y-box-binding protein 1 as a non-canonical factor of base excision repair. *Biochim. Biophys. Acta* **1864**, 1631–1640 (2016).
236. Chang, Y.-W. *et al.* YB-1 disrupts mismatch repair complex formation, interferes with MutSα recruitment on mismatch and inhibits mismatch repair through interacting with PCNA. *Oncogene* **33**, 5065–5077 (2014).
237. Fomina, E. E. *et al.* Y-box binding protein 1 (YB-1) promotes detection of DNA bulky lesions by XPC-HR23B factor. *Biochemistry* **80**, 219–227 (2015).
238. Naumenko, K. N. *et al.* Regulation of Poly(ADP-Ribose) Polymerase 1 Activity by Y-Box-Binding Protein 1. *Biomolecules* **10**, (2020).
239. Alemasova, E. E., Naumenko, K. N., Kurgina, T. A., Anarbaev, R. O. & Lavrik, O. I. The multifunctional protein YB-1 potentiates PARP1 activity and decreases the efficiency of PARP1 inhibitors. *Oncotarget* **9**, 23349–23365 (2018).
240. Kim, E. R. *et al.* The proteolytic YB-1 fragment interacts with DNA repair machinery and enhances survival during DNA damaging stress. *Cell Cycle* **12**, 3791–3803 (2013).
241. Ghanawi, H. *et al.* Loss of full-length hnRNP R isoform impairs DNA damage response in motoneurons by inhibiting Yb1 recruitment to chromatin. *Nucleic Acids Res.* **49**, 12284–12305 (2021).
242. Fujita, T. *et al.* Increased nuclear localization of transcription factor Y-box binding protein 1 accompanied by up-regulation of P-glycoprotein in breast cancer pretreated with paclitaxel. *Clin. Cancer Res.* **11**, 8837–8844 (2005).
243. Chattopadhyay, R. *et al.* Regulatory role of human AP-endonuclease (APE1/Ref-1) in YB-1-mediated activation of the multidrug resistance gene MDR1. *Mol. Cell. Biol.* **28**, 7066–7080 (2008).
244. Sengupta, S., Mantha, A. K., Mitra, S. & Bhakat, K. K. Human AP endonuclease (APE1/Ref-1) and its acetylation regulate YB-1-p300 recruitment and RNA polymerase II loading in the drug-induced activation of multidrug resistance gene MDR1. *Oncogene* **30**, 482–493 (2011).
245. Mo, D. *et al.* Human Helicase RECQL4 Drives Cisplatin Resistance in Gastric Cancer by Activating an AKT-YB1-MDR1 Signaling Pathway. *Cancer Res.* **76**, 3057–3066 (2016).
246. Chua, P. J. *et al.* Y-box binding protein-1 and STAT3 independently regulate ATP-binding cassette transporters in the chemoresistance of gastric cancer cells. *Int. J. Oncol.* **53**, 2579–

2589 (2018).
247. Lasham, A. *et al.* The Y-box-binding protein, YB1, is a potential negative regulator of the p53 tumor suppressor. *J. Biol. Chem.* **278**, 35516–35523 (2003).
248. Homer, C. *et al.* Y-box factor YB1 controls p53 apoptotic function. *Oncogene* **24**, 8314–8325 (2005).
249. Zhang, Y. F. *et al.* Nuclear localization of Y-box factor YB1 requires wild-type p53. *Oncogene* **22**, 2782–2794 (2003).
250. Tong, H., Zhao, K., Zhang, J., Zhu, J. & Xiao, J. YB-1 modulates the drug resistance of glioma cells by activation of MDM2/p53 pathway. *Drug Des. Devel. Ther.* **13**, 317–326 (2019).
251. Feng, M. *et al.* YBX1 is required for maintaining myeloid leukemia cell survival by regulating BCL2 stability in an m6A-dependent manner. *Blood* **138**, 71–85 (2021).
252. Setoguchi, K. *et al.* Antisense Oligonucleotides Targeting Y-Box Binding Protein-1 Inhibit Tumor Angiogenesis by Downregulating Bcl-xL-VEGFR2/-Tie Axes. *Mol. Ther. Nucleic Acids* **9**, 170–181 (2017).
253. Kawaguchi, A., Asaka, M. N., Matsumoto, K. & Nagata, K. Centrosome maturation requires YB-1 to regulate dynamic instability of microtubules for nucleus reassembly. *Sci. Rep.* **5**, 8768 (2015).
254. Perner, F. *et al.* YBX1 mediates translation of oncogenic transcripts to control cell competition in AML. *Leukemia* **36**, 426–437 (2022).
255. Sánchez, B. J. *et al.* The formation of HuR/YB1 complex is required for the stabilization of target mRNA to promote myogenesis. *Nucleic Acids Res.* **51**, 1375–1392 (2023).
256. Bommert, K. S. *et al.* The feed-forward loop between YB-1 and MYC is essential for multiple myeloma cell survival. *Leukemia* **27**, 441–450 (2013).
257. Tailor, D. *et al.* Y box binding protein 1 inhibition as a targeted therapy for ovarian cancer. *Cell Chem Biol* **28**, 1206–1220.e6 (2021).
258. McSwain, L. F. *et al.* Medulloblastoma and the DNA Damage Response. *Front. Oncol.* **12**, 903830 (2022).
259. Thomas, A. & Noël, G. Medulloblastoma: optimizing care with a multidisciplinary approach. *J. Multidiscip. Healthc.* **12**, 335–347 (2019).
260. Martin, A. M., Raabe, E., Eberhart, C. & Cohen, K. J. Management of pediatric and adult patients with medulloblastoma. *Curr. Treat. Options Oncol.* **15**, 581–594 (2014).
261. Inc., K. N. & Kernel Networks Inc. Evaluation of LY2606368 Therapy in Combination With Cyclophosphamide or Gemcitabine for Children and Adolescents With Refractory or Recurrent Group 3/Group 4 or SHH Medulloblastoma Brain Tumors. *Case Medical Research* Preprint at https://doi.org/10.31525/ct1-nct04023669 (2019).
262. Taylor, L., Kerr, I. D. & Coyle, B. Y-Box Binding Protein-1: A Neglected Target in Pediatric Brain Tumors? *Mol. Cancer Res.* **19**, 375–387 (2021).
263. Alkrekshi, A., Wang, W., Rana, P. S., Markovic, V. & Sossey-Alaoui, K. A comprehensive review of the functions of YB-1 in cancer stemness, metastasis and drug resistance. *Cell. Signal.* **85**, 110073 (2021).
264. Toulany, M. *et al.* Impact of oncogenic K-RAS on YB-1 phosphorylation induced by ionizing radiation. *Breast Cancer Res.* **13**, R28 (2011).
265. Liu, D. *et al.* The interaction between PDCD4 and YB1 is critical for cervical cancer stemness and cisplatin resistance. *Mol. Carcinog.* **60**, 813–825 (2021).
266. Ke, J. *et al.* Nucleolin Promotes Cisplatin Resistance in Cervical Cancer by the YB1-MDR1

Pathway. *J. Oncol.* **2021**, 9992218 (2021).
267. Kleinerman, E. S. & Gorlick, R. *Current Advances in the Science of Osteosarcoma: Research Perspectives: Tumor Biology, Organ Microenvironment, Potential New Therapeutic Targets, and Canine Models*. (Springer Nature, 2020).
268. Guay, D., Gaudreault, I., Massip, L. & Lebel, M. Formation of a nuclear complex containing the p53 tumor suppressor, YB-1, and the Werner syndrome gene product in cells treated with UV light. *Int. J. Biochem. Cell Biol.* **38**, 1300–1313 (2006).
269. Berman, D. M. *et al.* Medulloblastoma growth inhibition by hedgehog pathway blockade. *Science* **297**, 1559–1561 (2002).
270. Neradil, J. & Veselska, R. Nestin as a marker of cancer stem cells. *Cancer Sci.* **106**, 803–811 (2015).
271. Pei, Y. *et al.* An animal model of MYC-driven medulloblastoma. *Cancer Cell* **21**, 155–167 (2012).
272. Mehta, S. *et al.* Critical Role for Cold Shock Protein YB-1 in Cytokinesis. *Cancers* **12**, (2020).
273. Small, W. & Donnelly, E. D. Leibel and Phillips Textbook of Radiation Oncology. *JAMA* **307**, 93–93 (2012).
274. Cappelli, E., Townsend, S., Griffin, C. & Thacker, J. Homologous recombination proteins are associated with centrosomes and are required for mitotic stability. *Exp. Cell Res.* **317**, 1203–1213 (2011).
275. Mao, Z., Bozzella, M., Seluanov, A. & Gorbunova, V. Comparison of nonhomologous end joining and homologous recombination in human cells. *DNA Repair* **7**, 1765–1771 (2008).
276. Tanaka, T., Halicka, H. D., Traganos, F., Seiter, K. & Darzynkiewicz, Z. Induction of ATM activation, histone H2AX phosphorylation and apoptosis by etoposide: relation to cell cycle phase. *Cell Cycle* **6**, 371–376 (2007).
277. Penninckx, S., Pariset, E., Cekanaviciute, E. & Costes, S. V. Quantification of radiation-induced DNA double strand break repair foci to evaluate and predict biological responses to ionizing radiation. *NAR Cancer* **3**, (2021).
278. Maréchal, A. & Zou, L. RPA-coated single-stranded DNA as a platform for post-translational modifications in the DNA damage response. *Cell Res.* **25**, 9–23 (2015).
279. Shi, W. *et al.* The role of RPA2 phosphorylation in homologous recombination in response to replication arrest. *Carcinogenesis* **31**, 994–1002 (2010).
280. Panier, S. & Boulton, S. J. Double-strand break repair: 53BP1 comes into focus. *Nat. Rev. Mol. Cell Biol.* **15**, 7–18 (2014).
281. Shibata, A. & Jeggo, P. A. Roles for 53BP1 in the repair of radiation-induced DNA double strand breaks. *DNA Repair* **93**, 102915 (2020).
282. Bhargava, R. *et al.* C-NHEJ without indels is robust and requires synergistic function of distinct XLF domains. *Nat. Commun.* **9**, 2484 (2018).
283. Sorokin, A. V. *et al.* Proteasome-mediated cleavage of the Y-box-binding protein 1 is linked to DNA-damage stress response. *EMBO J.* **24**, 3602–3612 (2005).
284. Kosnopfel, C. *et al.* YB-1 Expression and Phosphorylation Regulate Tumorigenicity and Invasiveness in Melanoma by Influencing EMT. *Mol. Cancer Res.* **16**, 1149–1160 (2018).
285. Zhang, J. *et al.* Structural basis of DNA binding to human YB-1 cold shock domain regulated by phosphorylation. *Nucleic Acids Res.* **48**, 9361–9371 (2020).
286. Mehta, S. *et al.* Dephosphorylation of YB-1 is Required for Nuclear Localisation During G2 Phase of the Cell Cycle. *Cancers* **12**, 315 (2020).

287. Schellenbauer, A. *et al.* Phospho-Ku70 induced by DNA damage interacts with RNA Pol II and promotes the formation of phospho-53BP1 foci to ensure optimal cNHEJ. *Nucleic Acids Res.* **49**, 11728–11745 (2021).
288. Falk, M., Lukášová, E. & Kozubek, S. Chromatin structure influences the sensitivity of DNA to γ-radiation. *Biochimica et Biophysica Acta (BBA) - Molecular Cell Research* **1783**, 2398–2414 (2008).
289. Khanna, K. K. & Shiloh, Y. *The DNA Damage Response: Implications on Cancer Formation and Treatment*. (Springer Science & Business Media, 2009).
290. Chatterjee, M. *et al.* The Y-box binding protein YB-1 is associated with progressive disease and mediates survival and drug resistance in multiple myeloma. *Blood* **111**, 3714–3722 (2008).
291. Davies, A. H. *et al.* YB-1 Transforms Human Mammary Epithelial Cells Through Chromatin Remodeling Leading to the Development of Basal-Like Breast Cancer. *Stem Cells* vol. 32 1437–1450 Preprint at https://doi.org/10.1002/stem.1707 (2014).
292. Ramaswamy, V., Nör, C. & Taylor, M. D. p53 and Medulloblastoma. *Cold Spring Harb. Perspect. Med.* **6**, a026278 (2016).
293. Okamoto, T. *et al.* Direct interaction of p53 with the Y-box binding protein, YB-1: a mechanism for regulation of human gene expression. *Oncogene* **19**, 6194–6202 (2000).
294. Hallahan, A. R. *et al.* The SmoA1 mouse model reveals that notch signaling is critical for the growth and survival of sonic hedgehog-induced medulloblastomas. *Cancer Res.* **64**, 7794–7800 (2004).
295. Hatton, B. A. *et al.* The Smo/Smo model: hedgehog-induced medulloblastoma with 90% incidence and leptomeningeal spread. *Cancer Res.* **68**, 1768–1776 (2008).
296. Tamagnone, L. *et al.* Plexins Are a Large Family of Receptors for Transmembrane, Secreted, and GPI-Anchored Semaphorins in Vertebrates. *Cell* vol. 99 71–80 Preprint at https://doi.org/10.1016/s0092-8674(00)80063-x (1999).
297. van der Zwaag, B. *et al.* PLEXIN-D1, a novel plexin family member, is expressed in vascular endothelium and the central nervous system during mouse embryogenesis. *Dev. Dyn.* **225**, 336–343 (2002).
298. Cheng, H. J. *et al.* Plexin-A3 mediates semaphorin signaling and regulates the development of hippocampal axonal projections. *Neuron* **32**, 249–263 (2001).
299. Worzfeld, T. & Offermanns, S. Semaphorins and plexins as therapeutic targets. *Nat. Rev. Drug Discov.* **13**, 603–621 (2014).
300. Torres-Vázquez, J. *et al.* Semaphorin-plexin signaling guides patterning of the developing vasculature. *Dev. Cell* **7**, 117–123 (2004).
301. Risau, W. Mechanisms of angiogenesis. *Nature* **386**, 671–674 (1997).
302. Kim, J., Oh, W.-J., Gaiano, N., Yoshida, Y. & Gu, C. Semaphorin 3E–Plexin-D1 signaling regulates VEGF function in developmental angiogenesis via a feedback mechanism. *Genes & Development* vol. 25 1399–1411 Preprint at https://doi.org/10.1101/gad.2042011 (2011).
303. Kwiatkowski, S. C., Ojeda, A. F. & Lwigale, P. Y. PlexinD1 is required for proper patterning of the periocular vascular network and for the establishment of corneal avascularity during avian ocular development. *Dev. Biol.* **411**, 128–139 (2016).
304. Hurtado, C. *et al.* Disruption of NOTCH signaling by a small molecule inhibitor of the transcription factor RBPJ. *Sci. Rep.* **9**, 10811 (2019).
305. Rehman, M., Gurrapu, S., Cagnoni, G., Capparuccia, L. & Tamagnone, L. PlexinD1 Is a Novel Transcriptional Target and Effector of Notch Signaling in Cancer Cells. *PLOS ONE*

vol. 11 e0164660 Preprint at https://doi.org/10.1371/journal.pone.0164660 (2016).
306. Yang, W.-J. *et al.* Semaphorin-3C signals through Neuropilin-1 and PlexinD1 receptors to inhibit pathological angiogenesis. *EMBO Mol. Med.* **7**, 1267–1284 (2015).
307. Sawada, M. *et al.* PlexinD1 signaling controls morphological changes and migration termination in newborn neurons. *EMBO J.* **37**, (2018).
308. Chauvet, S. *et al.* Gating of Sema3E/PlexinD1 signaling by neuropilin-1 switches axonal repulsion to attraction during brain development. *Neuron* **56**, 807–822 (2007).
309. Bellon, A. *et al.* VEGFR2 (KDR/Flk1) signaling mediates axon growth in response to semaphorin 3E in the developing brain. *Neuron* **66**, 205–219 (2010).
310. Casazza, A. *et al.* Sema3E–Plexin D1 signaling drives human cancer cell invasiveness and metastatic spreading in mice. *J. Clin. Invest.* **120**, 2684–2698 (8 2010).
311. Tseng, C.-H. *et al.* Sema3E/plexin-D1 mediated epithelial-to-mesenchymal transition in ovarian endometrioid cancer. *PLoS One* **6**, e19396 (2011).
312. Sakurai, A. *et al.* Semaphorin 3E initiates antiangiogenic signaling through plexin D1 by regulating Arf6 and R-Ras. *Mol. Cell. Biol.* **30**, 3086–3098 (2010).
313. Sakurai, A. *et al.* Phosphatidylinositol-4-phosphate 5-kinase and GEP100/Brag2 protein mediate antiangiogenic signaling by semaphorin 3E-plexin-D1 through Arf6 protein. *J. Biol. Chem.* **286**, 34335–34345 (2011).
314. Casazza, A. *et al.* Tumour growth inhibition and anti-metastatic activity of a mutated furin-resistant Semaphorin 3E isoform. *EMBO Mol. Med.* **4**, 234–250 (2012).
315. Rankin, E. B. & Giaccia, A. J. Hypoxic control of metastasis. *Science* **352**, 175–180 (2016).
316. Li, J. *et al.* Prognostic Value of PLXND1 and TGF-β1 Coexpression and Its Correlation With Immune Infiltrates in Hepatocellular Carcinoma. *Front. Oncol.* **10**, 604131 (2020).
317. Vivekanandhan, S. *et al.* Role of PLEXIND1/TGFβ Signaling Axis in Pancreatic Ductal Adenocarcinoma Progression Correlates with the Mutational Status of KRAS. *Cancers* **13**, (2021).
318. Lyabin, D. N., Eliseeva, I. A. & Ovchinnikov, L. P. YB-1 protein: functions and regulation. *Wiley Interdiscip. Rev. RNA* **5**, 95–110 (2014).
319. Friedel, R. H. *et al.* Plexin-B2 controls the development of cerebellar granule cells. *J. Neurosci.* **27**, 3921–3932 (2007).
320. Lyabin, D. N. *et al.* YB-3 substitutes YB-1 in global mRNA binding. *RNA Biol.* **17**, 487–499 (2020).

Clinical Trials Bibliography

1ct. National Library of Medicine (US). (2019, July -). Evaluation of LY2606368 Therapy in Combination With Cyclophosphamide or Gemcitabine for Children and Adolescents With Refractory or Recurrent Group 3/Group 4 or SHH Medulloblastoma Brain Tumors. ClinicalTrials.gov Identifier: NCT04023669. https://clinicaltrials.gov/ct2/show/NCT04023669

2ct. National Library of Medicine (US). (2017, July -). Olaparib in Treating Patients With Relapsed or Refractory Advanced Solid Tumors, Non-Hodgkin Lymphoma, or

Histiocytic Disorders With Defects in DNA Damage Repair Genes (A Pediatric MATCH Treatment Trial). ClinicalTrials.gov Identifier: NCT03233204. https://clinicaltrials.gov/ct2/show/NCT03233204

3ct. National Library of Medicine (US). (2019, April -). Testing the Safety and Tolerability of CX-4945 in Patients With Recurrent Medulloblastoma Who May or May Not Have Surgery. ClinicalTrials.gov Identifier: NCT03904862. https://www.clinicaltrials.gov/ct2/show/NCT03904862

4ct. National Library of Medicine (US). (2017, July -). Samotolisib in Treating Patients With Relapsed or Refractory Advanced Solid Tumors, Non-Hodgkin Lymphoma, or Histiocytic Disorders With TSC or PI3K/MTOR Mutations (A Pediatric MATCH Treatment Trial). ClinicalTrials.gov Identifier: NCT03213678. https://clinicaltrials.gov/ct2/show/NCT03213678

5ct. National Library of Medicine (US). (2018, August -). Phase 1 Study of the Dual MDM2/MDMX Inhibitor ALRN-6924 in Pediatric Cancer. ClinicalTrials.gov Identifier: NCT03654716. https://clinicaltrials.gov/ct2/show/NCT03654716

6ct. National Library of Medicine (US). (2004, August - 2009, February). Gene Therapy in Treating Patients With Recurrent or Progressive Brain Tumors. ClinicalTrials.gov Identifier: NCT00004080. https://clinicaltrials.gov/ct2/show/NCT00004080

7ct National Library of Medicine (US). (2004, July - 2018, June). Gene Therapy in Treating Patients With Recurrent Malignant Gliomas. ClinicalTrials.gov Identifier: NCT00004041. https://clinicaltrials.gov/ct2/show/NCT00004041